Development of an Inkjet Printing System on a Flatbed Router

by

Dayna Chan

A thesis
presented to the University of Waterloo
in fulfillment of the
thesis requirement for the degree of
Master of Applied Science
in
Mechanical Engineering

Waterloo, Ontario, Canada, 2010

© Dayna Chan 2010

Author's Declaration

I hereby declare that I am the sole author of this thesis. This is a true copy of the thesis, including any required final revisions, as accepted by my examiners.

I understand that my thesis may be made electronically available to the public.

Abstract

Manufactured products, such as furniture, laminate flooring, and large signs, are very labour intensive, time-consuming, and costly to produce as they require multiple coating and cutting operations on a series of independent machines, which can each introduce manufacturing errors between the tools and the work piece. By combining the processes of printing and milling, printing integrated manufacturing has the potential to eliminate some of these steps, significantly reduce errors, and preserve resources. Inkjet printing is an ideal method for both image transfer and coating operations due to its non-contact method of directly depositing various types of fluid onto a substrate. With improved positioning accuracy and droplet miniaturisation, inkjet printing could even be used for future applications like the mass-production of MEMS devices, which are traditionally fabricated with a highly complex process involving photolithography.

This thesis presents the integration of a Xaar 126 inkjet printing system with an existing industrial flatbed CNC router to develop a combined printing and cutting system. This integration required modification to the overall system through mechanical, electrical, and software means to the existing 3-axis CNC milling system. A secondary z-axis was installed onto the router gantry for positioning of the printheads relative to the substrate, which required development of a separate homing routine to consistently position the printheads to a specified location. Based on the identified frequency response of the machine, a loop-shaping controller was designed for improved y-axis positioning, which is one of the main contributions to droplet placement accuracy. This resulted in a continuous motion tracking accuracy within ±20.2 µm at 250 mm/sec along a print pass (measured by 1.22 nm resolution linear encoder), which is significantly better than the industrial benchmark of ±100 µm.

Extensive image processing and calibration methods were utilised on various substrate preparations of paper, wood, and coatings, to demonstrate the capability of the printing system and quantify the quality of print resolution. Calibration results tested on high-gloss Hewlett-Packard paper showed that the swath angle could be aligned within ±1°. Also, bidirectional printing could be used to reduce print time by at least 15% in multi-colour printing with comparable droplet placement accuracy to unidirectional printing. The inkjet system was successfully used to print custom designs on paper and, to a certain extent, on medium density fibreboard at a feed rate of 250 mm/sec. It was difficult to achieve satisfactory image results on wood, as the wood or paint grain was visible through the ink. Thus, without a white pre-coat, the printed image would appear significantly darker than the original image, even after adjusting the image in a graphics editor. For better quality results, it is recommended that greyscale printheads be implemented for greater resolution and a UV system should be investigated for more versatility in printing on different substrates such as glass, metals, plastics, and ceramics.

Acknowledgements

This research was funded in part by the Ontario Centres of Excellence. This project would not have been possible in such a short time without the help of a great group of people at the University of Waterloo. Robert Wagner, our laboratory's CNC technician, provided invaluable advice and support in the mechanical assembly of the router and printing system. Jason, Charlie, and Fred from the Engineering Machine Shop did an amazing job machining components for the printing assembly and were always friendly and helpful. Andy Barber and Neil Griffett were a great help in figuring out the necessary electrical connections, building the signal converter and cables, and troubleshooting. AJung Moon hugely facilitated in getting the project started with the motor and actuator selection and assisting in the design of the printhead mounting assembly. Mark Podbevsek was a terrific help with his knowledge of machinery and for machining components in preparation for the initial setup with the Xaar field engineer. Greg Derrington was the field engineer from Xaar and he was an excellent advisor in implementing the printing system, providing years of experience and knowledge, and giving comprehensive instruction on using Xaar software. The redesign of the bottom plate for bidirectional printing was completed with the help of Turker Izci. Jeff Gorniak, Ammar Alzaydi, and Sui Gao roughed some of the plates for the printhead mount. Dan Gordon provided great insight in implementing the Control Desk real-time program for manually controlling the router and general discussion. Everyone here and the rest of the members from the Precision Controls Laboratory were a tremendous support. Thanks for the good times.

To my thesis committee readers, Prof. Ehsan Toyserkani and Prof. Michael Mayer, thank you for the great feedback and taking the time to review my thesis. I would like to thank my supervisor, Prof. Kaan Erkorkmaz, for giving me the opportunity to work with such an exciting project. His guidance and insight were an invaluable part of my experience.

Finally, I am very grateful to my friends and family, especially Jayna Chan, Heather Van Winckle, and Rana Chan, for pushing me to finish and believing in me. See, I do listen to you. Thanks to Ivan Chin, my main reason for getting a Master's degree, for understanding and supporting me (including distractions and food) through the good times and bad. I'll get working on those robots soon...

Dedication

This thesis is dedicated to my mom and dad.

Table of Contents

Author's Declaration ii

Abstract iii

Acknowledgements iv

Dedication v

List of Figures viii

List of Tables x

Chapter 1: Introduction to Printing Integrated Manufacturing 1

Section 1.1: Applications 2

Section 1.2: Experimental Setup and Previous Work 3

Section 1.3: Scope of Thesis 5

Chapter 2: Literature Review 6

Section 2.1: Printing Methods 7

Section 2.2: Printing Resolution and Colour Generation 13

Section 2.3: Theory of Droplet Formation in Inkjet Printing 15

Section 2.3.1: Kinetics 21

Section 2.4: Recent Developments in Industrial Inkjet Printing Applications 24

Section 2.5: Conclusions 26

Chapter 3: Design of a Flatbed Printing System 28

Section 3.1: Printing Component Selection 29

Section 3.2: System Integration 34

Section 3.2.1: Mechanical Integration 36

Section 3.2.2: Electronics and Software Integration 42

Section 3.3: Conclusions 44

Chapter 4: Servo System Design 45

Section 4.1: Sliding Mode Controller Design 47

Section 4.2: Frequency Domain Identification of Axis Dynamics 50
Section 4.3: Loop-Shaping Controller Design 53
Section 4.4: Trajectory Generation & Axis Homing 62
Section 4.5: Conclusions 70
Chapter 5: Inkjet Printing Calibration 71
Section 5.1: Printhead Calibration Methodology and Operation 73
Section 5.2: Calibration Experiments 77
Section 5.2.1: Unidirectional Monochrome Printing 79
Section 5.2.2: Unidirectional Multi-colour Printing 82
Section 5.2.3: Unidirectional Multi-swath Monochrome (Large Image) Printing 84
Section 5.2.4: Unidirectional Multi-swath Multi-colour Printing 89
Section 5.2.5: Bidirectional Monochrome Printing 92
Section 5.2.6: Bidirectional Multi-colour Printing 94
Section 5.3: Additional Issues 98
Section 5.4: Conclusions 100
Chapter 6: Printing on Different Media 101
Section 6.1: Conclusions 111
Chapter 7: Conclusions and Recommendations 112
References 115
Appendices:
Appendix A: Xaar Printhead Specifications 118
Appendix B: Printhead Angle Calculations 119
Appendix C: Operation of Printing System 123
Appendix D: Additional Calibration Measurements and Calculations 138

List of Figures

Figure 1.1: Industrial Flatbed Router 4
Figure 2.1: Continuous Inkjet (CIJ) 8
Figure 2.2: Drop on Demand (DOD) 8
Figure 2.3: Various Methods of Droplet–Substrate Interaction 12
Figure 2.4: Stages of Droplet Formation in a Drop on Demand System 15
Figure 2.5: Effects of Different Nozzle Shapes 17
Figure 3.1: Previous System Schematic for Operation of the Router 28
Figure 3.2: Main Ink System Components 30
Figure 3.3: Xaar 126 Printhead 31
Figure 3.4: Printhead and Header Tank Assembly With Ink Trap Bottle 32
Figure 3.5: Overall System Schematic for Operation of Printing System 35
Figure 3.6: Demonstration of How the Alignment Angle Generates 309 DPI 37
Figure 3.7: Bottom Mounting Plate 37
Figure 3.8: Printhead Mount 38
Figure 3.9: Additional Mechanical Integration 40
Figure 3.10: Router After Ink System Modifications 41
Figure 4.1: Structure of SMC Implementation 48
Figure 4.2: SMC Tracking Performance 49
Figure 4.3: Sinusoidal Excitation Overlaid on Top of the Control Signal (u) 51
Figure 4.4: Identified Position Frequency Response 52
Figure 4.5: Loop-shaping Controller 53
Figure 4.6: Simplified Controller 54
Figure 4.7: Effect of Proportional Gain Integrator 56
Figure 4.8: Sensitivity After Adding PI 56
Figure 4.9: Effect of Adding a Notch Filter 58
Figure 4.10: Sensitivity Plot After PI, Notch, and Lead Filters 58
Figure 4.11: Final FRF 59
Figure 4.12: Final Sensitivity Analysis 60
Figure 4.13: SMC vs. Loop-shaping Tracking Error 61
Figure 4.14: Homing Trajectory 63
Figure 4.15: Homing 63
Figure 4.16: Axis Jogging Interface 65

Figure 4.17: Jerk Limited Profile for the y-axis 66
Figure 4.18: Unidirectional Printing Trajectory 67
Figure 4.19: Bidirectional Printing Trajectory 68
Figure 5.1: Direction of Printhead Adjustment 73
Figure 5.2: Piezoelectric Shear Mode Printhead 75
Figure 5.3: Droplet Placement Error due to A-B-C Firing 76
Figure 5.4: Calibration Image Shown rotated 90°clockwise 77
Figure 5.5: Test Image After XUSB Angle Compensation 78
Figure 5.6: Unidirectional Printed Microscope Results 79
Figure 5.7: Angle Measurements 81
Figure 5.8: Microscope Image of Cyan Printed After Calibration 81
Figure 5.9: Multicolour Unidirectional Printed Microscope Results 83
Figure 5.10: Microscope Image Printed After Realignment of Magenta 83
Figure 5.11: Alignment Errors 84
Figure 5.12: Measuring Droplet Radius and Position 85
Figure 5.13: Calibration Results 88
Figure 5.14: Unidirectional Multi-swath Multi-colour Test Image 90
Figure 5.15: Scan of Unidirectional Multi-swath Multi-colour Image Printed on Xerox Paper 91
Figure 5.16: Scan of Colour Disparity in Bidirectional Printing 95
Figure 5.17: Mounting Plate for Bidirectional Multicolour Printing (Top View) [mm] 97
Figure 5.18: Image Processing for a Bidirectional Image 97
Figure 5.19: Print from Damaged Magenta Nozzle 98
Figure 5.20: Damaged Nozzle on Magenta Printhead 99
Figure 6.1: Wood Pattern Test Image 102
Figure 6.2: Wood Pattern Printed on Hammermill Paper 104
Figure 6.3: Wood Pattern Printed on Xerox Inkjet Paper 104
Figure 6.4: Wood Pattern Printed on MDF 105
Figure 6.5: Wood Pattern Printed on Varnished MDF 105
Figure 6.6: Wood Pattern Printed on MDF Painted with Rust Paint 106
Figure 6.7: Wood Pattern Printed on Drywall 107
Figure 6.8: Wood Pattern Printed on Primed Drywall 108
Figure 6.9: Wood Pattern Printed on Plywood 108
Figure 6.10: Wood Pattern Printed on Pre-coated MDF 109
Figure 6.11: Wood Pattern Printed on Gesso 109

List of Tables

Table 1: Dot Radii Measured from Microscope Images 80
Table 2: Droplet Placement Accuracy [degrees] 80
Table 3: Vertical Offset Measurements 86
Table 4: Horizontal Offsets for Unidirectional Printing 86
Table 5: Droplet Radius [µm] Comparison for Different Substrate Clearances 87
Table 6: Bidirectional Horizontal Offsets [µm] 93

Chapter 1: Introduction to Printing Integrated Manufacturing

Recent advances in printing technology over the past few decades have made printing systems commercially available for home and office environments, with industry constantly pushing the limits in terms of speed, accuracy, resolution, minimising noise level, improving portability, and finding new uses. These printers depend on a wide range of deposition methods such as thermal and piezoelectric inkjet, dot-matrix, or even laser printing. Inkjet printing, in particular, is finding more and more applications in industry due to its advantages of being very low-cost when compared with laser printing, can have variable droplet size, and has shown potential for applications in markets outside of paper products due to its non-contact method of depositing ink droplets. Various companies such as Zünd have developed industrial-scale flatbed inkjet printing systems that print on large sheets of paper or textiles and cut them into several smaller sheets for high-throughput mass-production. Direct printing has also been used to produce decorative surfaces for many years, though only for areas of low visibility such as drawer bottoms or backers since the quality of print is poor. [1]

Companies that produce customisable manufactured products such as furniture, laminate flooring, and large signs typically process these materials with multiple coating and cutting steps through a series of independent machines, which can be costly. This setup also has the disadvantage of transferring parts from one machine to the next, which adds the risk of misalignment between the tool and the substrate. For line assemblies, as each machine would need to be tuned to the specific line velocity to maintain accuracy. The finishing step is typically the bottleneck in the process as different shapes or contours are required and many companies resort to hand-cutting, which is labour intensive, inconsistent, poor quality, and can lead to costly remakes.

Printing integrated manufacturing, where printing and cutting processes are instead combined into one apparatus, has become more relevant to the manufacturing industry due to the savings in cost of machinery, labour, time, and accuracy. Inkjet printing is highly compatible with cutting/milling technology, given that each of these technologies requires tight tolerances in positioning accuracy for droplet placement to produce good quality images, and for precise milling designs. However, integrating the processes of printing and machining is highly complex in that it requires the knowledge of diverse fields such as controls, microfluidics, mechanical design, electronics, programming, graphics, and colour. Despite the complexities, there are many benefits to integrating printing and machining. For example, inexpensive, easy-to-machine, readily available wood, or recycled wood could take on the appearance of high-quality wood from trees that are scarce or expensive to harvest by applying images of the wood grain and colour, thereby saving valuable resources. [2]

Section 1.1: Applications

Inkjet printing has valuable applications in the sign and furniture industries, though other printing methods are equally capable. However, inkjet printing has the most desirable features of being cost-effective, being compatible with different fluids including water- and oil-based inks, metals, and heat-sensitive biomaterials, and depositing droplets without contacting the substrate, which makes it promising for the manufacture of other intricate products. Current research has emphasised inkjet printing for layered products, since an impact printing method would damage the underlying layers. For example, instead of depositing ink, fluid metals could be deposited to create three-dimensional structures such as microchips, light emitting diodes, circuit boards, and flat screen displays. Current microfluidics and microelectromechanical (MEMS) systems are fabricated using complex multi-step photolithography, deposition, and etching steps, and require patterned masks to transfer the patterns. These steps use experimental wafers made of several layers of different materials, where an alignment mark is necessary for each mask so that every layer is deposited directly above the previous layer. Photoresist deposition on wafers, which is often done with a spin coating machine, wastes 95% of the photoresist while coating the smooth surface layer. Inkjet printing could replace the process of lithography since it is capable of precisely depositing material, thereby improving accuracy and reducing waste. As well, large-scale inkjet printing would not be limited to the size of a single wafer as in typical microfabrication processes and thus opens up the possibility of high-throughput mass-manufacturing. Since inkjet printing has the versatility of using a variety of different fluids, the applications can be virtually limitless. Other applications include soldering circuit board connections, precise placement of lubricants, fabrication of displays using organic LEDs, thin film coating for heat radiators to improve surface area and radiate heat efficiently, and printing of difficult to replicate characters and logos for security documents. [3, 4, 5, 6, 7]

Section 1.2: Experimental Setup and Previous Work

A commercially available Computer Numerical Control (CNC) industrial flatbed router was donated to the Erkorkmaz Precision Controls Laboratory for the purpose of research (Figure 1.1). The suction bed area is 1200 mm wide and 2400 mm in length. This suction bed holds the material stationary, while the spindle moves with respect to the material. A vacuum close to the spindle removes any chips and dust during cutting. An internal controller communicates to a computer using an RS232 cable and is used when manually jogging the axes with the joystick. Various programs such as SignLab can be used to program the cutting trajectory. However, this thesis focuses on using MATLAB and a dSPACE controller environment to develop advanced controllers that override the internal controller from the router. The dSPACE controller provides high processor power for the Simulink model and interfaces to the inputs and outputs of the machine.

Three axes allow for gantry movement along parallel ball screws (x-axis), spindle motion along the gantry (y-axis), and adjustment of spindle height (z-axis), with positioning speeds up to 250 mm/sec for x and y, and 75 mm/sec for z. All axes are powered by DC motors that can be monitored using rotary encoders that produce a digital signal. The x-axis has two motors, which are referred to as x-left and x-right, one for each ball screw. For the x-axes, the motors move with the gantry and the pulley belt actuates a nut along a stationary ball screw. The y-axis motor drives a pulley belt, which instead rotates the ball screw, thus translating the nut and components along the axis. Most of the weight on these axes is supported by the linear guiderails and bearings. x- and y- axes have the same pulley ratio of 4.8 and the rotary encoders have a resolution of 500 counts/rev plus quadrature interpolation. Having a lead of 25 mm (the linear travel distance per revolution), this corresponds to an encoder resolution of 2.6 μm. With the same rotary encoder, though a different pulley ratio of 2.4 and a lead of 5 mm, the z-axis encoder resolution is 1.042 μm.

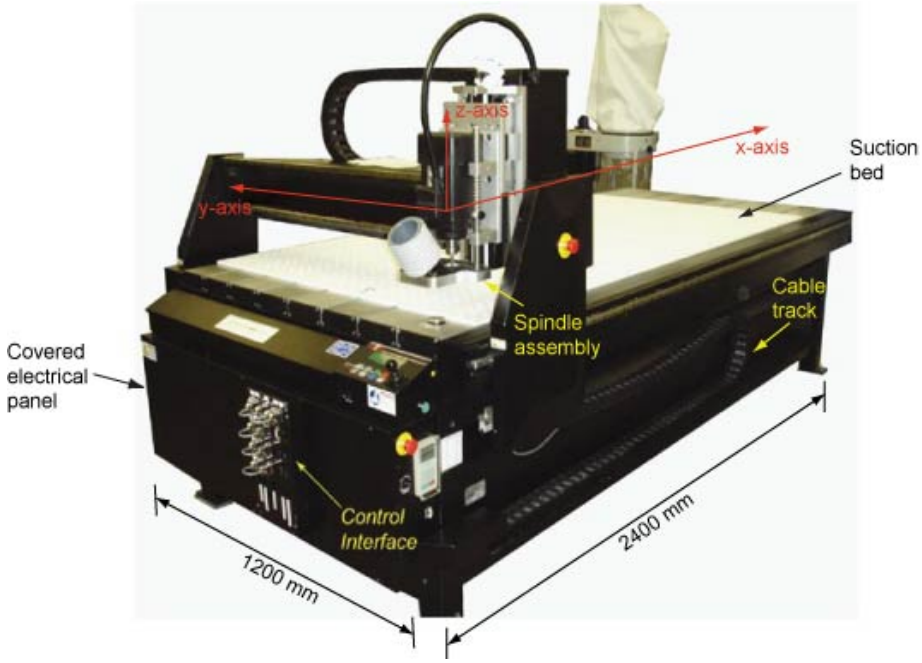

Figure 1.1: Industrial Flatbed Router

Previously, the x- and y-axes were retrofitted with LIDA 485 linear encoders from Heidenhain, since it was found that the original rotary encoders experience backlash when changing directions and are unable to detect vibrations outside of the motor. Given that the linear encoder is entirely optical, where a beam of light reflected off the encoder strip determines the position readings, the feedback is thus essentially unaffected by electrical noise. The linear encoder outputs sinusoidal signals to two channels, A and B, which lags one quarter of a period behind output A. With a signal period of 20 µm with 4-fold interpolation and 4096 counts per period, the linear encoders have a resolution of 1.22 nm. Though more susceptible to vibration noise, the results showed that the linear encoder error was more repeatable since it does not depend on direction or suffer from backlash as does the rotary encoder. [8]

Various tests have also been performed on the router for smooth, time-optimal trajectory generation and precision controller model design. In trajectory generation the use of Non-Uniform Rational B-spline toolpaths provides faster feed rates, higher accuracy, and better surface finish in machining parts with complex geometry. The results of that study showed approximately 13% - 26% reduction in cycle time [9]. Improvements in the controller design and modelling of the dynamics of ball-screw systems have shown higher motion accuracy at high speeds is possible [10].

Section 1.3: Scope of Thesis

This chapter introduced the concept of printing integrated manufacturing and its advantages and potential applications. Previous research in the Erkorkmaz Precision Controls Laboratory has improved both the position tracking control and the optimised trajectory generation for the performance of a low-grade, CNC router, resulting in the ability to manufacture high-quality, high-accuracy products. The goals of the research described in this thesis were to integrate an inkjet printing system onto this existing industrial flat-bed router, modify the controller software design to further improve positioning accuracy, and demonstrate the ability to print high-quality images at high-speed onto porous substrates such as paper and medium density fibreboard (MDF).

To understand the process of inkjet printing, Chapter 2 presents a general overview of the science and terminology surrounding this technology, along with a synopsis of recent developments in industrial inkjet printing. The methodology, design, and steps taken to integrate the Xaar inkjet printing system with the CNC router can be found in Chapter 3. Chapter 4 explains how a high-accuracy motion controller was developed for improved image resolution and speed of the printing and milling processes. This is followed by Chapter 5, which describes the calibration process and characterisation of droplet placement accuracy for variations of monochrome, unidirectional, bidirectional, and multicolour prints. An analysis of printing on different substrate materials can be found in Chapter 6 before the final conclusions and recommendations in Chapter 7.

Chapter 2: Literature Review

Printing technology has advanced significantly over the past few decades, starting with dot-matrix printers, moving to the first commercial piezoelectric inkjet printers marketed in the late 1970s, then the first thermal inkjet printer with improved performance produced in 1984 by Hewlett-Packard, and most recently, laser printing [11]. Since then home and office printers have become commonplace; able to print quickly, in wide-format, and in full colour. Printer formats in which the printhead moves with respect to the substrate or the substrate moves while the printhead remains stationary are both common. Currently, most printers rely on inkjet or laser printing technology, both of which can be subdivided further based on their mode of operation. Unlike lithographic methods, both processes are classified as non-impact printing, which means that no mechanical device comes into contact with the substrate, and are thus ideal for substrates where contact with the surface would cause damage. In addition to this advantage, comparative quality, low noise, small size, low cost, and the ability to print in colour quickly pushed inkjet and laser printing ahead of traditional processes such as impact dot-matrix printing.

Various methods of inkjet printing are described in Section 2.1. The system selected for integration with a flatbed router was chosen based on ease of integration, maintenance, cost, and flexibility for future research. Some of the main terminology and issues in printing and image generation are discussed in Section 2.2, followed by a more extensive analysis of the fluid mechanics and composition in Section 2.3. There are many parameters to consider for stable droplet formation, including fluid and substrate selection, waveform shape and frequency, and maintenance. Section 2.4 will mention some of the companies that have successfully implemented printing integrated systems to directly print on non-traditional substrates for use in a diversity of industries. Conclusions from the literature review can be found in Section 2.5.

Section 2.1: Printing Methods

Inkjet printing is defined by the ability to generate a sequence of fluid micro-drops with predetermined size and precisely controlled trajectories. This technology has been used to deposit a very wide range of materials, for many different applications, with the only restriction being that the material must be in liquid form with appropriate rheological properties at the time and location of printing. There is a broad range of applications for inkjet printing simply due to all the possible fluid to substrate combinations. This makes it applicable to industries such as print media, MEMS, and photolithography. Materials which have been printed include metals, ceramics, and artificial polymers, as well as various biological materials including living cells. An early application for the direct printing of liquid metal was to form solder droplets on electronic printed circuits. Metallic particles suspended in a suitable liquid can be printed by inkjet processes, and are used for both structural and electrical applications. Inkjet printing is typically divided into two specific droplet formation methods known as continuous inkjet (CIJ), in which individual droplets are diverted from a continuous stream, and drop-on-demand (DOD), in which droplets are formed only when needed. These two groups can be further classified based on the mechanism of operation, including acoustic, thermal, and piezoelectric, with each having its own advantages and disadvantages. [5]

In acoustically disrupted CIJ, a continuous fluid jet is produced by pressurising the fluid reservoir (Figure 2.1). The printhead is excited with acoustic waves that generate nodes in the fluid stream as it emerges from the nozzle, where the maxima of the waves then form into individual droplets. By changing the waveform frequency to produce nodes at different intervals, the droplet diameters can be varied to a limited extent. Smaller wavelengths should decrease the size of droplets; however, the fluid jet becomes unstable for a wavelength less than three times the jet diameter. Similarly, the maximum droplet diameter producible is determined by larger wavelengths. However, long distances between nodes make the jet susceptible to secondary nodal points. These can create extra droplets, which are known as satellite droplets, and may be deposited on the substrate in undesirable locations. Stable droplet breakup depends on fluidic properties such as surface tension and viscosity. For example, lower viscosity suppresses satellite droplet formation. Image printing is typically done by electro-statically charging the droplets and then using deflection electrodes to direct droplets into the targeted locations, while non-deflected droplets are returned to a tank for recycling. Control of the droplet trajectory can be implemented by either modulating the potential between external deflection electrodes or by modulating the induced charges on the droplets. This means that the liquid requires enough electrical conductivity for the charge to pass along the stream from the nozzle. [4, 5, 12]

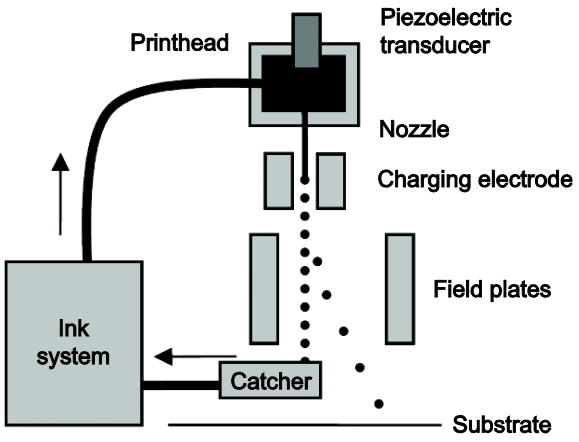

Figure 2.1: Continuous Inkjet (CIJ) - Ink droplets fall continuously into a tank, while electrical charges are used to deflect select droplets to the desired locations. Courtesy of IOP Publishing Ltd. [12]

In DOD, the most commonly used method in industry, short duration fluid jets are made such that each jet condenses into a single micro-drop of the desired diameter. The principle of DOD makes it ideal for many other manufacturing processes since small marks can be made and ink is conserved by only marking where necessary. A low fluid impedance nozzle of approximately the same diameter as the droplet to be ejected and a controllable actuator that can generate microsecond scale pressure impulses in the fluid are needed. These actuators are most commonly piezoelectric elements or thermally generated gas bubbles created by resistive heating elements in contact with the working fluid. Usually in a large array, each nozzle is individually activated to generate a single droplet on demand. The droplets then travel in straight lines from the nozzle to deposit on the substrate. After deposition, the material usually becomes solid by evaporation of solvent, chemical changes, or through cooling. Figure 2.2 shows a typical DOD system. [5]

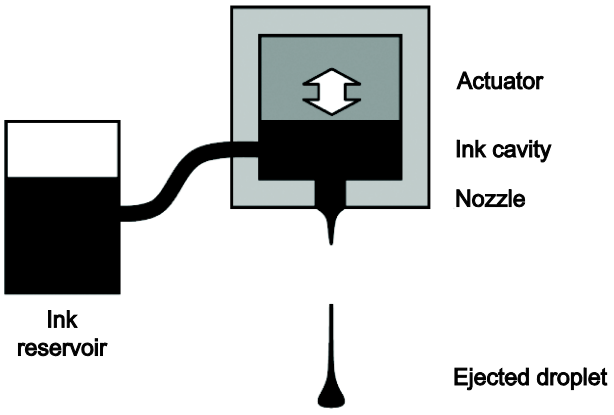

Figure 2.2: Drop on Demand (DOD) - The ink reservoir is actuated only when it is time to eject a droplet. Courtesy of IOP Publishing Ltd. [12]

One of the main differences between CIJ and DOD methods is the frequency of droplet generation. CIJ is capable of producing droplets at MHz rates and even its minimum operating range in the tens to hundreds of kHz is higher than the maximum operating frequencies of DOD. The maximum frequency in DOD is constrained by the sequential, discrete time steps it takes for fluid ejection and cavity replenishment. To make up for a lower maximum rate of droplet production, DOD utilises miniaturisation and massive paralleling of independently operating ejectors into a common functional unit, suitable for fabrication with well-established integrated circuit processes. Although early CIJ systems used single or small numbers of nozzles, while DOD is typically operated with tens or hundreds, both are now capable of handling many hundreds of nozzles and there is significant convergence between the two technologies. Generally, CIJ systems operate with fluids of lower viscosity, higher droplet velocity, and tend to require larger quantities of fluid for pumping and recirculation than DOD. However, certain DOD nozzle arrays also circulate the fluid through the nozzle manifold to improve reliability. Current trends in research are to increase droplet generation rates in DOD and develop the ability to generate droplets of variable size by using complex drive waveforms, which produces a stream of micro-droplets merging into a single, large droplet before contacting the substrate. Despite its quick droplet generation rates, integrating a system based on CIJ would have the disadvantage of higher hydraulic complexity and significant maintenance. As well, due to very high minimum operating fluid volumes and a substantial amount of ink wasted in evaporation, CIJ is unsuitable for applications in which small quantities of high-value fluids must be micro-dispensed. While droplet diameters for DOD printing are larger than in CIJ, the advantages of DOD include flexibility with substrates and deposition materials, relative mechanical simplicity, smaller minimum fluid operating volumes, lower hardware cost, lower maintenance, and ease of use. [4, 5]

Thermal inkjet, or bubble jet, is a DOD method widely implemented in home and small office printers by companies such as HP and Canon. Electrical pulses are applied to heating elements in contact with the fluid near the nozzle. This rapid transient heating of the ink creates a short-lived bubble of vapour which produces pressure impulses to drive a jet of ink out of the nozzle. With the correct drive levels, the fluid will form into a single droplet. The bubble then collapses, drawing ink from the reservoir to refill the cavity, and the process can then be repeated. Thus, no moving part or direct electrical contact with fluid is needed and this technique is easily integrated into a dense array on an inkjet printhead with low maintenance. Thermal inkjet relies on high nozzle count and firing frequency to print at high speeds. Since thermal DOD involves the vaporisation of a small volume of the ink, this places significant restrictions on materials which can be jetted by this method as the fluid must be relatively volatile. Although thermal inkjet printheads are known for lower cost, they have a shorter

lifespan in part due to higher operating temperatures causing material stresses. Some other disadvantages are that they lack flexibility in modifying the rise and fall time of the pressure pulse for optimising control over the ejected fluid jet and the local chemical reactions that take place during each vaporisation and cooling cycle, which can change the chemical composition of the fluid over time. [4, 5]

Piezoelectric inkjet is similar to thermal, except that a piezoelectric element is used to change the internal volume of the ink cavity on the application of an electric field in order to generate pressure waves, which in turn eject ink from the nozzle and then refill the cavity. This method is more common in industrial inkjet systems and is used by companies such as Epson. Once the jet emerges from the nozzle, surface tension causes it to form a main droplet followed by a long globule which may collapse into one or several smaller satellite droplets. As in CIJ, the surface tension and rheological properties of the liquid strongly influence the formation of droplets and satellite droplets. Pressure pulse rise and fall times can be modified to optimise monodisperse droplet production free from satellite droplets and dynamically alter the diameter of the ejected droplets. Piezoelectric inkjet does not chemically alter the composition of the fluid like in thermal inkjet, so there is much less restriction on the materials which can be ejected. Although laser printing is known for higher resolution than inkjet printing, it may also be limited by the types of deposition material since the deposition material is melted onto the substrate, whereas inkjet printing can handle various fluids including heat-sensitive biomaterials. Shear-mode designs utilise piezoelectric elements in which the direction of polarisation of the drive element is nonparallel to that of the applied electric field. Piezoelectric printheads have low power consumption and high firing frequency, relying on rapid dry time for its solvent-based inks, which may bleed when exposed to wet conditions. There are no stresses caused by cycled heating or moving parts, meaning that the lifespan of the equipment is lengthened. However, the components are often difficult to service, making it necessary to buy full replacements if they do fail. [4, 5, 13]

Three-dimensional printers use starch or plaster-based powder and a binder to print a part layer by layer. The printer places a thin layer of powder on a platform and then the binder is applied in areas where the part is to be printed in order to solidify the powder. The platform is then lowered very slightly, another thin layer of powder is spread on the platform, and the binder is applied again where needed. This process repeats until the entire part is printed. The part can then be lifted off the platform and excess powder brushed away. Waxes and resins can be applied to strengthen the result so that the 3D prototype can be used as part of an engineering design process. [14, 15]

Some systems also use solid or UV curable inks. Solid inks are melted in the printhead and solidify after they are deposited on the substrate and cool. Solid or UV inks would not require a special coating since there is some mechanism such as heat or light that cures the ink onto the substrate and very little spreading and absorption occurs. UV ink cures when exposed to UV light, so solvent evaporation is not really a factor. It has good adhesion, durability, and chemical and solvent resistance for a wide variety of semi-porous and non-porous substrates, which includes more exotic materials such as leather, stone, and wood. This also means no over-laminate is needed to protect the print from rain, sun exposure, or fingerprints. A UV system has low energy and heat requirements, which is beneficial for temperature-sensitive substrates. However, UV ink performs poorly under conditions with high levels of abrasion since UV ink deposits are among the thinnest and erode more quickly. The curing itself is very fast, within 0.2 seconds depending on the colour of the ink and intensity of the UV light source. The inks are sensitive to proper cure procedures for adhesion between coatings and proper cure level for each colour, making it less flexible than other ink systems. As multiple colours can be done in succession by placing a UV light source between each printhead, care must be taken to avoid over-curing. If too much radiation is applied, then the next colour may not adhere properly, and the effects are cumulative as over-cured ink can become brittle and flake off. Naturally, UV inks must be kept in a light-free environment to prevent unwanted curing. The print has excellent colour value, ranging in opacity from very transparent to translucent, where high levels of transparency produce a very clean colour gamut. There are no real opaque UV inks since the UV light must reach all the way through the ink layer to polymerize the ink. This means UV ink does not print well on dark substrates. UV inkjet would be even more preferable than piezoelectric for printing on a greater variety of substrates; however, it has a higher initial hardware cost and would be much more complicated to implement due to the addition of a curing system and also necessary safety measures for working with UV light. [16, 17]

Figure 2.3 shows what happens after depositing a droplet for some of the various printing methods on different substrates.

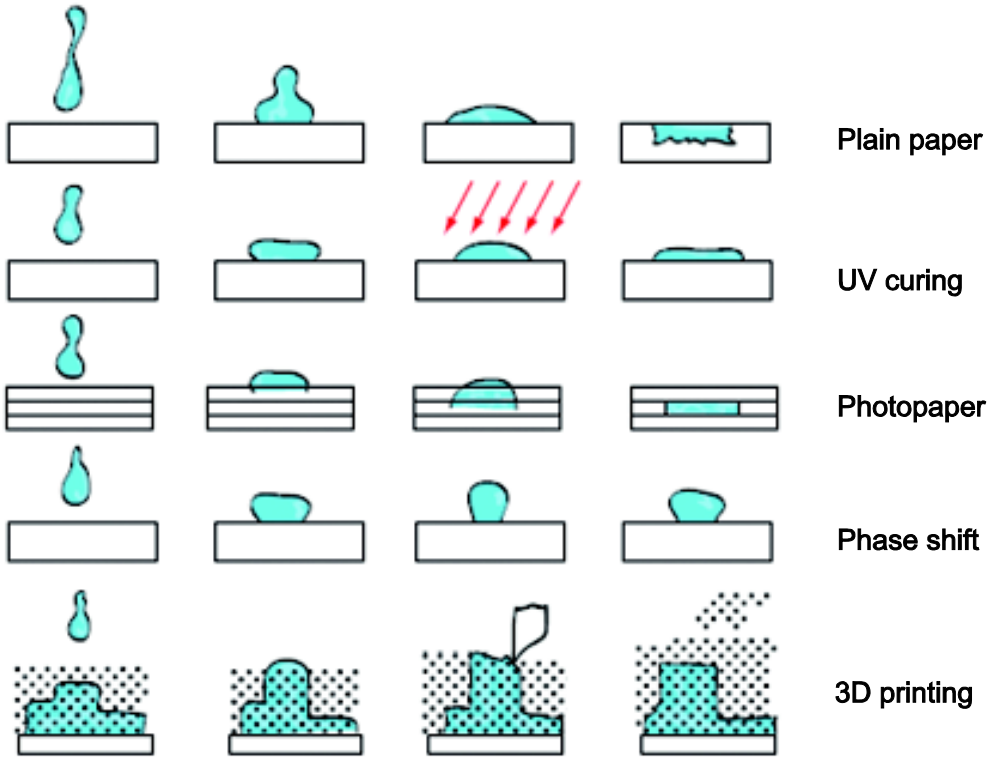

Figure 2.3: Various Methods of Droplet–Substrate Interaction . Reprinted from Comprehensive Microsystems, Heinzl, J., Ink Jets, pp. 335-368, 2008, with permission from Elsevier [14]

There are numerous problems that can be encountered when working with inkjet printheads. Damaged nozzles or cracks can create irregularly shaped, enlarged holes, which can generate abnormally large droplets regardless of settings, ingest air at low negative pressures, misdirect droplets, or create satellite droplets. To verify if the printhead is damaged, it is necessary to observe it under a microscope. Holes can easily be damaged by cleaning and physical contact. Partially clogged holes, asymmetric or over-wetting, debris build-up, or mistuned drives can also trigger misdirected droplets. Clogged nozzles are one of the major problems encountered when operating an inkjet system, and should be prevented by implementing the largest nozzle diameter possible and clean handling procedures. To test whether the nozzles are clear, a positive pressure is applied and if a continuous fluid jet is seen perpendicular to the aperture, then it is clear. For particles that cannot be removed by wiping the nozzles with a lint-free cloth or swab, it may be necessary to flush the nozzles with cleaning fluid. The mechanical mounting of the printheads may also influence droplet generation in that any mechanical resonance may be excited. Ejectors that are loosely mounted and shifting position require tuning based on contact with the holder. [4]

Section 2.2: Printing Resolution and Colour Generation

The overall print quality (resolution and colour) for inkjet printing relies on several variables, including dot resolution, substrate, ink composition, and deposition method, while the deposition method and dot resolution will determine how accurately the ink droplets are placed. A swath is one pass of a printhead, where the width of the swath is determined by the distance from the first nozzle to the last nozzle and a large image is composed of multiple swaths. Printers create an image by applying ink or toner to a page in very small dots, where the resolution is typically measured in dots per inch (DPI). The resolution of the image is based on the separation between successive nozzles. The quality of the print is based on the size of the coloured dots and how closely they are spaced. Smaller dots that are more closely packed produce a better quality of output. Higher resolution is thus attainable by reducing droplet size, which can be controlled by using smaller nozzles. However, the efficiency of the nozzle varies proportionally with the length of channel to the diameter of nozzle, and thin nozzle material is difficult to handle. Absorption of the ink depends on both the viscosity of the ink and the porosity and compatibility of the substrate material. Substrate properties can affect ink application since, for example, ink tends to spread along fibre grains and into any grooves of the substrate material. As well, the absorption of ink is often too slow to absorb multiple droplets of ink in the same location within a short period of time. This results in poor image quality since the ink spreads and colours mix together. Thus, the substrate should be specially tailored with the ink and vice versa based on variables such as droplet volume, evaporation rate, penetration rate, coating thickness, and porosity, or else a special coating is required. [11]

Inks use a subtractive model to generate colour, where the more an element is added, the more it subtracts from white. The combination of all the colours would theoretically result in black. Since the result is actually more of a brownish grey and utilises a lot of ink, black ink is often used in addition to cyan, magenta, and yellow. The hue of the ink is defined as the colour, while saturation is the amount of colour. Some colour printers place dots of ink very close together to simulate different colours in the same way that a computer monitor has a triad of colours for a single pixel close together. Other colour printers use transparent inks and place different colours on top of each other like an artist mixing colours. Greyscale printers control the size of droplets to vary the colour at each droplet position. The eye integrates the dots to produce an impression of shade or colour. Image colour will change for different printers, since each type of output device has a slightly different set of colours that it produces. Adjustments are necessary to accurately reproduce a colour on a variety of devices, which is sometimes not possible. [12, 14, 15]

Solvent inks are inexpensive, can be fast drying, and are a good match for semi-porous and non-porous substrates. Most common solvents are water and oil, which are less hazardous (non-volatile) than organic solvents and have been found to be well-matched to most porous and semi-porous substrates. However, solvents will spread along the surface of the substrate unless special coatings are applied prior to printing. The advantages of using oil-based ink rather than water-based ink are absence of cockle (rippling) on paper substrates and high light-fastness, which describes how resistant the ink is to degradation from light sources. [18][19]

If there is no white ink and the ink is somewhat transparent, then the natural colour of the substrate will show through the ink and deteriorate the image colours. Most printers use CMYK colours, though there are expanded sets which provide a wider colour gamut or improved tonality. For example, a new opaque white allows a printer to image directly onto non-white substrates by first laying down the opaque white coat, then printing the remaining colours on top. The ability to generate droplets with accuracy is thus crucial to resolution and colour. [11]

Section 2.3: Theory of Droplet Formation in Inkjet Printing

Micro-drops can be generated on demand with diameters ranging from a few microns to tenths of a millimetre, having well-defined shape and composition, small size, low mass, and the ability to be ejected with a precise predetermined trajectory. Droplets with identical diameters and ejection speeds are repeatable to within a fraction of a percent. There are many requirements for reliable droplet generation. It is not as simple as taking a fluid chamber with a small hole and pressurising it enough for fluid to emerge from the nozzle or allowing the printhead to leak. If that were the case, then fluid would accumulate and spread out until a large droplet breaks off when its weight exceeds the surface tension forces holding it onto the opening, which is not very controllable. Higher, steady pressures would produce a continuous stream of fluid being pushed out, breaking up into undesirable randomly sized droplets. Instead, DOD requires special conditions to produce high-speed fluid jets of a certain diameter and then control the behaviour of the jets precisely enough to allow consistent formation of uniformly sized droplets. These include the nozzle shape and size, drive pulse shape and frequency, and fluids of a certain composition. After a droplet is ejected, there are still a significant number of factors to consider, such as the speed and position of droplets, environmental influence, splashing, and various printhead malfunctions. Figure 2.4 shows the general process of droplet formation for a DOD printer. [4]

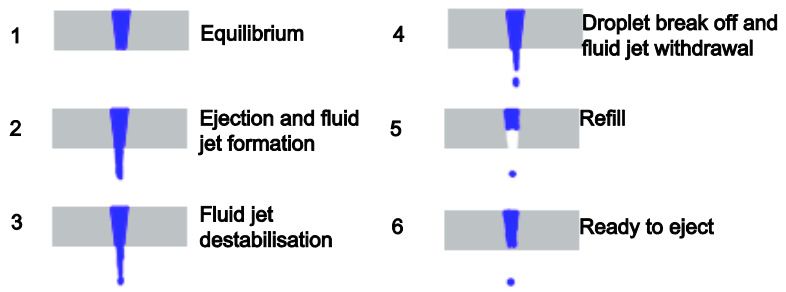

Figure 2.4: Stages of Droplet Formation in a Drop on Demand System - adapted from Microdrop Generation [4]

Fluid micro-drops are very easily given large electric charges that can be used to control their positions and velocities. Droplets that are produced with large amounts of charge can be drawn back into the ejection aperture surface by electrostatic attraction after breaking off from the fluid jet. Electrostatic forces between droplets can also affect stability. In DOD, it is difficult to predict electric charges, which can occur even in systems that do not require droplet charging. Fluid jet polarisation can occur due to stray electrostatics. Electric double layer (EDL) charging is the formation of a high concentration of charge (electron affinity) along a fluid-solid interface and spray charging is the same as EDL though at the fluid-air interface. However, EDL thickness is typically in the range of 1 to 100 nm, which becomes negligible for much larger nozzle diameters. Overall, it is unlikely that droplet charging will be a factor for micrometre sized droplets that are not actively charged. [4]

Highly charged droplets may redeposit onto the ejection aperture surface, forming a layer of fluid and debris that may impair droplet ejector operation. Also, some fluids have a minimum ejection rate since the fluid hardens on contact with air or evaporates off volatiles, leaving a locally more viscous fluid. Both these problems emphasize the need for frequent cleaning of the nozzles and pressurised purging. As the interval between droplet ejection increases, the amplitude of the required pulse energy also increases. Printheads may sit nonoperational for unpredictable periods of time. Many inkjet printers solve this by initiating a print job, which physically wipes the surface of the nozzles over a pad and into a fluid reservoir prior to depositing droplets onto a target. Another solution is to continuously actuate the ejector with pulses sufficient enough to only push the fluid jet out of the nozzle and back without breaking off a free droplet, though this method is not very good for fluids which harden in air. The ejector can also be capped if it is known in advance when the printheads are not going to be in use. [4]

Negative internal pressurisation reduces the pulse energy needed to eject droplets and increases reliability. A high positive internal pressure level will create a forced ejection from the nozzle in the form of a slow leak, which prevents DOD since a thick, fluid layer covering the nozzle acts as an obstacle before a free droplet can be formed. This is especially the case when high surface tension causes the fluid to bind to itself. A thin layer of fluid over the nozzle plate is typically desired, however, if the meniscus is asymmetric, then droplet direction becomes unpredictable. Some fluids with low viscosity and surface tension will leak out of the nozzle without negative pressurisation and also form a thick layer outside of the nozzle. As well, at high droplet generation rates, some fluids leave residue on the surface near the nozzle hole that builds over time and eventually stops droplet ejection. Negative internal pressurisation tuned to the fluid and size of the ejection aperture helps by pulling the fluid back in. Tuning is time dependent, as changing the pulse width will have a settling time where the meniscus must adjust to the new equilibrium value and can be on the order of minutes. A combination of fluids and surface coatings for the ejection aperture that minimises this kind of surface wetting should be chosen. Ideally, the fluid should easily wet the interior of the ejector, yet avoid creating a thick meniscus on the plate, which can be improved by Teflon coating the outside and leaving the interior uncoated. A coating inside can raise the energy needed to eject a jet by causing the fluid to fail to wet the aperture so that it must be driven into contact with the surface of the aperture near the hole before forming an external jet. Fluids with higher surface tension may need no negative pressurisation at all to operate as they are not likely to break the meniscus and there is less of a tendency to flow out of the ejector. [4, 14]

An ideal nozzle is a tapered cross-section ending in a short cylindrical hole with an aspect ratio approximately equal to 1:1 as shown in Figure 2.5. This minimises fluid impedance without compromising mechanical rigidity if the structure is formed on a flat plate. A straight hole would have excessively high fluid impedance, which requires much higher drive impulse and also limits the refill rate near the tip, thereby reducing the maximum droplet generation rate. Non-symmetrical aperture holes create directional deflections as small as a few microns. However, fluid characteristics are far more important than aperture geometry in having satellite free droplets. If the holes are hand-formed, then each hole is unique and causes problems for systems requiring parallel, identically operating units. [4]

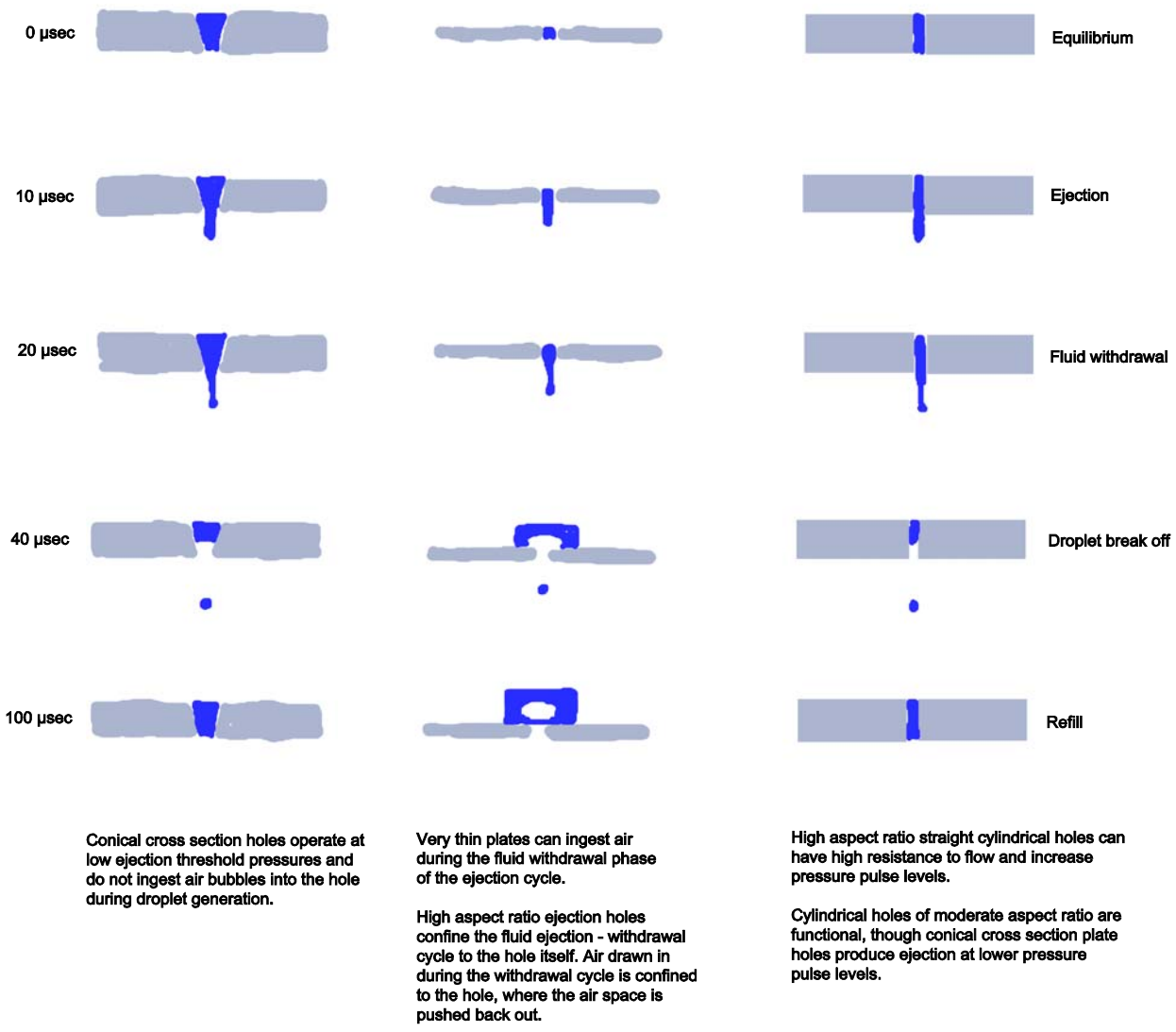

Figure 2.5: Effects of Different Nozzle Shapes - Adapted from Microdrop Generation [4]

The conditions needed for monodisperse DOD operation are generally tuned by trial and error until a fluid jet is pushed out at a high enough speed to form a cylindrical column. Tuned standing waves cause the fluid column to destabilise so that an end node condenses into a separate droplet. The end node breaks off as the fluid column withdraws back into the ejector as a result of a negative pressure wave on the interior of the fluid chamber. The pulse shape of the waveform has a wide range of effects on the tuning for a given fluid and is critical to setting up the system. Excitation of different vibration modes in the ejected jet and mechanical structure of the droplet ejector is difficult to model, as it varies for different fluids and even for different fluid-fill levels within the same droplet ejector. Non-optimal pulse waveforms can cause instability in the form of non-ejection, misdirection, and satellite droplets. If the drive pulse amplitude is too low, a fluid jet is ejected from the aperture and then drawn back on the negative pressure cycle of the excitation before the jet has destabilised enough to form discrete, separate droplets. A large enough amplitude range is needed that will release a single droplet with each pulse, such that the droplets have uniform size and identical velocities. Higher drive amplitudes may generate larger droplet size and higher ejection velocity, yet if the amplitude is too large, then satellite droplets will form. However, the formation of these satellite droplets may not cause an issue due to its repeatability and common direction of travel of the primary droplet and satellites, which could allow them to merge back into one droplet. Though, for even larger amplitudes, a chaotic spray of multi-disperse droplets with random directions of travel is often observed. Overdriving the printhead with large amplitudes or high frequencies may also cause cavitations in the fluid and air ingestion into the interior of the droplet generator. Internal air bubbles will act as fluidic shock absorbers and increase the drive amplitudes required for droplet formation. In addition, during filling, there would be excessively high negative pressure and high drive pulse amplitudes as the bubbles do not re-dissolve quickly enough. Minimum amplitude, on the other hand, immediately produces multiple droplet ejection or random spray. Location and size of satellites can be altered by varying the excitation waveform by trial and error to optimise the droplet formation. If the pulse rate is too high, then the fluid builds up at the nozzle, and if the build-up is too low, then evaporation occurs, which changes the rheological properties of the fluid such that high ejection amplitude is needed. While size of droplets is determined primarily by the size of the nozzle hole, shorter pulse widths produce smaller droplets, though they also require higher amplitudes to eject them. Some pulse widths have no amplitude window at which stable monodisperse droplets are produced. The amount of change in pulse width that can be tolerated before no longer producing stable droplets is mostly dependent on the fluid used. [4]

Fluids having unfavourable rheological characteristics for stable ejection usually require more precise control over the drive to piezoelectric elements. Large diameter particles randomly distributed

throughout the working fluid can cause unstable operation by making the break-off of the droplet from the ejected jet unpredictable since it can act as an instability node. Changes in temperature, back pressure, fluid level, and humidity (determines meniscus thickness) can also alter the optimal settings for exciting an ejector to produce monodisperse single droplets on demand. Ejection characteristics can be enhanced at elevated fluid temperatures, which have a minor effect on surface tension, yet a large effect on viscosity. Some fluids not stable at room temperature will produce reliable monodisperse droplets at a slightly elevated temperature since there is a reduction of energy required for ejection. [4]

Of course, it is expected that not all fluids can be jetted from DOD to form monodisperse droplets. Developing a working fluid for micro-drop ejectors is an extremely difficult process. The starting materials may consist of combinations of powders, surface coatings, binders, and solvents, all of which require customised chemical and rheological properties. A long list of material parameters has to be considered, including viscosity, melting temperature, mean particle size distribution, specific heat, thermal conductivity, diffusivity, substrate material, and porosity. In a well-engineered micro-drop ejection fluid the fluid jet and micro-drop formed by each actuation impulse are nearly identical. Thus, inks contain many different additives to help control the characteristics of the fluid. [4, 5]

Payload is the material put into the micro-drop in order to deposit, react, take a measurement with, or aerosolise, such as pigments and dyes. Solvents are used to suspend or dissolve the payload. Humectants prevent drying out or solidification in the ejection cavity. As most low molecular weight fluids like water and gasoline are Newtonian, viscosity modifiers are used to increase the viscosity of the fluid in order to extend the period of time that suspended solids will remain mixed and not settled out. Polymeric fluid elasticity agents (long chain soluble molecules) prevent satellite formation by suppressing fragmentation of the fluid jet into random-sized spray. Long chain molecules give elasticity which causes the fluid jet to have a greater tendency to remain in a cohering mass that ultimately pulls together into a single droplet rather than disintegrating into many smaller separate satellite droplets. Anti-fungal agents (biocides and preservatives) are added to inks since the aqueous media for many micro-drop ejection fluids may deteriorate due to growth of microorganisms. Chelating agents bind to metal ions to prevent formation of scale deposits upon evaporation of fluids near the ejection aperture. Additives specific for inkjet image printing include penetrants that aid in penetration of ink into fibrous media such as paper and fabrics. Without penetrants, some inks may bead up on the surface of paper, suffer smearing, and have excessively long drying time. Mechanical immobilisation of dye pigments, once deposited as an image, is important for documents that may be frequently handled or stacked and rubbed against other documents. Thus, fixatives and binders (resins and polymers) are added to increase smear resistance of printed images. Anticockel additives reduce the tendency for ink, when absorbed

into paper, to wrinkle, curl, or otherwise mechanically distort the final document. Ultraviolet blockers, free-radical inhibitors, and antioxidants are utilised to protect the image from fading, which is mostly a result of sunlight exposure. There are three main causes of chemical degradation of dyes and pigments: exposure to light (particularly UV components), atmospheric oxygen, and chemical free radicals. [4]

Surfactants are added to ejection fluids to alter surface tension for stable droplet ejection. Some surfactants double as effective dispersants, which aid in the maintaining of solids such as pigment particles in stable suspension. High shear forces and surfactants are required to break up particle agglomerations. Surfactants aid in wetting since structurally, the molecules facilitate suspension by having one portion that binds to the solid particle and another portion that is strongly philic with fluid. Particles are coated with a surface layer that suppresses van der Waals mediated agglomeration of particles into larger solids, which would gravitationally settle or jam ejection aperture holes. The coating must be matched to both the solvent and type of particles to be suspended. Another method of preventing re-agglomeration includes rotary mixers to generate high shear forces to break up particles. The method and duration of mixing can make a strong difference in the quality of the final suspension as poor mixing can result in particles settling within a short time. [4, 5]

Other provisions exist for making suspensions of ground solids able to be ejected from a nozzle, as there is a difference between stable particle suspension and fluid particle slurry. Small particles are generally favoured as the suspensions are more stable. The reasons are that the particles do not sediment and nozzle clogging is avoided. The maximum diameter for a particle that can be stably suspended depends upon the material. Ink pigments typically have a diameter of 0.1 μm, while inkjet printer droplets range from 15 to 40 μm. Larger particles will gravitationally settle in a timeframe too short for most applications. Since the size of the particles approaches the diameter of the ejection aperture hole, the presence in random locations of large particles unpredictably destabilises the ejected fluid jet, leading to unreliable droplet formation. Crushing and grinding is ineffective when the particle diameter is from 10 to 100 μm. Solids subjected to mechanical stress will also fracture along lines of weakness. The number of such defects decreases as the particles are fractured into smaller sizes. The force required to fracture a defect-free small particle is far higher than that needed to break it along a crystal plane dislocation. Re-agglomeration occurs as small, freshly fractured particles with clean crystal planes that contact each other in the correct manner fuse back together into a single particle. The necessary diameter that the suspended particles must be reduced to varies with the specific gravity of the fluid and solids, as well as the viscosity of the fluid. It is difficult to predict the ability of a fluid to be ejected based on its components alone. In the end, the only way to determine the quality of the inkjet fluid is to test it. [4]

Section 2.3.1: Kinetics

Micro-drops of different diameters falling in air can be imaged to study the transition between the dominance of turbulent and laminar flow for drag resistance of objects of different sizes. While the naked eye can observe droplet diameters as small as 10 μm, micro-drops are usually imaged in an area backlit against a dark background with a stroboscope [4, 12]. In terms of fluid dynamics, inertia, viscosity, and surface tension are the dominant forces which control the behaviour of liquid jets and droplets. A micro-drop is small enough that its associated Reynolds Number causes the forces associated with viscous flow resistance to motion defined by Stokes Law to be dominant. Reynolds number is a measure of the ratio of the dynamic pressure drag force to the Stokes viscous drag force on a given object moving through a fluid media such as air:

$$\mathrm{Re} = \rho D v / \eta \qquad (1)$$

where η is the dynamic viscosity of air (182.7×10^{-6} g/cm·s at standard temperature and pressure), ρ is the density of air (0.0011206 g/cm^3), v is the velocity with respect to air, and D is the characteristic diameter, which is usually taken to be the jet or droplet diameter. Weber number *We* is:

$$We = \rho D v^2 / \sigma \qquad (2)$$

Where σ is the surface tension, describes the ratio between kinetic energy and surface energy (between inertial and surface forces). Sometimes Ohnesorge number *Oh* is a more useful value to consider, as it describes the relative importance of viscous and surface forces:

$$Oh = We^{1/2} / \mathrm{Re} = \eta / (\rho \sigma D)^{1/2} \qquad (3)$$

Stable DOD printing of a fluid may occur only if *Oh* is between about 0.1 and 1. For *Oh* greater than 1, viscous dissipation in the fluid prevents droplet ejection, while for *Oh* less than 0.1, multiple droplets form rather than a single well-defined droplet. The ability of a fluid to be ejected thus involves both its viscosity and also the Ohnesorge number. [5, 12]

The drag force is given by:

$$F_{drag} = \frac{1}{2} \rho C_d A v^2 \qquad (4)$$

where C_d is the drag coefficient and A is the frontal area. Stokes Law drag factor dominates over dynamic pressure drag in determining both terminal velocity in air and the relaxation time constant. Cunningham's correction factor, C_c, corrects for atmosphere not being a perfect continuum. Resistance of air is slightly less than that predicted by Stokes Law by $1/C_c$ and the error is larger for smaller droplets. [4]

Terminal velocity is calculated by setting the gravitational force on the droplet equal to that of the velocity dependent drag forces and keeping in mind the following guidelines:

$$D < 100\mu m, use\ Stokes\ Law\ and\ Cunningham\ slip\ correction$$

$$D < 0.1\mu m, use\ Brownian$$

$$D = 0.1\mu m, use\ v_t = 9.0 \times 10^{-4} mm/sec$$

An initial velocity of 1 to 10 m/s is typical for DOD inkjet, about three orders of magnitude faster than the final velocity of ejected droplets in air. How rapidly the droplet decelerates is critical to determining the distance between the droplet ejector and the substrate surface. The relaxation time constant, τ, is the parameter that characterises motion of the fluid droplet that has not come into equilibrium with externally applied forces. It is a measure of how fast the motion of the droplet comes to steady state after initial ejection, changes in local air speed, or application of external forces induced by electric or magnetic fields. There are large differences in impact behaviour of the droplet depending upon how much the droplet has slowed in air from its initial ejection velocity. Micro-drops with diameters ranging below 10 microns are difficult to precisely deposit due to perturbing effects of air convection. While the droplet is moving at high velocity just after ejection it is much less vulnerable to deflection by convection currents. Operation in totally convection-free air may be impractical, particularly if the droplet ejector is being continuously moved and repositioned by a robotically controlled motion stage. Outside of a convection-controlled chamber, the target should be positioned such that the droplet traverses the distance between the ejector and the target at a high enough velocity that local air currents do not significantly deflect the droplet. This may be difficult for small droplets since deceleration is rapid and maximum stable droplet ejection speed tends to be slower the smaller the droplet size. As mentioned, past a certain drive level, stable droplet production ceases and the droplet ejector starts to produce satellite droplets and spray. Thus, as large a droplet as possible should be used for any application requiring accurate positioning in open air. [4]

The extent of the high velocity region of an ejected droplet trajectory can be estimated by multiplying the relaxation time by the initial ejected speed of the droplet. The relaxation time constant τ can be calculated as follows, where g is the gravitational acceleration, y_h is the horizontal distance travelled by a horizontally ejected droplet as a function of time, y_v is the vertical distance, v_{hi} is the initial horizontal ejection velocity, and v_{vi} is the initial vertical velocity:

$$\tau = \left(\frac{1}{18}\right)\left(\frac{D^2}{\eta_{air}}\right)\rho_{droplet}$$
$$y_h(t) = v_{hi}\tau\left(1 - e^{(-t/\tau)}\right) \qquad (5)$$
$$y_v(t) = \tau g t + \tau\left(v_{vi} - \tau g\right)\left(1 - e^{(-t/\tau)}\right)$$

A wide range of behaviour is possible when a liquid droplet strikes a solid surface. The dynamics of droplet spreading can be characterised primarily by the Weber and Ohnesorge numbers in equations (2) and (3), where the value of *We* determines the origin of the driving force for spreading, while *Oh* describes the force that resists spreading. There are generally four stages of development in the diameter of a liquid droplet after impact onto a solid surface, identified as the kinematic phase, the spreading phase, a relaxation phase, and a wetting or equilibrium phase. In the initial kinematic phase the droplet has its initial spherical shape, truncated by the plane of the surface, and the contact circle diameter increases. The non-dimensional diameter of the spreading film is the ratio of the final impacted droplet diameter to the original diameter and is known as the spread factor. This phase of the impact is completely described by the impact velocity and initial diameter. In the next phase, the spreading depends most strongly on the viscosity of the liquid, with less effect of surface tension. Less viscous liquids attain larger diameter droplets than more viscous liquids. During the spreading phase the diameter is constantly increasing. As the spreading liquid comes to rest, the effects of surface tension are more significant. Depending on the wettability and roughness of the surface and the balance between inertial and viscous forces up to this point, the contact angle at the end of the spreading phase may be greater or less than the appropriate (advancing or receding) equilibrium value. The droplet may therefore continue to expand, or retract, during the relaxation phase. For longer times and if the surface is well wetted (rough) by the liquid, the droplet continues to expand. In practical applications of inkjet printing, the first three stages of droplet spreading last only a few tens of microseconds. [5]

Splashing is generally undesirable if precise droplet placement is required. For a droplet to splash and break up on impact the kinetic energy must be sufficient to supply the surface energy for the new droplets, which requires relatively large droplets travelling at high speed. Since surface energy of a single large droplet is smaller than that of the same volume of fluid dispersed among smaller droplets, the kinetic energy of fluid droplets, with the exception of the largest droplets at highest speed, is insufficient to break the droplet into smaller droplets on impact. When hitting a nonporous surface the droplet will remain a single cohered mass with diameter determined by the surface tension of the fluid and the contact angle of the fluid with the substrate. Splashing will be more likely for a larger droplet, higher impact velocity, lower fluid surface tension, lower viscosity, or a rougher substrate. [5, 20, 21]

Section 2.4: Recent Developments in Industrial Inkjet Printing Applications

Flatbed inkjet systems have been introduced to industry within the past few years. The substrate can either be placed directly on the flatbed while the printheads move or the substrate can move relative to the printheads. Most flatbed inkjet systems use ultraviolet-curable inks and the traditional CMYK colour gamut. Some systems have begun to use opaque white, which allows the ink to be printed on substrates that are not white by first printing the opaque white coat before the remaining colours. A final varnishing coat can also be printed after the image. Again, this provides the opportunity to expand printed products to such industries as signage and furniture. [22]

Various printing component and ink suppliers such as Dimatix, Spectra, Xennia, Xaar, KonicaMinolta, and Hewlett-Packard recognise the benefits of using their technology to develop custom printing systems for applications like coding and marking, light-emitting polymers, conductive fluids, signage, addressing, decor, textiles, wall and floor coverings, and MEMS. There are some companies like Zünd and Hymmen that have further developed printing technology outside of traditional applications. It is only a matter of time before direct printing approaches the precision and repeatability necessary for MEMS fabrication.

Zünd is a company in Switzerland that specialises in flatbed printing and cutting sheet material for mass-distribution. Four colours (CMYK) and white or six colours (CMYK, light cyan, light magenta) are available for higher apparent resolution, smoother gradients, and better skin tones. White ink can be printed either before (under), after (over), or with other colours to achieve all possible optical effects, while the white density is controllable through software settings. Their systems are versatile, modular, and allow for straightforward and accurate double-sided printing and edge to edge capabilities of virtually any media in any size. This includes both uncoated rigid and flexible materials, smooth, uneven, or perforated surfaces, and boards, sheets, or rolled materials such as plexiglass, wood, cardboard, glass, metal, polyester, polycarbonate, polystyrene, PVC, perforated plates, fabrics, mesh, stone, foamboard, wallpaper, canvas, ceramics, leather, cork, aluminum, and vinyl. Applications include indoor/outdoor signage, advertising and decorations, posters, exhibition and stage graphics, banners, flags, billboards, vehicle graphics, furniture, architecture, and showrooms. The UV ink system is environmentally friendly and free from any solvents (VOC), outdoor durable with excellent colour vibrancy, and shows good adhesion to a wide variety of materials, economical in use, and has minimal startup time. Print materials can be up to 40 mm thick, 2150 mm wide, and have unlimited length. Maximum resolution is 360 DPI at a print speed of 38 m^2/h (typically 7 – 20 m^2/h). Ink consumption is about 80 m^2/L. Zünd is capable of plotting, cutting, milling, and engraving at a maximum 10 mm depth for soft materials and 2 mm for hard materials, with a foam cutter at 1-1000 mm/sec speed, +/- 0.02 mm

repeatability, 30 mm material clearance, max feed speed of 250 mm/sec, feed accuracy of +/-0.1 mm; and 0.005 mm measuring system resolution. A vacuum table is used for material fixation. [23]

Hymmen is another company that provides surface finishing of board (MDF, particle, etc.) or roll material and the production of decorative and technical laminates. They develop, manufacture, and distribute machinery and lines such as their DecoPrint coating line (DPR). The decor printing machine is a fast and economic alternative to laminating of decor paper, for the printing of wood and fantasy decors onto veneer and wooden work pieces. A water-based (environmentally friendly) ink, water-based varnishes, and UV build-up are used. The process typically consists of several steps, beginning with a dry base coat, followed by base colour, print, corundum, varnish for smoothness and hardness, counter-coating, and ending with lacquering. The final hardness layer creates a pore structure. Hymmen is the first company to successfully produce printed laminate flooring, using Xaar 1001 printheads for their Jupiter line. However, there is still a long way to go based on easy handling, adequate production performance, and high surface quality. Decorative finishes are done in film or melamine resin impregnated paper to MDF or particleboard. The finishes are similar to natural wood in appearance and can be superior in terms of durability and damage resistance. Line speeds range from 167 to 2000 mm/sec and include roll press for boards, foils, and glue. DPR flooring is up to 20% quieter than traditional laminate flooring and a uniform product structure prevents stresses in the floor. This flooring also remains more stable during temperature changes (i.e. heating in winter). [24, 25, 26]

The Hymmen GmbH digital printing machine (DGP) relies on very sensitive deposition control (dosing) of the ink output leading to an equally precise printing image. It consists of a single-pass printing station, an ink supply, a conveyor system, and a drying module. This setup relies on the material to be printed being positioned on a transport slide that passes under fixed printing heads, allowing a substrate to be printed across the double width of the printing zone in two steps. Small differences in the dot size provide subtle grey shades, which in conjunction with low ink consumption keep operating costs low. Xaar 1001 printheads feature a resolution of 360 DPI (binary vs. greyscale nearly triples optical resolution), low sensitivity to contamination of printing station, minimum risk of blockage of ink nozzles, and insensitivity to vibrations and crashes. Hymmen discusses a gravure process which contains inaccuracies due to tolerances in the wood panel, different pressures of the application rollers, differences in velocity between printing machines, and process and machinery related tolerances. [1, 24, 25, 26]

Section 2.5: Conclusions

The basic principles of printing have been investigated thoroughly by many, such as the characteristics of droplet formation, colour, and motion control. However, the theory of droplet generation is still not exact and the specific concept of printing integrated manufacturing is still a relatively new area of research that has not been widely explored. Given the proprietary and commercial nature of the printing research field, availability of literature references and publicly available documents describing the engineering design of existing systems is minimal. It is often necessary to experience much of the already established knowledge of printing firsthand in order to understand the complications of the process. Though similar technology exists, the focus of this research was to improve the results of current technology and also the machining of materials such as wood and metal. Little research has been done specifically on the combination of printing and manufacturing, likely due to the problems with noise and vibration, which could affect printhead firing and accuracy. There are numerous tolerance areas between the work piece and apparatus where inaccuracy could be introduced, such as work piece surface finish or straightness, printhead calibration, and machine structure. Dust from the air or particles from the cutting process could easily clog the nozzles and prevent the flow of ink, requiring constant cleaning and maintenance. Also, the amount of material research would be quite extensive as different substrates require different inks and methods of surface preparation.

This chapter has presented background information on inkjet printing and materials deposition technologies, introduced the terms and concepts involved, and also reviewed recent developments in both printing mechanisms and applications. As discussed, there are a number of challenges in inkjet printing. Greater understanding of the processes and quantitative parameter relationships need to be developed for modelling more accurate and reliable processes such as droplet formation, droplet impact, and drying or curing. This would allow for a more methodical approach rather than relying on trial and error testing, and could potentially lead to further miniaturisation for MEMS and nanotechnology applications. More research should be done to establish resolution, absorption, and colour interactions for different substrates and deposition materials, including the composition of the materials themselves. Faster deposition rates would encourage the use of inkjet deposition for mass-production and commercialisation. Laser-based direct printing technologies are slow to commercialise due to high hardware cost and limitations in deposition materials and substrate dimensions.

A piezoelectric inkjet system, which is used in the work described in this thesis, is well-suited for integration with the existing flatbed router due to its simpler mechanisms, ease of use, and potential for future applications requiring more sensitive deposition fluids compared to CIJ, thermal inkjet, and

laser methods. However, the minimum droplet size may limit its use for MEMS and nanotechnology development. There are several things that should be noted for the implementation of an inkjet printing system. For example, they are susceptible to dust and vibration, which are prevalent in manufacturing environments. Maintenance of the printheads includes daily wiping of the nozzle plates and occasional flushing to ensure no debris is blocking the nozzles and to remove excess ink for accurate droplet formation and positioning. Also, significant research and testing may need to be done to obtain satisfactory image results on wood substrates, most likely by using a white pre-coat. A UV system will provide better results on different substrates, though it has a higher initial hardware cost and added system complexity. It may be possible to predict the positioning error of the droplets, though the calculations would be quite complicated. Convection may be a factor depending on how quickly a droplet is ejected from the printhead and the distance between the nozzle and the substrate.

Flatbed inkjet systems similar to the work described in this thesis have been recently developed in industry. Zünd manufactures a flatbed system with specifications similar to that of the router used in this research, and can thus provide an industrial comparison in terms of tracking control. Their router is capable of a maximum feed of 250 mm/sec with a feed accuracy of +/- 0.1 mm and 0.005 mm encoder resolution. Hymmen has also successfully printed laminate flooring using MDF, Xaar 1001 printheads, and water-based ink.

Chapter 3: Design of a Flatbed Printing System

A printing system consists of a printhead, printhead drive electronics, printhead support and maintenance, ink or fluid, and substrate. Motion control hardware, electronics, and software are necessary to position the printhead and substrate relative to each other [27]. Section 3.1 reviews the selection process for these components and their functions. The design process for the addition of a printing system to an industrial flatbed router can be found in Section 3.2 and was divided into subsections for the overall system, mechanical integration, and electronics and software integration so that the reader can more easily follow the elements of the design.

The integration underwent several iterations of redesign as understanding of the system and software developed. All 3D models and sketches were created in SolidWorks 2007/2008. Components that did not have an available drawing were roughly measured and drawn in order to visualise how they fit in the design before fabricating the matching components. The design was limited to the features of the existing flatbed router as well as budget considerations and available resources. As shown in Figure 3.1, the existing setup consists of encoder measurements that get sent to a computer, which sends the trajectory commands through a dSPACE controller back to the router to control the motor positions. Conclusions for the chapter are provided in Section 3.3.

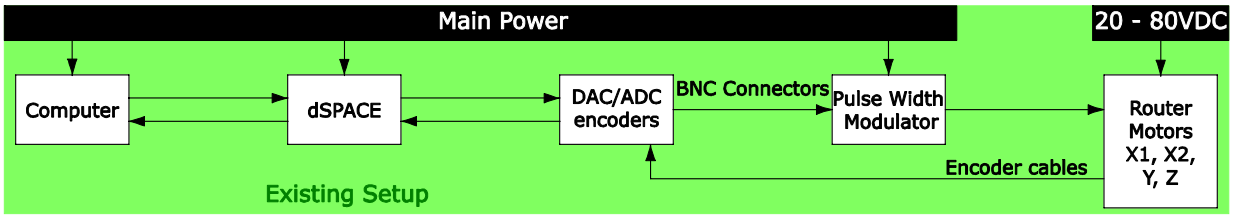

Figure 3.1: Previous System Schematic for Operation of the Router

Section 3.1: Printing Component Selection

As digital printing is application specific, no manufacturer has all the components necessary to develop a complete printing system. Printhead suppliers provide limited electronics and software together with generic application notes and technical support based on their experience [27]. Thus, the main concern was finding a system as complete as possible that could be readily assembled onto the existing machine at a reasonable cost (less than $30 000). Most companies like Xerox and Canon only offer completely assembled printers for certain applications. Other companies such as Fujifilm Dimatix, Global Inkjet Systems, Accu Automation, and Xaar sell customisable kits, which are suitable for integration with the router. However, Fujifilm Dimatix does not supply systems to small end-users or researchers and Global Inkjet Systems does not provide all the necessary components. It was also found that the system from Accu Automation was much more expensive than the Xaar system, despite the convenience of the company location in Cambridge, and offered more high-end functionality then required in the initial prototype. Thus, Xaar was chosen as the supplier for the printing system.

Xaar provides printing kits that can be readily assembled onto existing machines to fit the applications of different companies. They design various printheads and their corresponding peripherals and supply inks depending on the application. It was decided that the Xaar 126 printheads would be the best choice to start learning about the printing process due to their simple design, light weight, low cost, ease of integration, and compatibility with a variety of different ink types such as oil-based and UV-curable to allow for future modifications. Oil-based ink was selected for its absorption properties with wood, non-toxicity, and low maintenance. The Xaar 126 printheads are binary, which means that the printhead nozzles fire in two modes: on or off. As a result, the image generation and droplet formation are also slightly easier to understand than higher resolution greyscale printheads, whose droplet sizes can be variable. However, the drawbacks of its simple design are limited resolution, difficulty in alignment, susceptibility to dust and damage, and limited colour. Specifications for the Xaar 126 printheads can be found in Appendix A.

The kit came with all the components necessary for printing, except the actuation system and position encoder, which are chosen by the system designer. It included four pumps, four filters, four header tanks, four manual valves, a supply of cyan, magenta, yellow, and black ink bottles, various luer fittings, clear Teflon tubing, an ink supply controller (ISC), a printhead controller (XUSB), USB 2.0 cable, XUSB power supply, software for the XUSB and ISC, head personality card (HPC unit), two power cables, two link cables, four printhead mounting plates (not used), eight adjustment screws, four ribbon cables, and four printheads. Items that were requisitioned elsewhere include two USB 2.0 repeaters, two RS232 extension cables, extra Teflon tubing (only available in imperial measurements),

DC motor, linear actuator, linear encoder signal splitter, encoder interpolator, and the machined parts necessary to mount all the components to the router. Some 3D models of the main components can be found in Figure 3.2.

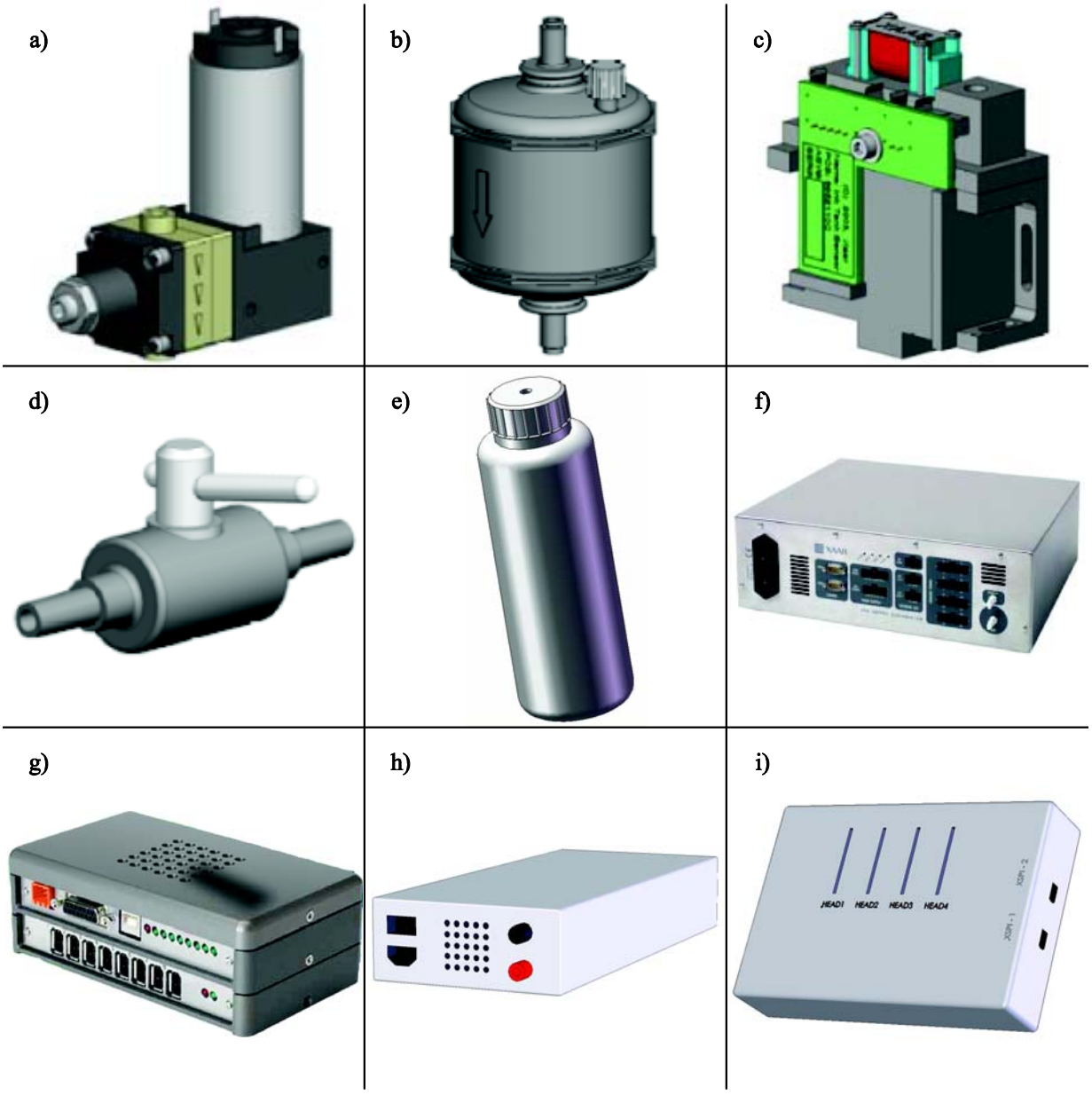

Figure 3.2: Main Ink System Components - Not to scale, a) Pump, b) Filter, c) Header Tank, d) Manual Valve, e) Ink Supply Bottle, f) Ink Supply Controller, g) XUSB, h) XUSB Power Supply, i) Head Personality Card Unit. Courtesy of Xaar [28]

An XJ-126 printhead, shown in Figure 3.3, has 126 functional nozzles. The resolution of the image depends on the angle at which the printheads are mounted, though the software only handles specific angles corresponding to 200, 309, and 360DPI. Angles can be fine-tuned with the adjustment screws that hold the printhead chassis in place, which also acts as a cooling surface for heat generated by the printhead driver chips. Four printheads are necessary for colour printing, one each for Cyan, Magenta, Yellow, and Black inks. Ink enters the printhead through the inlet port, while the normally plugged outlet port is used for the initial filling of the printhead to remove air inside the printhead and for purging the printhead for storage. A serial number identifies each printhead so that a nozzle firing efficiency factor can be applied through software. Mechanical variations due to manufacturing will cause variance in efficiency factor values, which are used with temperature compensation to achieve the specified average drop speed. The ribbon cable powers the printhead and sends the image information from the XUSB software corresponding to which nozzles should fire at a specific time. Physical contact with the nozzle plate should be avoided to prevent damaging the nozzles.

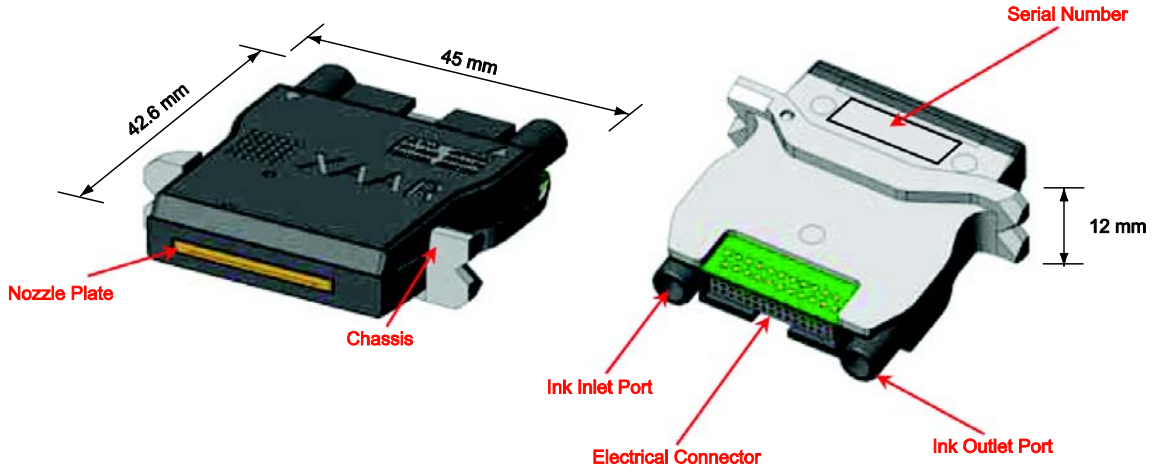

Figure 3.3: Xaar 126 Printhead - Courtesy of Xaar. [28]

Each printhead has its own header tank, which should be centred above the printhead inlet as close as possible to minimise tube length and pressure variations between the printhead and header tank (Figure 3.4). The ink supply controller controls the vacuum and the pumps, which provide ink from the supply bottles to the header tanks. Negative vacuum pressure maintains a thin film of ink on the nozzle plate for reliable printing and is based on printhead size, ink properties, and the height of the header tanks above the printheads. If the pressure is too high, then the ink will flow toward the vacuum. Conversely, if the pressure is too low, then the ink will leak out through the nozzles. This pressure was determined by trial and error. Waveforms defined in the XUSB software are applied to the piezoelectric wall to produce a pressure wave in the channel, which can control the droplet size. However, they are

tuned for the specific printhead and ink for optimal droplet formation to prevent issues such as satellite droplets. The print frequency of any specific printhead or waveform is dependent on the number of grey levels and the sample clock value. Since the printheads are binary, there is only one grey level. Thus, any attempt to overdrive the printhead would result in undefined behaviour of the XUSB and/or printhead [28]. Filters between the ink bottles and the pumps prevent particles from entering the printhead and blocking the nozzles. The Teflon tubing connecting all these components has an outer diameter of 4 mm and an inner diameter of 3 mm.

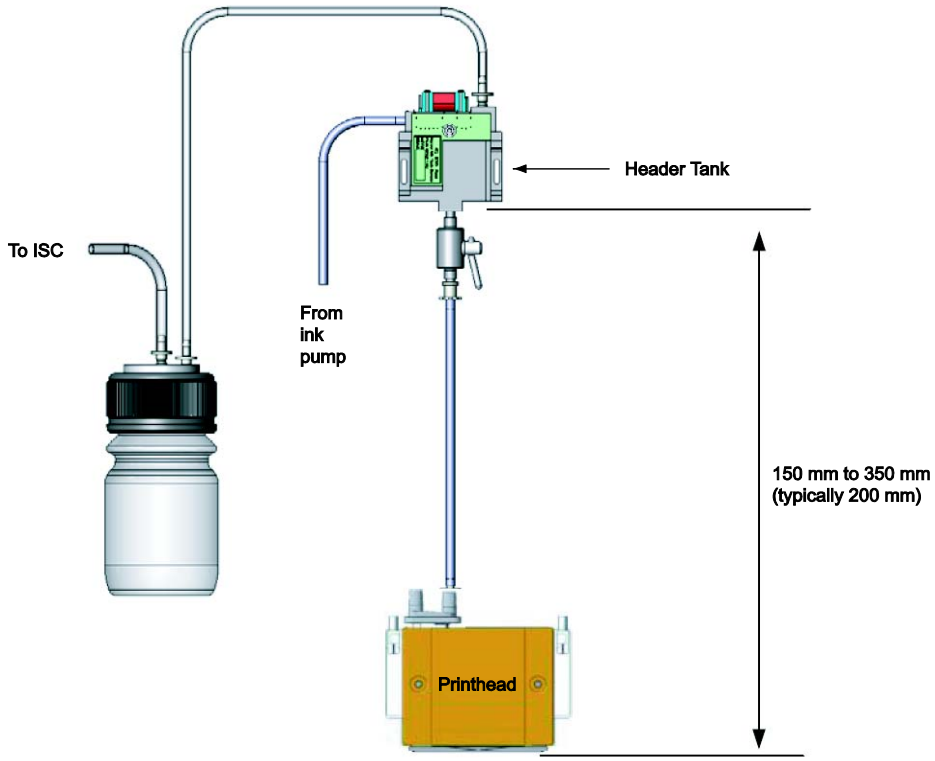

Figure 3.4: Printhead and Header Tank Assembly With Ink Trap Bottle - Courtesy of Xaar. [28]

While printing, the printheads need to be positioned 1 mm above the substrate, which can be of varying thickness. Since a height of 1 mm above the substrate is the optimal position there is no specific tolerance, as anything less than or greater than 1 mm will degrade the image in terms of droplet positioning accuracy and aesthetics. This required the design of a secondary z-axis that can be controlled separately from the spindle axis. In order to differentiate them, the spindle axis is designated as Z1 and the axis for the printhead mount is Z2. The Z2 axis consists of an actuator with at least 7" of vertical travel length, a motor capable of carrying a minimum estimated load of 3 kg and a positioning speed of 38 mm/sec or higher, a rotary encoder with resolution less than 10 µm of equivalent linear motion, bearings for the gantry guideway, an amplifier, a motor power supply, and a budget of $3000

CAD [29]. It was also desirable to minimise the width of the drive system, since its addition to the gantry will reduce work area where both the printheads and spindle can reach. The spindle can no longer travel to the far left of the gantry, the printhead cannot access the far right, and the distance between printheads also limits the working area since the Black printhead will not be able to reach the same position as the Cyan printhead.

A ball-screw drive was chosen for its high efficiency, speed, duty cycle, tool life, accuracy, and repeatability, as well as constant backlash. A LinTech Series 130 linear stage was selected, having a precision grade ball-screw of 0.625" diameter with 0.2" (5.08 mm) lead and a maximum travel length of 8", along with a DC servo motor and rotary encoder. The negatives of this design are that it is easily back-driven and the price is higher for an increase in speed compared to other options such as a belt and pulley. It was indeed found that earlier self-locking calculations for the DC servo motor based on the weight of 3 kg and safety factor of 5 were correct. Based on the SolidWorks model, the total weight of the assembly is approximately 5 kg. However, when the motor is powered off the ball-screw is easily back-driven due to the weight on the assembly, which causes an issue when developing the homing routine in Section 4.4. The electrical motor brake was ineffective in holding the ball-screw in place for situations where the router is turned on and no control signals are being sent to the motor. The rotary encoder with quadrature is capable of 4000 counts per revolution. There is no pulley system in the Z2 axis, so the motor directly controls the ball-screw. Thus, given the lead of the ball-screw, the resolution of the encoder is 5.08 mm/rev divided by 4000 counts/rev, which is 1.27 μm. [29]

Section 3.2: System Integration

Figure 3.5 shows the overall system schematic for retrofitting the router with printing capability using the components discussed in Section 3.1. While each area can be loosely separated into controls, fluid, software, electrical, and mechanical assemblies, establishing communication between components and conversion of signal formats is important. The XUSB receives the linear encoder position from the y-axis to determine the print frequency of droplets, and also controls which printheads should be firing based on information from the computer. The ISC monitors the pressure readings from the header tanks to ensure that the correct vacuum pressure is constantly applied.

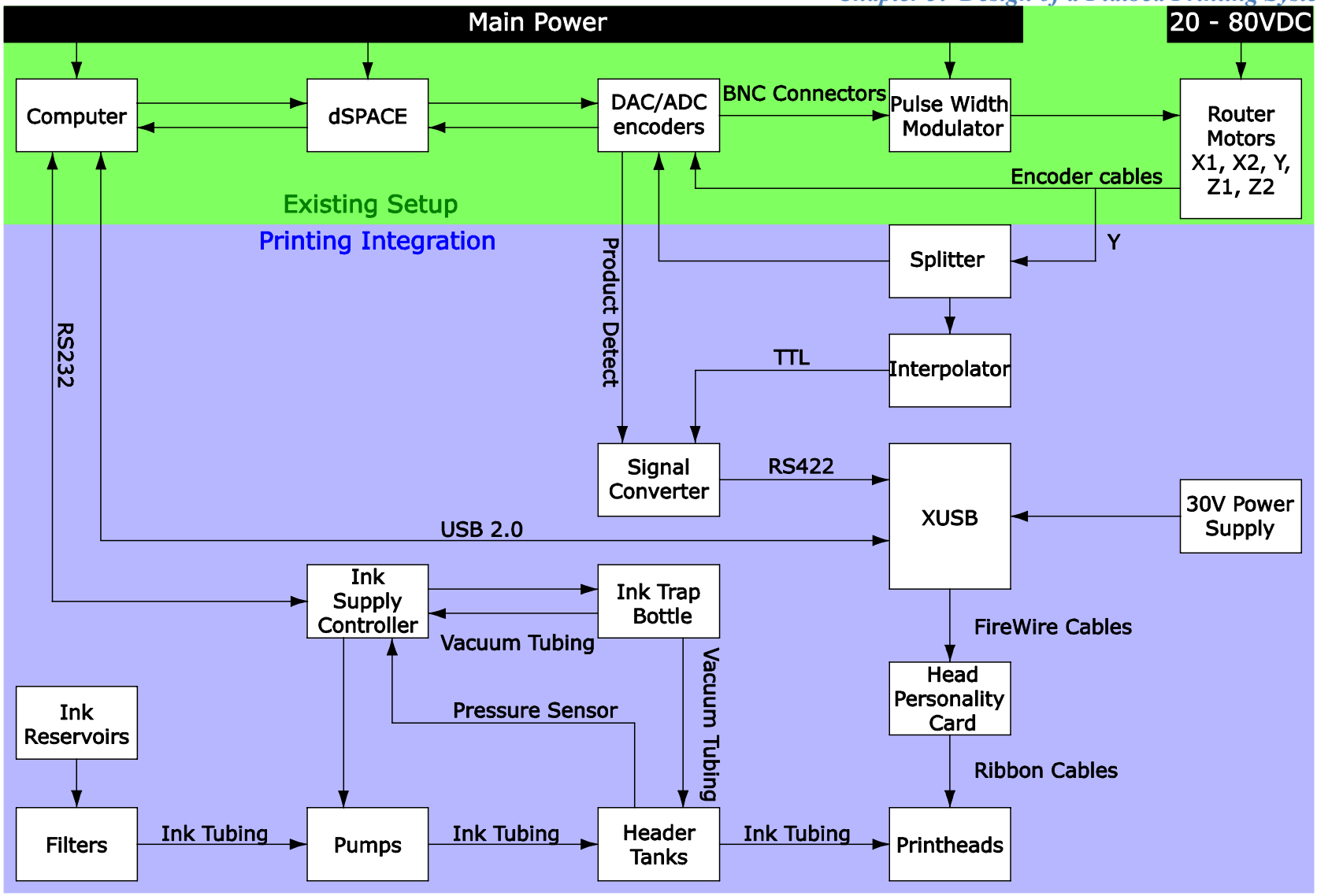

Figure 3.5: Overall System Schematic for Operation of Printing System

Section 3.2.1: Mechanical Integration

The back of the linear stage was attached to a metal plate, which was constructed to fasten to two bearings along the lower and upper y-axis guideways. Couplings were made to connect the new Z2 axis to the spindle assembly so that when the spindle assembly is driven across the y-axis the Z2 axis is also pushed alongside. Next, the mounting assembly was designed for the four printheads and the components that require close proximity to the printheads, which include four header tanks, the ink trap bottle, and the Head Personality Card (HPC) unit. The position of the HPC unit was limited by the length of the ribbon cables, though its cooling fan makes it susceptible to chips and dust from machining. When designing the plate to hold the printheads, there were several factors to consider. The distance between printheads should be minimized to reduce droplet placement errors as a result of substrate stretch and velocity variation over the time and distance between the first and last printheads. However, the distance between printheads was slightly constrained by the size of the header tanks, since it is necessary to have the printhead inlet positioned directly below the header tank to reduce fluid pressure losses. Component positions were also designed keeping in mind that tubing lengths should be minimized to avoid fluid pressure losses.

For the printheads to print at a specific resolution they must be angled with respect to the printing direction. Figure 3.6 shows how an angle of 36.9° produces a resolution of 309 DPI, which was recommended by Xaar even though a resolution of 360 DPI was also available. However, there are numerous discrepancies in the Xaar manual which have an effect on the calculation of the angle at which the printhead should be placed and the displacement in the x-direction from swath to swath. At one point, the manual mentions the angle of the printhead should be 36.9°, while the swath width is 10.3 mm. The manual also gives the distance from the first nozzle to the last nozzle as 17.2 mm, whereas the technical documentation obtained from the Xaar website states this distance as 17.1 mm. A resolution of 300 DPI was written in the manual, though this value was ignored as the resolution in the XUSB software is shown as 309 DPI. When the angles and travel distances from swath to swath are calculated based on the different combinations of parameters, the results range from 36.7867° to 37.2784° and 10.3421 mm to 10.4401 mm, respectively. Appendix B shows the detailed calculations for each variation.

Though the mechanical calibration can compensate for the angle to produce a straight image, the variations have an influence over how far the x-axis should travel from swath to swath. It also adds difficulty in analyzing the results, since it would not be known whether errors are due to the printhead angle or the trajectory. Based on these calculations it was determined that the parameters given in the manual yield values in the middle of each range, so a swath travel distance of 10.41 mm and printhead

angle of 36.9° were used in the trajectory generation, the design for the bottom mounting plate, and later in the design of a new mounting plate for bidirectional printing. Figure 3.7 shows the SolidWorks model for the bottom mounting plate. The rectangular holes are larger than the printhead, such that, without the adjustment screws and thrust pin, the printhead is free to move.

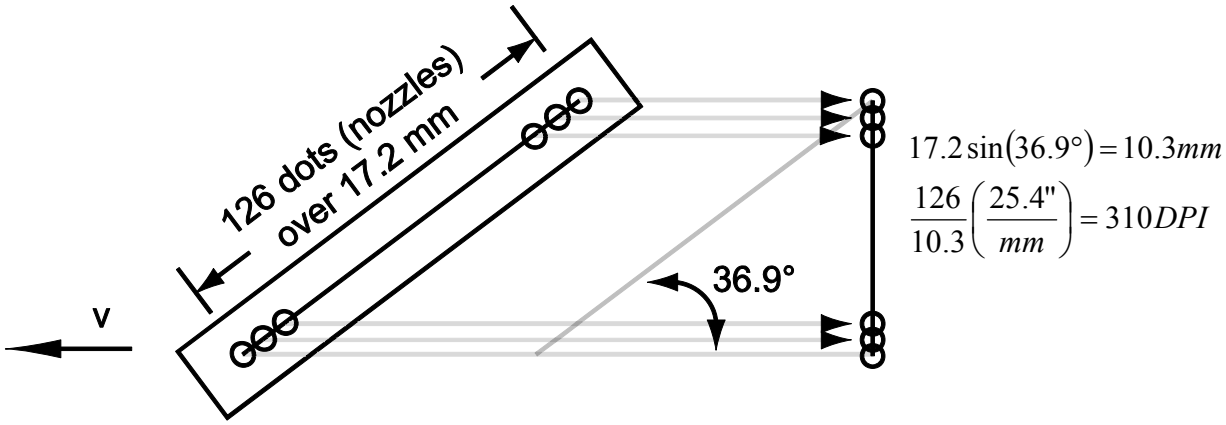

Figure 3.6: Demonstration of How the Alignment Angle Generates 309 DPI

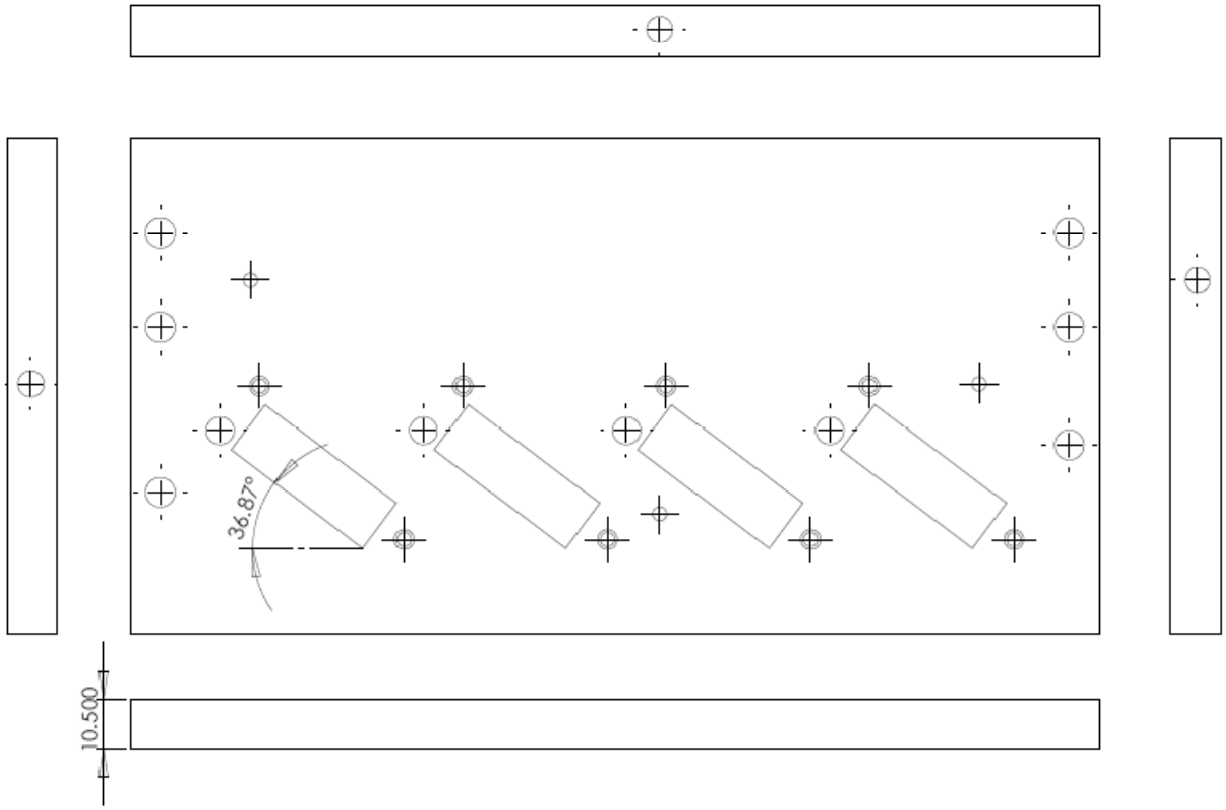

Figure 3.7: Bottom Mounting Plate- plate thickness was later changed to 10.3 mm to avoid smearing rough surfaces; the angle of 36.87° was also found to be an inaccurate representation for 36.9°.

Since the angle of the printheads is crucial, the bottom plate was CNC machined whereas the other plates were done with a manual mill. A cover was made out of sheet metal for the bottom plate to protect the nozzle plates from dust and damage while the printheads are not in operation, especially when the spindle is in operation. It was also necessary to ensure that the bottom plate is as level as possible over the surface of the substrate. Thus, the bottom plate was mounted to the vertical plate using carefully machined triangular supports at 90°. To verify that the bottom plate was level within ±0.1 mm, a dial gauge was placed along the bottom while the y-axis was slowly jogged back and forth. It should be noted that this is a very rough measure of alignment since the design of the router itself does not use dowel pins or other methods of calibration. Figure 3.8 shows the final printhead mounting assembly attached to the router.

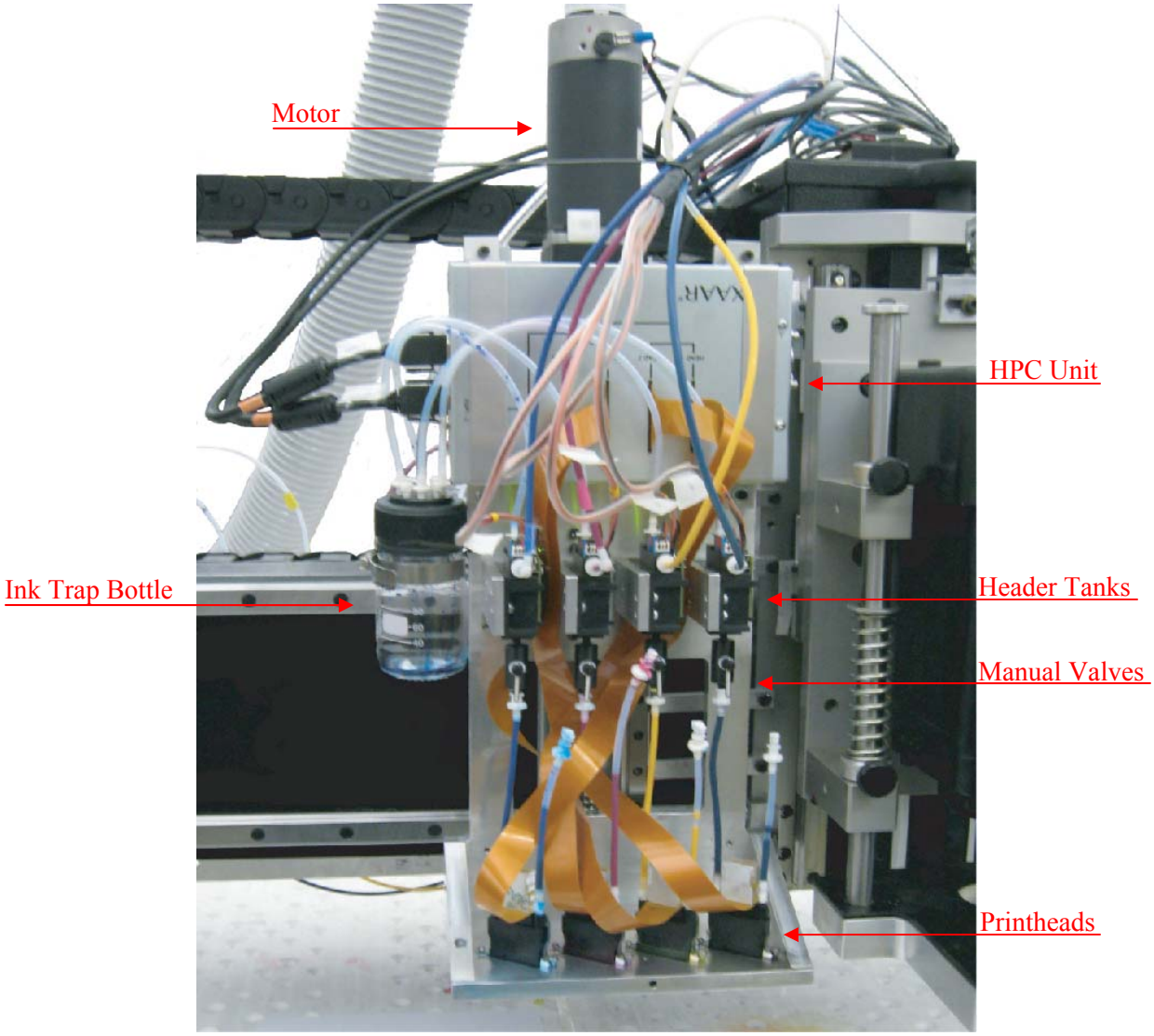

Figure 3.8: Printhead Mount

Positioning of components such as the ISC and XUSB were limited due to the lengths of the cables and tubing, which were fed through the existing cable tracks. Thus, it was also necessary for the XUSB to move along with the gantry. The XUSB was assembled to the right side of the gantry, while two USB repeaters were used to extend the 5.0 m connection between the XUSB and the computer. The cables from the XUSB to its power supply were extended so that the power supply could be placed stationary underneath the cable track on the right side of the router. To minimise tubing length, the ink supply bottles, pumps, and filters were attached to the back of the gantry; symmetrically to avoid putting an uneven distribution of weight on the gantry, which could affect positioning accuracy. It was still necessary to obtain extra Teflon tubing of 1/8" ID and 5/32" OD. Two RS232 extension cables were used to connect the ISC, located at the lower left-hand side of the router, to the computer, at a distance greater than the original 10 ft cable. An extension was also made for the cables between the header tanks and the ISC. Since the length of the vacuum tubing that needed to reach from the ISC to the ink trap bottle was greater than the 4 m of tubing supplied by Xaar, though less than the 10 m maximum length, clear PVC tubing of 1/8" ID and 1/4" OD was obtained. Teflon tubing for reduced friction and wettability was not necessary as the vacuum tubing should only transport air. The power supply for the Z2 motor was placed inside the front panel of the router and the amplifier was set on top of the spindle motor housing. Close-ups of the assemblies are found in Figure 3.9 and the final integrated system is shown in Figure 3.10.

In addition to the physical integration with the router, there are a number of steps that must be carried out for the general maintenance of the printing system. Before starting to print, the printhead nozzle plates need to be gently wiped clean of dust and excess ink with a lint-free swab or wipe. As an extra precaution, the printheads should be purged before wiping, which is a pressure applied to the ink so that the ink flows freely and is activated through software. However, purging was often found to be unnecessary unless the printheads have been inactive for one day or longer. Wiping should be done in one direction only along the nozzles, swabs should not be reused, and extra care should be taken to ensure that the colours do not mix from one printhead to another, as it is difficult to remove the mixed colours. If a nozzle appears to be blocked by a particle during print, which cannot be wiped away, then a purge should be done. Soaking a swab in cleaning solution before wiping the printhead, or as a last resort, flushing the entire printhead with cleaning solution may be necessary. Otherwise, it is likely that the nozzle may have been damaged and the printhead must be replaced.

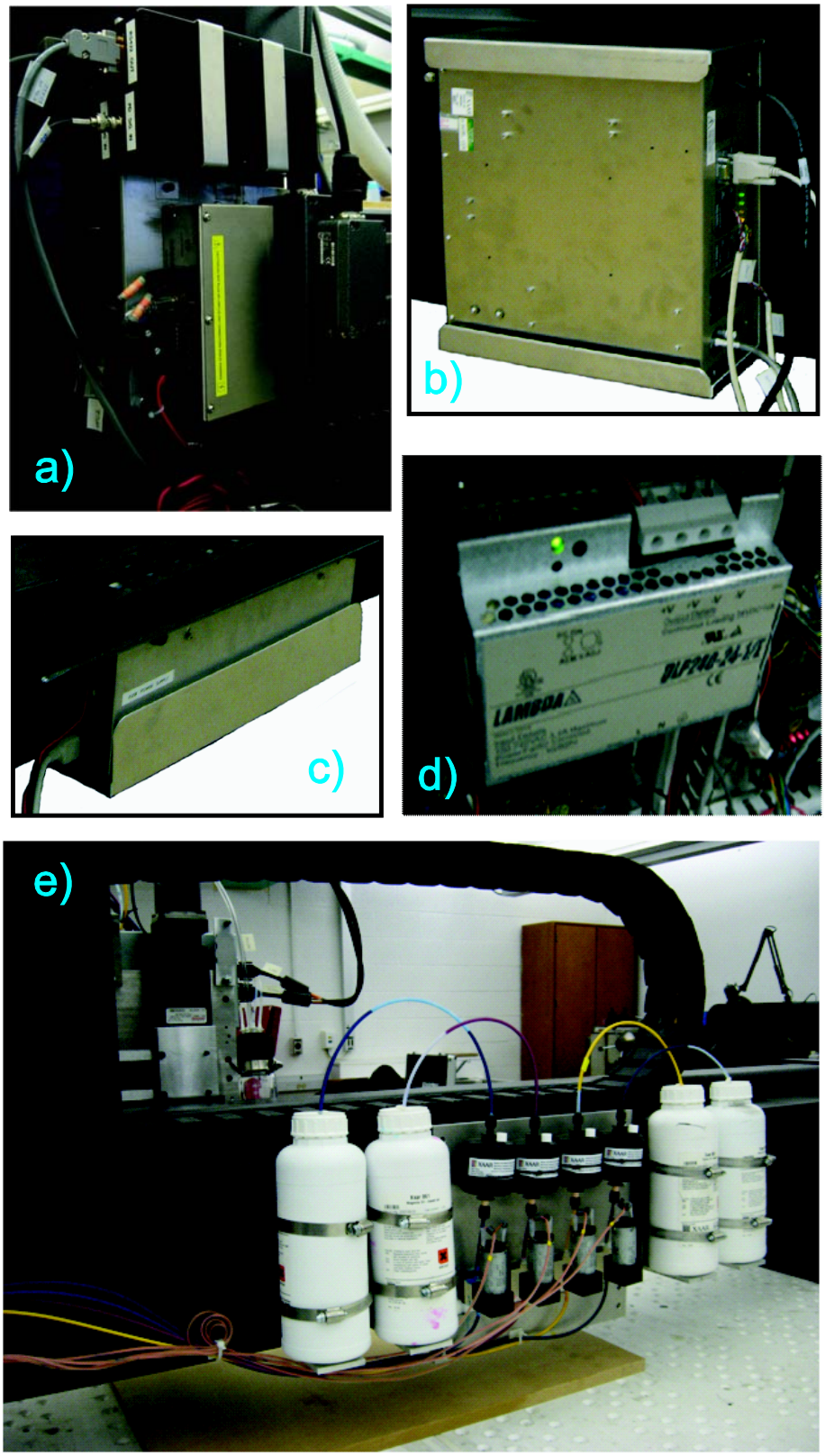

Figure 3.9: Additional Mechanical Integration - a) TTL to RS422 signal converter (black box), XUSB (middle), and Heidenhain interpolation electronics (right), b) ISC, c) XUSB power supply, d) Z2 motor power supply, e) Ink supply tanks with filters and pumps.

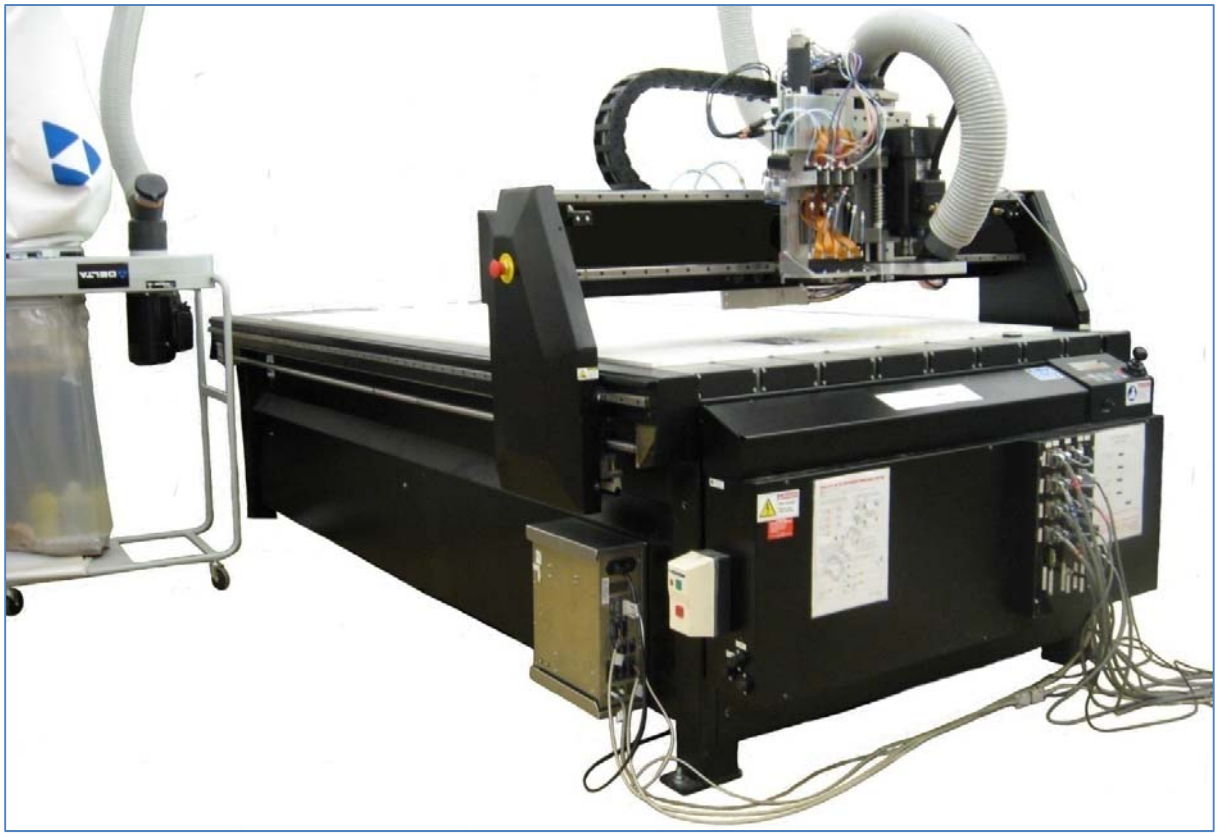

Figure 3.10: Router After Ink System Modifications

It was also found that the printheads would leak after long periods of inactivity. It is believed that this was a result of small leaks between the Teflon tubing and luer fittings, possibly due to the larger inner diameter tubing. If a purge tube is empty, then the printhead may need to be refilled, since allowing air to be pushed through the nozzles could damage the printhead. After printing, and especially when machining, the cover plate should be placed over the bottom of the printhead mount to protect it from chips and dust. The manual valves must always be closed before the ink supply controller is turned off, otherwise there will be no vacuum and the ink will flow freely out of the printheads. The ink level of the supply bottles should also be manually checked on occasion and replaced if necessary.

Incorporating a UV printing system involves the use of black, UV-light filtering tubing, flushing the ink from the system and replacing it with a UV-curable ink, and integrating a UV-curing lamp. Though this addition seems conceptually simple, there would be added complexity in determining light intensity and duration of cure settings for different inks and substrates. It would also be prudent to enclose the entire machine in an area free of UV light to prevent curing of the ink meniscus on the nozzles, accidental spills, or leakages.

Section 3.2.2: Electronics and Software Integration

The XUSB requires an encoder to determine the firing frequency of the printheads based on their position. A linear encoder was used since it provides a much higher resolution and accuracy than rotary encoder readings. Since it was also desirable to use the linear encoder for controller feedback, a splitter was made to feed one of the linear encoder signals to the dSPACE and the other to the XUSB. Originally, an interpolator was made to convert the y-axis linear encoder sinusoidal signal into TTL signals that the XUSB can read, as well as passing along the PD signal. However, it was thought that the makeshift converter added error to the analog signals and thus a splitter with an additional 2-fold increase in resolution was purchased from Heidenhain, along with an interpolator to increase the resolution of the signal sent to the XUSB by 10-fold. With quadrature encoding as well, the XUSB would then see an encoder resolution of 0.25 µm. [30]

The Xaar 126 printheads are binary, meaning that the nozzles can only be turned on or off and one pixel of an image represents one droplet from a single nozzle. However, most computer-generated images and real photos are made in greyscale, where the droplet size of the ink would need to be controlled. Thus, greyscale images must be converted to binary (bitmap) images of 309 DPI, which generally means a decrease in image resolution and quality. Diffusion dithering was used to convert the images, and although there may be other methods that would result in better image quality, they were not investigated here [31, 32]. The binary nature of the printheads also means that more bleeding will occur in dark images since the droplet size cannot be controlled. In printing, the absence of ink is considered white and the combination of all colours is black. In order to reduce bleeding, the colour levels are adjusted to preserve the lighter areas of the image, while making darker areas appear lighter. Thus, darker images will need to be lightened more in a graphics editor than lighter images (Photoshop was used for this thesis work). Since each printhead represents one of the C, M, Y, and K colours, the image must also be separated into the four images corresponding to each colour. In the XUSB software, the image swaths need to be angled according to the angle of the printheads, otherwise the image will be slanted. Figures and actual order of steps from the image conversion process can be found in Appendix C, along with the operation of the printing system.

MATLAB software is used to program the print trajectory and controller and is discussed in further detail in Chapter 4. A Product Detect (PD) signal is essential to notify the XUSB when to start each swath of print, which should be at precisely the exact same position along the y-axis. It is developed alongside the trajectory and is a single, short pulse that lasts at least 2 µsec on rising edge detection, sent to the XUSB once the y-axis motion acceleration has stopped. If the pulse is too long (i.e. longer than what it would take to print one swath of the image), then the next swath will continue

to print beside the previous swath. Likewise, if the pulse is too short, then the print will not start. PD signals that are not given at the precise location will result in jagged images due to swath misalignment. In bidirectional printing, a single PD (1PD) method can be used, which relies on the XUSB to determine where to start the reverse print, or a two PD method (2PD) can be used, which is dependent on the trajectory to generate a PD for both the forward and reverse swath. Section 4.4 will show how the PD signal behaves corresponding to both unidirectional and bidirectional trajectories (the PD signal the XUSB actually sees will be inverted). A separate cable for the PD signal was sent to a converter in order to change the PD signal into an RS422 signal that is readable by the XUSB hardware. The MATLAB program should be manually operated in conjunction with the XUSB software. Currently the print area is limited by the dSPACE memory in which large trajectories will cause an error. It is believed that if the recorded values are removed and since the trajectory from swath to swath is highly repetitive, then a repeating Simulink block instead of a large trajectory matrix could be used to reduce the amount of memory utilised.

Section 3.3: Conclusions

This chapter has presented the integration of printing capability onto a flatbed router to combine printing and machining into one system. The Xaar 126 printing system was chosen for its simple design, low cost, ease of integration, and potential for future research by using different inks. The disadvantages of this system are limited resolution and colour, difficulty in alignment, and vulnerability to dust and damage. The printhead operation is binary and no greyscale is possible. Nevertheless, the Xaar 126 printing system was deemed suitable for developing the first proof of concept prototype. Daily maintenance is necessary, which includes purging and wiping excess ink and particles from the nozzles.

Following the selection of printing technology components, the mechanical, electrical, and software integration issues were discussed. Some of the shortcomings of the design are the reduction of useable table area for both cutting and printing, the secondary z-axis motor being susceptible to back-driving due to the amount of weight from the printhead mount, the substrate being limited to flat surfaces, and limited trajectory size with the current controller implementation. For future studies, the motor for the secondary z-axis should be resized, the substrate surface should be level, and the work area could be enlarged by minimising the mechanical assembly of the spindle and printhead mount and by reducing memory usage in the dSPACE controller. Nonetheless, the proposed design is useful as a prototype for investigating new printing integrated manufacturing technologies, in particular for furniture, wood products, and signage industries.

UV printing capability can also be achieved by upgrading the tubing to black, UV filtering tubing, flushing the ink from the system and replacing it with a UV-curable ink, and integrating a UV-curing lamp. Print quality would also be improved with better printheads, such as the Xaar 1001, which feature easier calibration, greyscale droplet size variation, and lower maintenance due to a self-cleaning through-flow system that reduces nozzle blockage. Since this project was the pilot study, the focus has been limited to oil-based inks, which are relatively easier to work with than other fluids. In the following chapters, implementation and characterisation of the proposed printing system will be discussed.

Chapter 4: Servo System Design

Positioning accuracy is one of the most crucial requirements in developing a printing system, evident in three main areas: individual droplet positioning, swath-to-swath displacement, and start and end position alignment. First, printhead motion must follow the commanded trajectory with precision for the droplets within each swath to fall in their correct locations. Droplets that are too close together may result in dot merging or bleeding, leading to reduced image sharpness, while droplets that are too far apart may result in voids or distortions that can also diminish image features (particularly for solid lines). Next, each swath must be printed directly below the previous swath to prevent visible gaps or overlapping lines across the image in the y-direction (longitudinal). The ideal swath-to-swath distance travelled along the x-axis is equivalent to the width of the swath plus the distance between two successive dots. Finally, the starting (home) and ending positions of each swath must be aligned in the same location along the y-axis every time; otherwise, the image may have jagged edges or entire swaths appear shifted horizontally, creating a discontinuous image.

The flaws produced by not correctly achieving any one of these positioning elements are easily detectable by the human eye. The common keys to each issue are accurate positioning control and smooth trajectory generation. Unsmooth motion, shock, or vibration could affect the image, appearing as light and dark bands caused by pressure fluctuations and stitching errors [28]. Droplet positioning accuracy is also extremely important for future applications in areas such as MEMS fabrication, where features may require nanometre-scale accuracy. Similarly, the key elements of positioning accuracy translate to the milling process, consequently leading to rough or distorted surfaces from machining if they are not achieved adequately. In order to engrave features out of a printed image or cut out the printed image from a larger work piece, good positioning accuracy is needed to align the shape of the cut with the printed image.

Both printing and milling processes require a combination of physical adjustment (hardware) and controller tuning (software). With respect to physical modification to reduce environmental noise, design changes to the system could be made, such as stiffening the machine by strengthening couplings and frames and using shorter or larger diameter ball-screw shafts. This would increase the system spring constant, thereby raising the resonant frequency. Thus, bandwidth could also be increased, allowing the servo system to be more stable at higher frequencies. As physical adjustments can be costly, time-consuming, or difficult to assess, they are not covered in this research. The goal in this chapter is to improve the accuracy of an existing, commercially available machine using control theory.

The following sections describe the steps taken in order to achieve accurate motion control of the printheads. Section 4.1 discusses the implementation of a Sliding Mode Controller (SMC) used for the x-axes. Swath-to-swath alignment is mainly controlled by the SMC. The motion controller was developed in computational programming software, MATLAB, along with its modelling software, Simulink. Section 4.2 explains the process used to accurately identify the natural resonance of the system in order to develop a loop-shaping controller presented in Section 4.3 for improved motion tracking in the y-axis, which is the main mechanism in determining the positioning accuracy of droplets along a swath. Frequency response functions (FRFs) and sensitivity plots are used to evaluate the stability and bandwidth of the servo system. Section 4.4 provides the trajectory generation methods used to maintain smooth motion, as well as a homing routine for the secondary z-axis. As mentioned in Section 3.2.2, the Product Detect (PD) signal indicates when to start printing based on the position trajectory. This is followed by the conclusions in Section 4.5.

Section 4.1: Sliding Mode Controller Design

Sliding Mode Control (SMC) was first implemented for improved tracking control over the basic internal controller supplied with the router. SMC has inherent feed-forward and integral control action for improved tracking and disturbance rejection, and is as straightforward to tune as a simple PID controller. The concept is based on keeping the system states on a sliding surface (i.e. stable differential equation), so that their errors converge to zero as determined by the roots of the surface. Only rigid body dynamics are considered and the unknown disturbance is adapted for. The control signal for the sliding surface σ is given by the following equation [33]:

$$u_{smc} = K_s\sigma + \hat{m}\left[\ddot{x}_{ref} + \lambda\left(\dot{x}_{ref} - \dot{x}\right)\right] + \hat{b}\dot{x} + \hat{d} \tag{6}$$

Above, $\hat{b}$ is the viscous damping estimate [V/(mm/sec)], $\hat{d}$ is the disturbance estimate [V], $\hat{m}$ is the mass estimate [V/(mm/sec^2)], K_s is the feedback gain [V/(mm/sec)], and λ is the sliding surface bandwidth [rad/sec]. The following equations provide the disturbance estimate and sliding surface definition, where ρ is the adaptation gain [V/mm]:

$$\hat{d} = \rho\left(x_{ref} - x\right) + \rho\lambda\int_0^t\left(x_{ref} - x\right)dt \tag{7}$$

$$\sigma = \left(\dot{x}_{ref} - \dot{x}\right) + \lambda\left(x_{ref} - x\right) \tag{8}$$

The PID control equivalent proportional K_p, integral K_i, and derivative K_d terms appear as:

$$K_p = K_s\lambda + \rho \tag{9}$$

$$K_i = \rho\lambda \tag{10}$$

$$K_d = K_s + \hat{m}\lambda - \hat{b} \tag{11}$$

The resulting control model with feed-forward inertia, viscous damping, and friction compensation can be seen in Figure 4.1. The mass and viscous damping terms of the drives were determined by least squares identification. Effectively, the proportional control applies a control signal proportional to the error, the integral term adds disturbance adaptation (removes steady-state error), and the derivative gain will reduce oscillations and help achieve stability. For a more responsive system, λ, K_s, and ρ should be increased. However, if λ, K_s, and ρ are too large, then the system becomes too sensitive to noise and unmodelled dynamics, and turns unstable. [33]

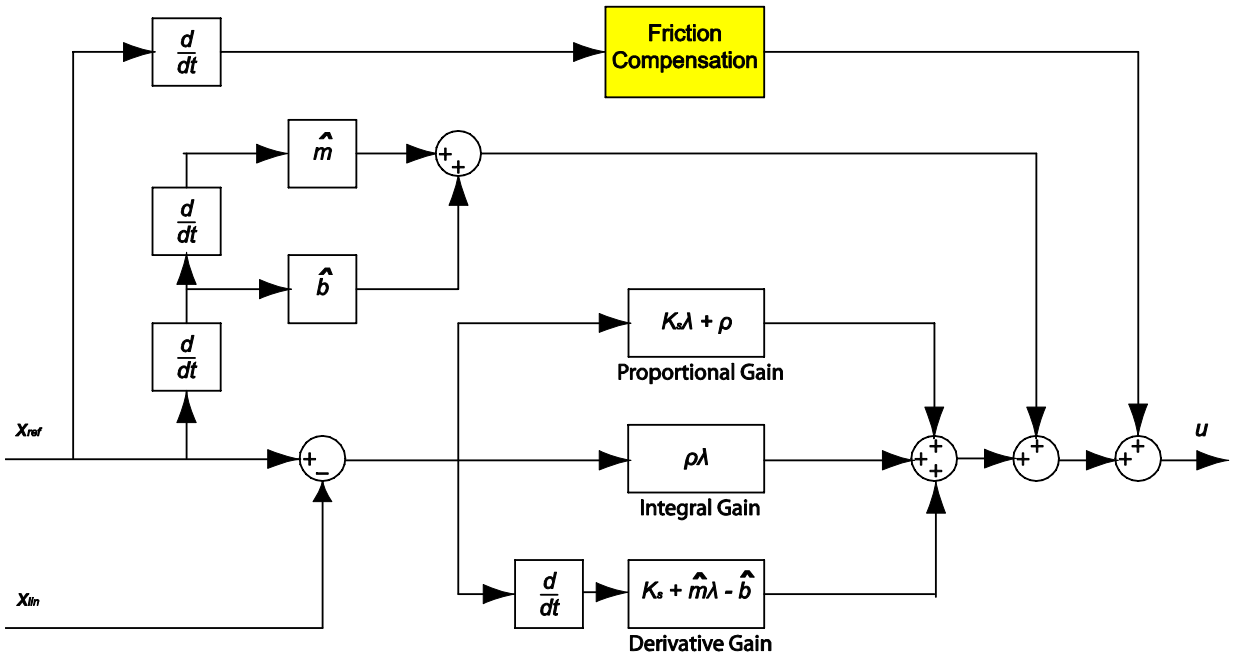

Figure 4.1: Structure of SMC Implementation

SMC works well for rotary encoder feedback. However, it is more desirable to rely on linear encoder feedback since the rotary encoder is attached to the motor, which means it can only measure relative position through the pulley and lead-screw. Thus, the rotary encoder does not directly measure the position at the point of interest. On the other hand, the linear encoder registers significant phase lag between the motor input and the translational motion, which can make it difficult to develop a stable controller. The ball-screw also acts as a spring-damper system, which means that any vibrations that occur would be more accurately observed by the absolute linear encoder rather than the rotary encoder. The added phase lag and sensitivity of the linear encoder to vibrations makes it much harder to tune the SMC when using linear encoder feedback since SMC is based on rigid-body dynamics. Figure 4.2 shows the results for the SMC at 250 mm/sec along the y-axis using rotary feedback with maximum tracking error of 80.75 µm. A piecewise constant jerk trajectory was used, as mentioned in Section 4.4, with maximum acceleration and deceleration magnitude of 500 mm/sec^2 and maximum jerk of 25 000 mm/sec^3. Although the feedback loop was closed using the rotary encoder, the tracking error was evaluated using the linear encoder. These tracking error results will be compared to the results of the loop-shaping controller in Section 4.3.

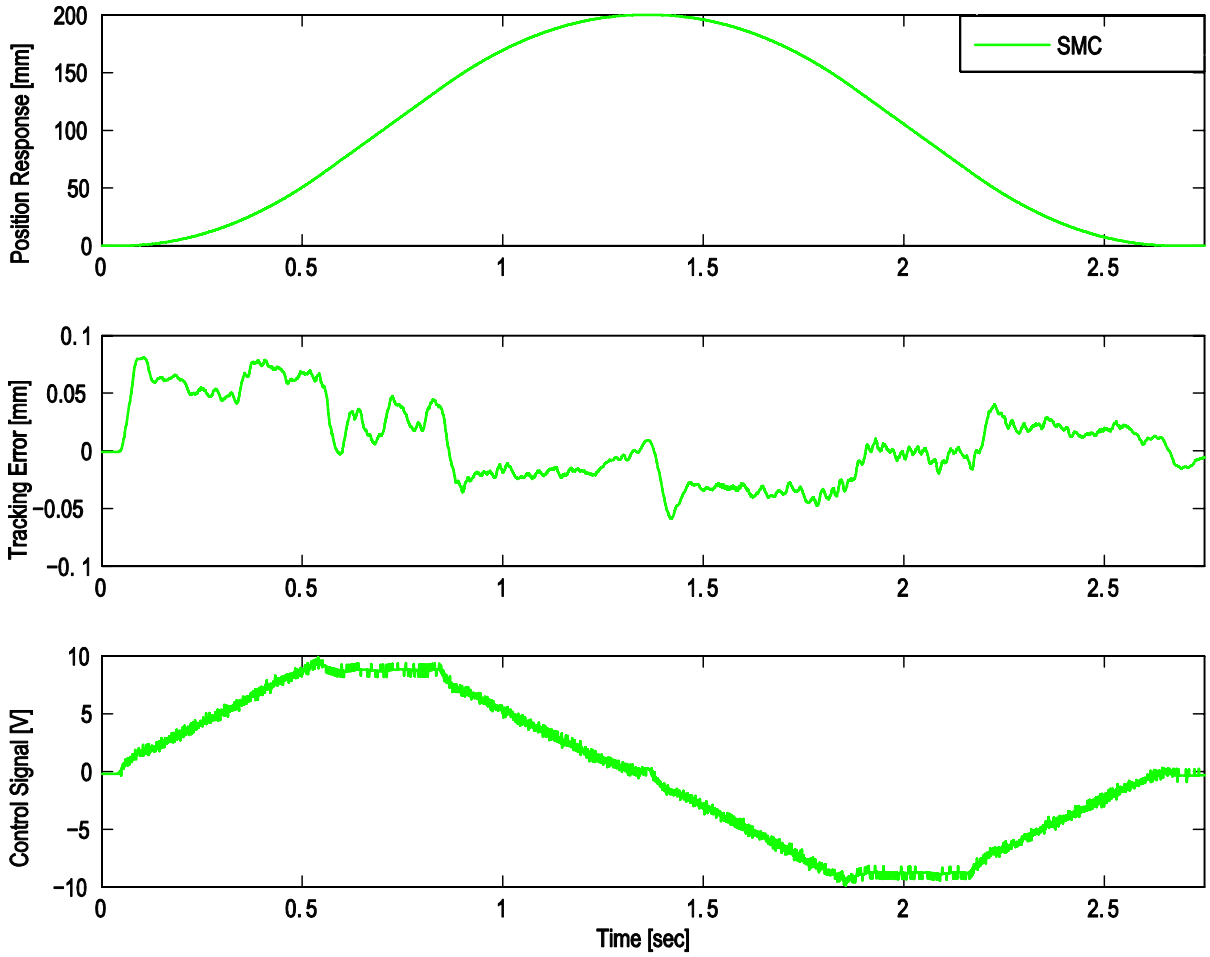

Figure 4.2: SMC Tracking Performance

Section 4.2: Frequency Domain Identification of Axis Dynamics

In high performance controller design, it is essential to have a good model of both the rigid body and friction dynamics, as well as the high frequency behaviour of a feed drive system. The resonance of the system is the frequency at which a matching input causes highly amplified oscillations. Resonances may also limit the bandwidth, or lead to instability if an attempt is made to push the performance further. In order to determine the high frequency behaviour and resonances, frequency response functions (FRF) are identified by injecting white noise or sinusoid signals of varying frequencies directly into a drive system. However, when there is a significant amount of guideway friction, identification becomes particularly difficult. Here, to overcome the nonlinear friction problem, sine waves of gradually increasing frequencies were injected into the control signal during y-axis travel at constant speeds. Although computation and run time are greater, the sine wave approach was chosen as more reliable compared to other methods, as it is better able to capture the nonlinear dynamics in the drive system, such as backlash and friction, which would exhibit as amplitude dependency. It was decided that performing the frequency identification was more crucial for the y-axis, since the swaths will be printed along the y-direction, thereby having a greater impact on the droplet positioning accuracy than the other axes.

Sinusoids of 1 V amplitude were added to the control signal, with frequencies varying from 2 to 400 Hz input for ten periods each, as shown in Figure 4.3. The SMC parameters were detuned, such that the controller provided low reactivity and no integral action, in order to capture the frequency response dynamics more accurately. Rotary and linear encoder data were recorded at a sampling rate of 1000 Hz. Each set of position data corresponding to a specific sine frequency input was evaluated individually, using least squares fitting to estimate input and output amplitude and phase values for the excitation input and actual position response. The output curve was approximated with an equation that incorporates both the linear trajectory motion and the injected sinusoids, where ω is the frequency in radians per second, t is the time elapsed in seconds, ϕ is the phase in radians, A is the amplitude, and a, b, c, $A\cos\phi$, and $A\sin\phi$ are the parameters to be identified:

$$y = at^2 + bt + c + (A\cos\phi)\sin\omega t + (A\sin\phi)\cos\omega t \qquad (12)$$

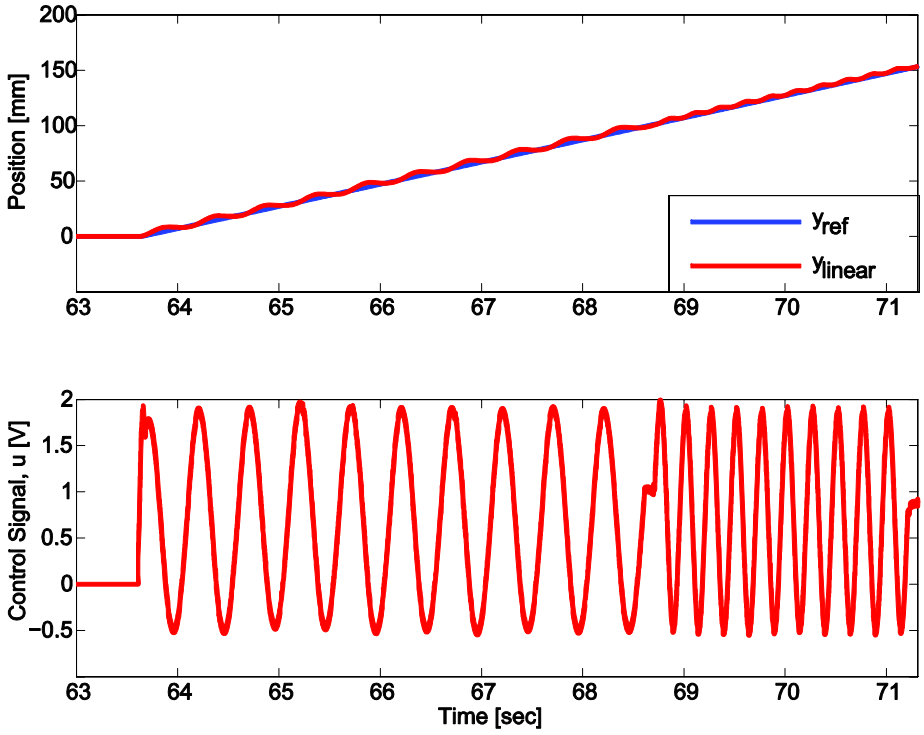

Figure 4.3: Sinusoidal Excitation Overlaid on Top of the Control Signal (u) - shown for 2 and 4 Hz waves

Equation (12) was rewritten in matrix form and the θ parameters were solved using the N elements of y position data obtained from experiment:

$$y = \Phi_y \theta_y$$

$$\begin{bmatrix} y(2) \\ \vdots \\ y(N) \end{bmatrix} = \begin{bmatrix} t(1)^2 & t(1) & 1 & \sin \omega t(1) & \cos \omega t(1) \\ \vdots & \vdots & \vdots & \vdots & \vdots \\ t(N-1)^2 & t(N-1) & 1 & \sin \omega t(N-1) & \cos \omega t(N-1) \end{bmatrix} \begin{bmatrix} a \\ b \\ c \\ A\cos\phi \\ A\sin\phi \end{bmatrix} \quad (13)$$

A similar matrix was made for the u control signal data. Thus, for each input frequency, the magnitude $|G|$ and phase φ were calculated as follows, where U and φ_u are the respective magnitude and phase of the control signal at that frequency (calculated similarly to Y and φ_y):

$$\text{Magnitude of output : } Y = \sqrt{\theta_{y4}^2 + \theta_{y5}^2}$$

$$\text{Plant gain : } |G| = \frac{Y}{U} \quad (14)$$

$$\text{Phase of output}: \varphi_y = \arctan\left(\frac{\theta_{y5}}{\theta_{y4}}\right)$$
$$\text{Phase of plant}: \varphi = \varphi_y - \varphi_u \qquad (15)$$

This resulted in the Bode plot in Figure 4.4, which verifies that for lower frequencies the rotary encoder data follows closely with the linear encoder data and differs significantly for higher frequencies. In the presence of unity feedback gain, the crossover frequency (where the gain is equal to 1) of the transfer function for the identified plant is approximately 4.5 Hz, which would result in a very poor tracking accuracy.

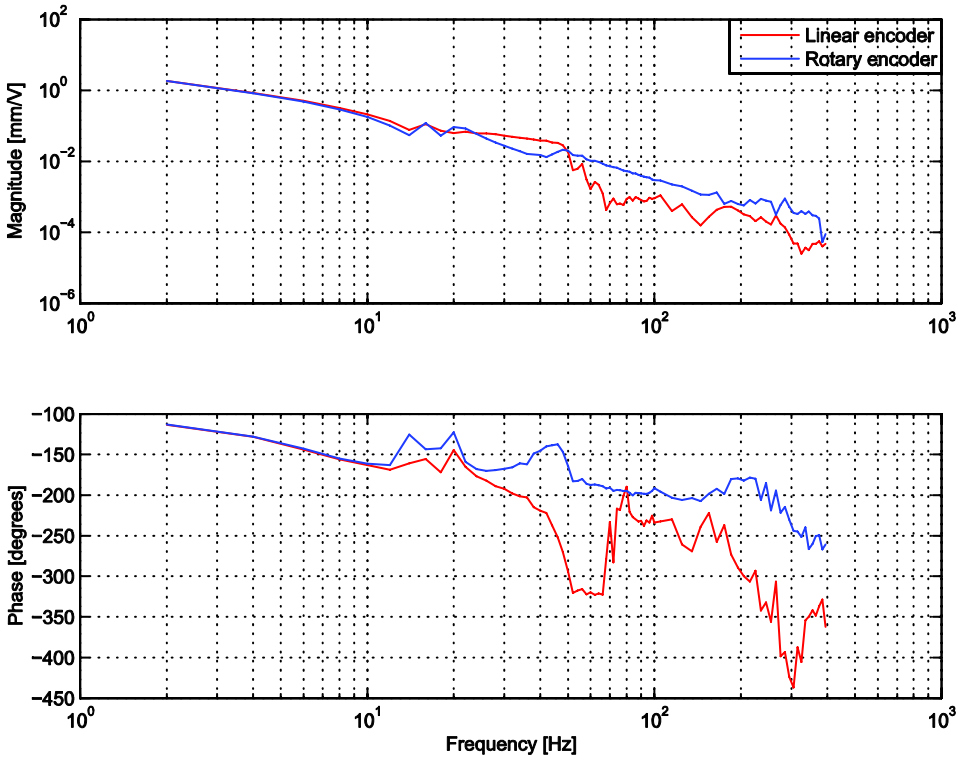

Figure 4.4: Identified Position Frequency Response

Section 4.3: Loop-Shaping Controller Design

By identifying the actual plant model, it is then possible to design a controller to shape the FRF for optimal positioning accuracy, which is known as loop-shaping. Using the plant model identified in the previous section and linear encoder feedback, the loop-shaping controller was designed for the y-axis to account for the natural resonance and high frequency dynamics of the servo system. This is accomplished through several objectives, such as high crossover frequency to allow operation over a wide range of frequencies, attenuation of uncertain dynamics at high frequencies, high gain at low frequencies for good position tracking, and low gain at high frequencies to reduce noise amplification. It is desirable to have the slope at the crossover frequency be -1 and then drop down quickly. For stability, the acceptable phase margin was defined as 30° and the gain margin must be greater than 2. The maximum sensitivity should be between 1.5 and 2.5. If the sensitivity is too high, then the controller may excite unwanted dynamics or be very close to being unstable. High sensitivity means that the controller will not react to command inputs and disturbances, resulting in poor tracking. The desired crossover frequency was chosen to be 18 Hz, a conservative value based on the FRF and previous experiments on the router, yet a significant improvement over the SMC bandwidth which could be achieved when only linear encoder was used (8 Hz).

This section will explain the iterative development of the overall loop-shaping controller as shown in Figure 4.5 with feed-forward inertia, viscous damping, and friction compensation. Figure 4.5 also provides the filter equations, which will be described further in this section. A more in depth background of some of the control theory can be found in reference [34].

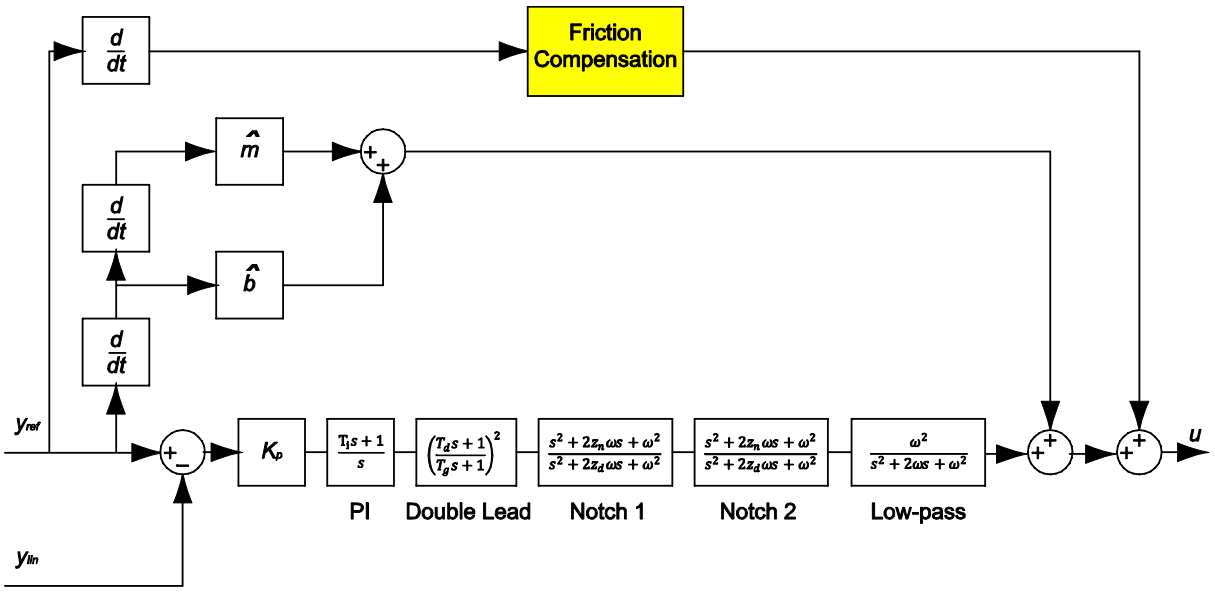

Figure 4.5: Loop-shaping Controller

The FRF in Figure 4.4 showed subtle peaks around 17 and 20 Hz, which were determined to be acceptable. The first step was to increase the gain at low frequencies with a proportional integral controller (PI). Only the low frequency area is affected by the integration action since $1/T_i$ is the frequency at which the PI term rolls off to a value of 1. The disadvantage is that the PI term introduces a phase lag to the system, which has to be compensated with lead filters. The phase lag for the PI term at the crossover was limited to -15°. The phase is calculated as:

$$\emptyset_{PI} = atan(w_c T_i) - 90° \quad (16)$$

For a crossover frequency of 18 Hz and a phase of -15°, $1/T_i$ is calculated to be 30.3043 Hz. The resulting effect of the PI term on the plant is shown in Figure 4.7. Though the phase margin at the 18 Hz crossover frequency is about 5°, which is less than the desired value, it will be considered acceptable for now.

Next, the feedback gain, K_p, was calculated to shift the curve such that the gain at the crossover frequency is 1:

$$\left|G(j\omega_c)\cdot K_p(j\omega_c)\right| = 1 \quad (17)$$

K_p is recalculated each time a new filter is added to the controller.

Sensitivity plots are used to evaluate the stability of the controller. Using the simplified controller in Figure 4.6, where d is the disturbance, G is the plant, K is the controller, e is the error, and n is the signal noise, the position response can be written as:

$$y = \frac{GK}{1+GK}\cdot y_{ref} - \frac{1}{1+GK}\cdot G\cdot d + \frac{GK}{1+GK}\cdot n \quad (18)$$

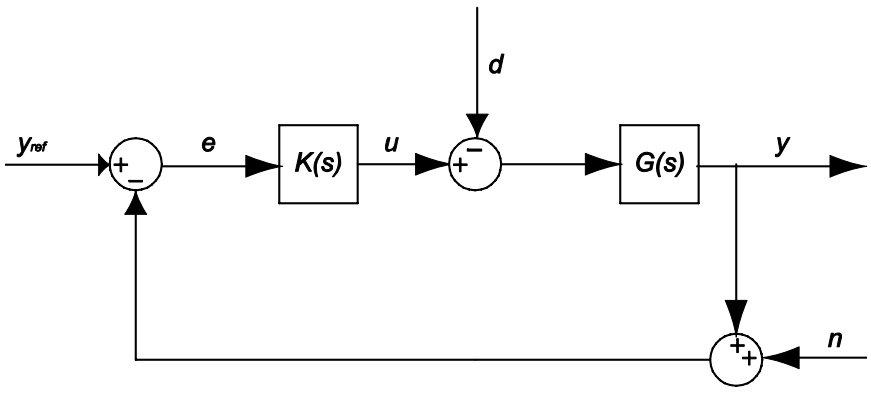

Figure 4.6: Simplified Controller

The open-loop transfer function L is defined as:

$$L = GK \tag{19}$$

Thus, Equation (18) can be rewritten as:

$$y = \frac{L}{1+L} \cdot y_{ref} - \frac{1}{1+L} \cdot G \cdot d + \frac{L}{1+L} \cdot n \tag{20}$$

And the error is:

$$e = \frac{1}{1+L} \cdot y_{ref} + \frac{1}{1+L} \cdot G \cdot d - \frac{L}{1+L} \cdot n \tag{21}$$

S and T are then defined as the sensitivity and complementary sensitivity functions:

$$\begin{gathered} S = \frac{1}{1+L}, T = \frac{L}{1+L} \\ S + T = 1 \\ e = S \cdot y_{ref} + S \cdot G \cdot d - T \cdot n \end{gathered} \tag{22}$$

Therefore, large values of L (small S) help attenuate disturbance and improves tracking in the low frequency range. However, small values of L (small T) are also desirable for immunity against noise and unknown dynamics in the high frequency range. The inverse of the sensitivity represents the distance from the loop transfer function at the crossover frequency to -1 in the Nyquist plot.

Looking at the sensitivity plots in Figure 4.8, a peak can be clearly seen. A notch filter was added to attenuate this peak at 28 Hz ($\omega = 56\pi$ radians), with $z_n = 0.15$ determining the amplitude of the notch and $z_d = 1.4$ influencing the width of the notch.

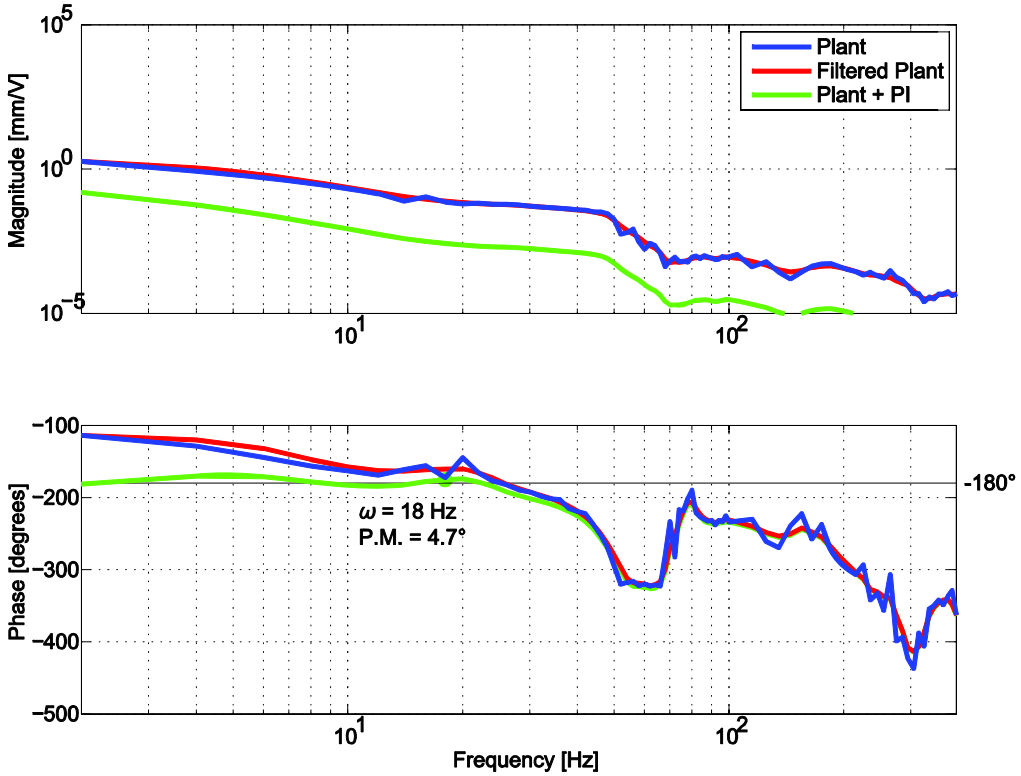

Figure 4.7: Effect of Proportional Gain Integrator

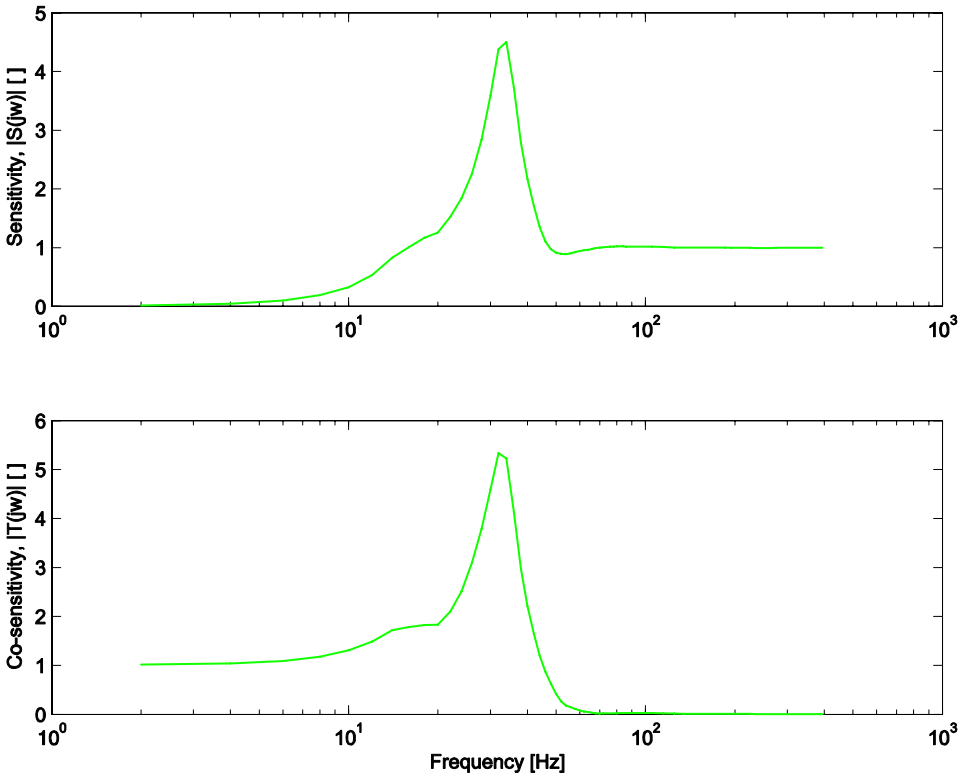

Figure 4.8: Sensitivity After Adding PI

As a result of adding the notch, the phase margin is 79° below the desired value, as shown in Figure 4.9. It is not recommended that a single lead filter be used for more than 71° phase. Therefore, a double-lead filter was introduced to increase the phase margin (*P.M.*) back to 30°, such that each lead filter provides:

$$\emptyset_{lead} = 0.5[-180° + P.M. - \emptyset_{PI} - \emptyset_{F1} - \emptyset_{G}] \quad (23)$$

where F represents the additional shaping filter and G is the identified plant. The parameters of each lead filter are calculated as follows [34]:

$$\beta = \sqrt{\frac{1 + \sin \emptyset_{lead}}{1 - \sin \emptyset_{lead}}} \quad (24)$$

$$T_d = \beta \omega_c$$

$$T_g = \beta / \omega_c$$

Essentially, two zeros and two poles are placed symmetrically around the desired crossover frequency to generate sufficient phase lead in order to recover the system stability with the desired phase margin. Figure 4.10 shows the effect of the PI, notch, and lead filters on the sensitivity plots.

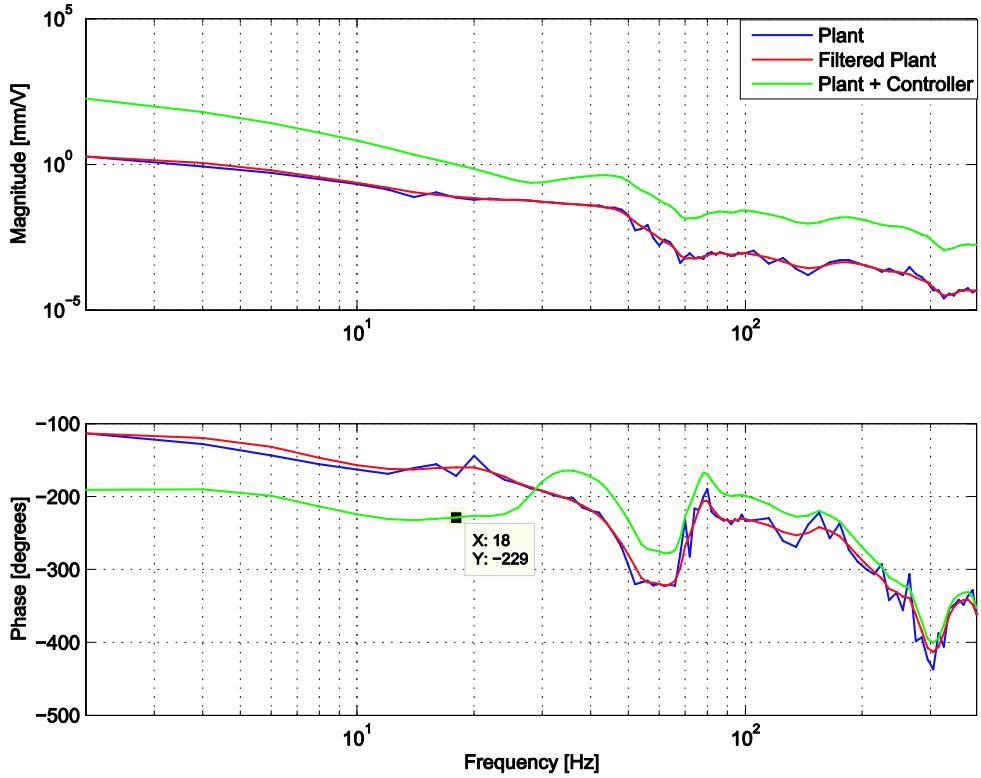

Figure 4.9: Effect of Adding a Notch Filter

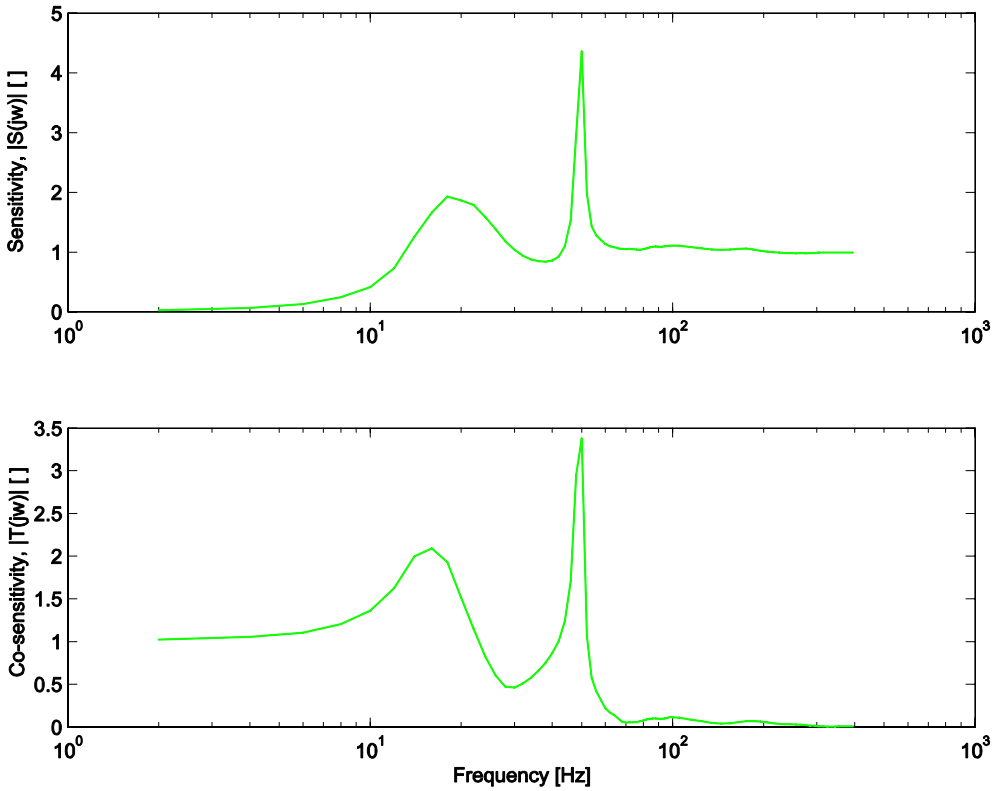

Figure 4.10: Sensitivity Plot After PI, Notch, and Lead Filters

A peak can now be seen at a frequency of 45 Hz, which was attenuated by adding a second notch filter with z_n = 0.09 and z_d = 0.7. The phase compensation from the lead filters was altered accordingly to include the second notch in ϕ_{F2} in Equation (19).To compensate for the decrease in phase margin from both notch filters, the double-lead filter would now have to make up approximately 82.6° of phase advance at 18 Hz.

Finally, a second order low-pass filter was introduced to lower the gain over high frequencies. Its disadvantage is that it generates additional phase lag, which also reduces the phase margin. Thus, its frequency was chosen as 200 Hz, which is more than 10 times the crossover frequency and would not significantly affect the phase margin. Again, the lead filters were changed to include the low-pass filter in ϕ_{F3} in Equation (19). Figure 4.11 and Figure 4.12 show the final controller FRF and sensitivity plot, respectively, satisfying the design constraints mentioned at the beginning of this section. Some attempt was made to increase the bandwidth to more than 18 Hz, however, the filters were very difficult to tune. Noise and unmodelled dynamics became a significant problem that caused vibrations and hampered accuracy.

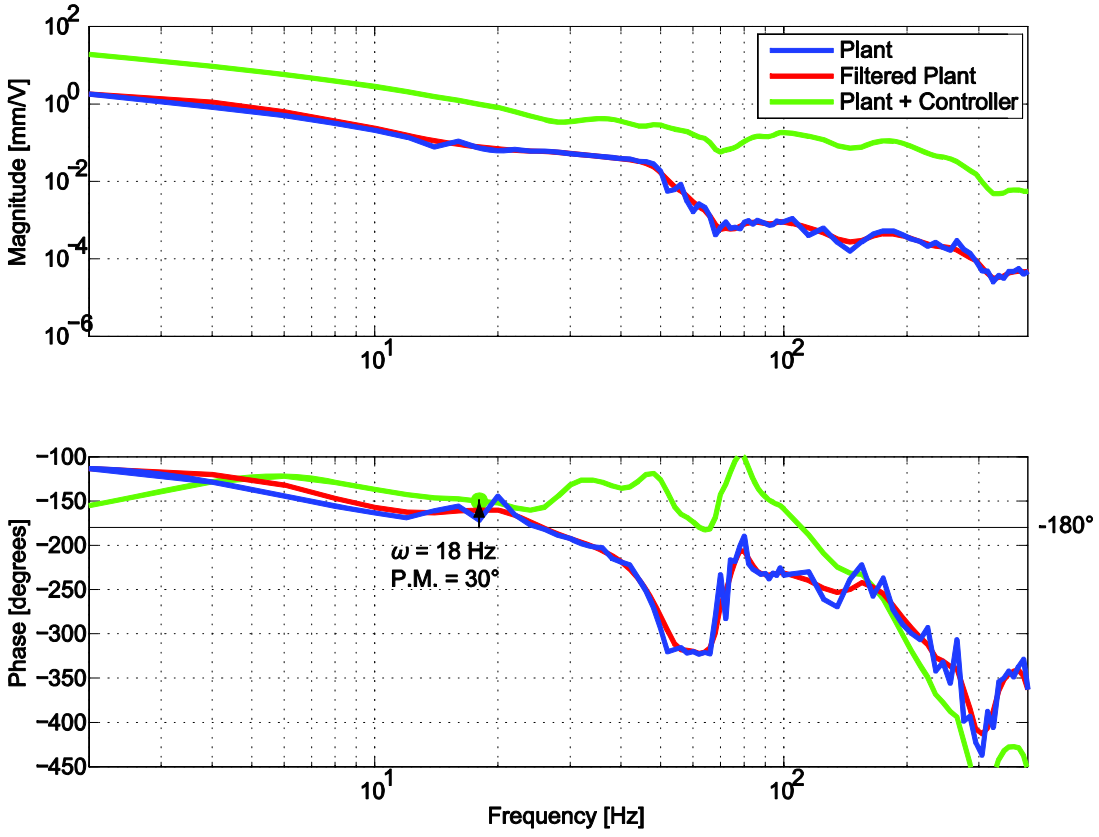

Figure 4.11: Final FRF

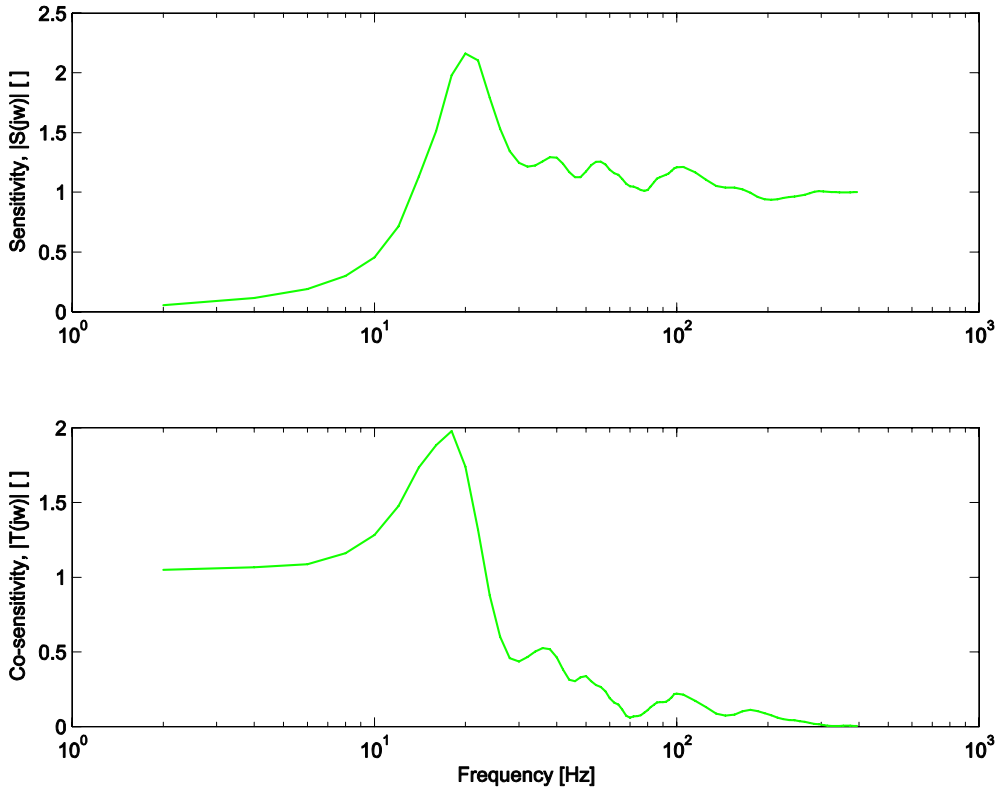

Figure 4.12: Final Sensitivity Analysis

Next, the loop-shaping controller was tested and compared with experimental results from the SMC using the same trajectory. As can be seen in Figure 4.13, over the constant velocity sections, the loop-shaping controller resulted in a maximum error of 20.2 µm, which is 75% better than the 80.75 µm from the SMC. The control signal for the loop-shaping controller is also less aggressive, decreasing the risk of vibration affecting the printing operation. It is believed that the friction model in the loop-shaping controller was not tuned as well as for the SMC, giving rise to the worse tracking error when the motor changes direction and stops. Considering the spacing between droplets is 82.2 µm (explained in Chapter 5.0), the tracking error for the loop-shaping controller is quite a significant improvement. A tracking error of 20.2 µm is also considerably better than the 100 µm currently achievable in industry, as noted in Section 2.2.

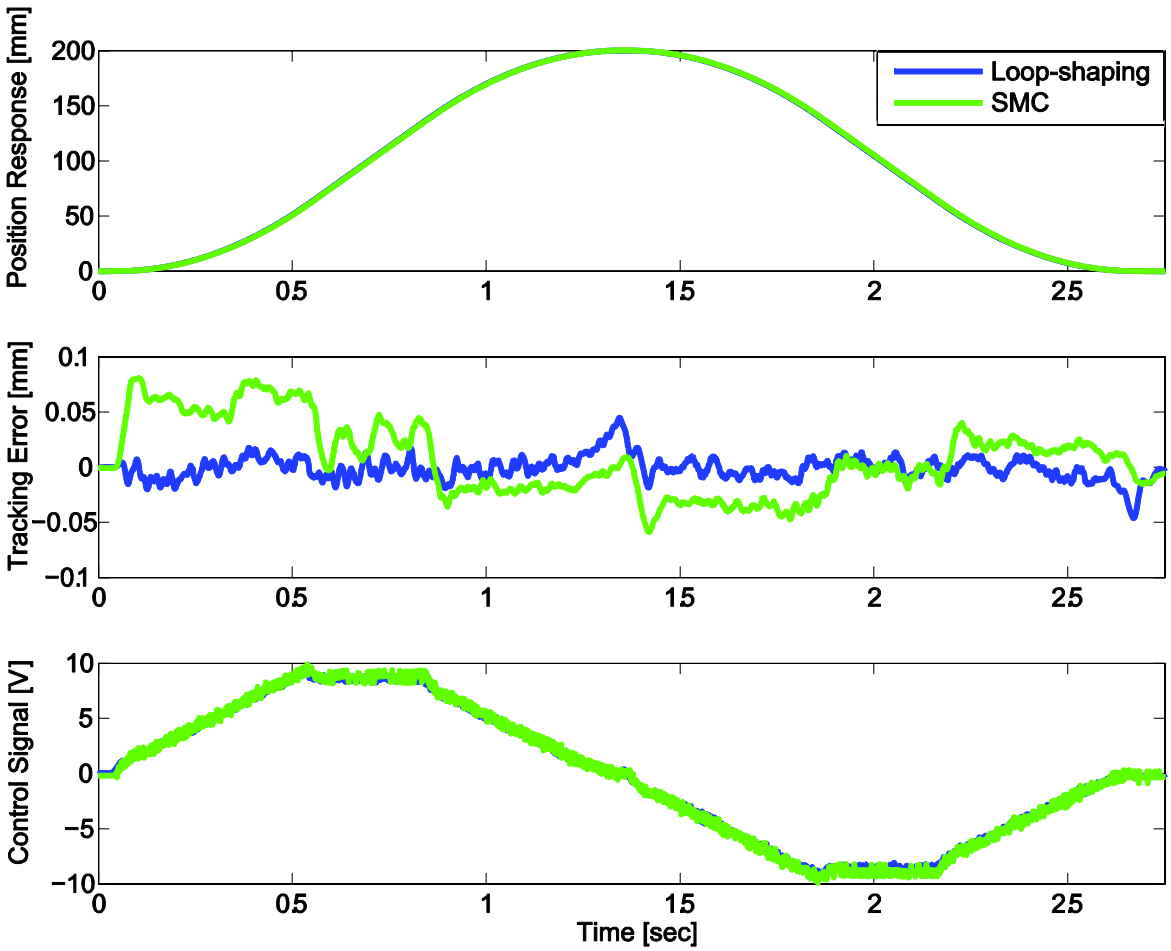

Figure 4.13: SMC vs. Loop-shaping Tracking Error

Section 4.4: Trajectory Generation & Axis Homing

While printing, the printheads must be kept at a height of 1 mm above the substrate. Since the thickness of the substrate can change, the printheads should start at a predefined zero location and drop down to the required 1 mm height. There is no vision detection for the substrate, so its thickness must be incorporated into the trajectory prior to motion in order to calculate how far the printheads should be lowered. When turning on the machine, the Z2 axis does not necessarily start at the zero location and must be homed. Otherwise the printheads could crash into the substrate, thereby risking damage to the printheads, the substrate, and the machine itself.

During the initial setup, the secondary z-axis was connected to the internal controller and the limit switches of the router. This meant that the basic internal controller used by the router to home the x, y, and z-axes could be used for the secondary z-axis instead of the spindle. It was found that the motor dynamics of Z2 were very similar to Z1, which allowed for the switch. Ideally though, the printhead mount and the spindle would both need to be in operation in order to print and machine without constantly switching connections. Thus, a separate homing routine and mechanism were developed for Z2 in MATLAB and Control Desk, which is a real-time program that can be used in conjunction with the Simulink model.

The homing routine makes use of an encoder pulse produced every full revolution of the Z2 lead screw, which has a lead of 5.08 mm. In other words, for any position the lead screw should be within 5.08 mm of the Z-pulse. Thus, as shown in Figure 4.14, the homing trajectory was designed such that the lead screw would turn π radians clockwise (2.54 mm) and then 2π radians counter-clockwise (5.08 mm), guaranteeing the detection of a single z-pulse. Once the pulse is detected, the Simulink program was designed to reset the Z2 encoder to zero and the trajectory would turn off by simply overriding the planned trajectory and sending zeroes to the controller instead. There is a slight positioning correction of the lead screw due to the delay between the encoder reset and the trajectory motion, where the linear stage will try to jump back to where it was before the encoder was reset, based on the new zero position (Figure 4.15).

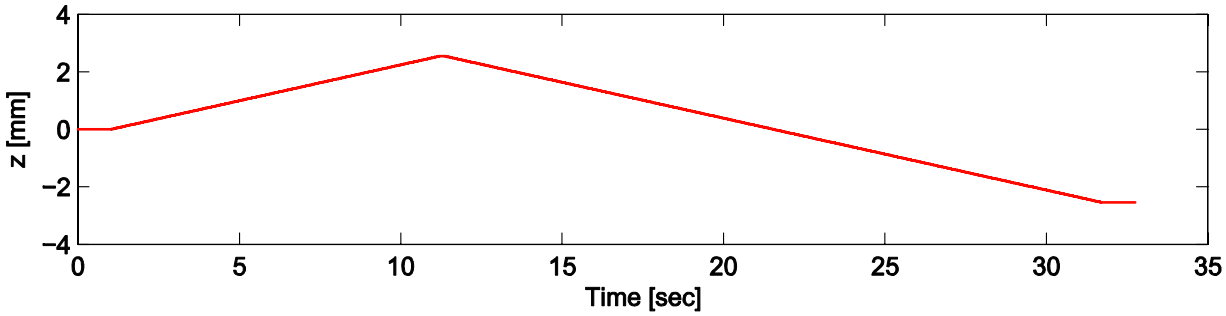

Figure 4.14: Homing Trajectory

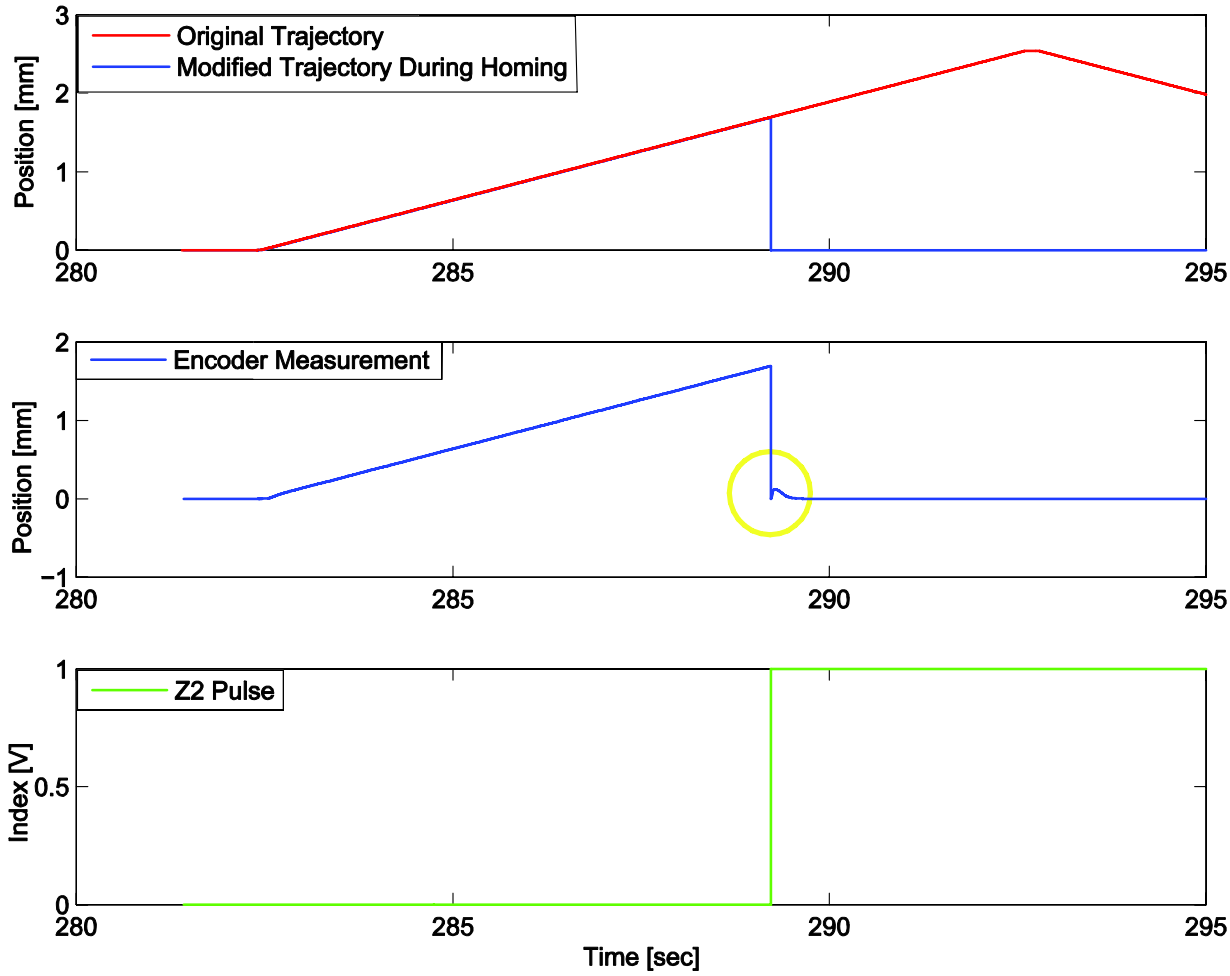

Figure 4.15: Homing- The actual position shows the positioning correction (highlighted in yellow) after detecting the Z2 pulse.

This homing routine does not take into consideration the actual position of the printhead mount, since there is no detection from the Z2 limit switches. The lead screw could be fully actuated, fully retracted, or at some position in between. Hence, a manual jogging routine was developed in Control Desk in conjunction with the Simulink model in order to position the printheads within range of a specific location physically marked as the home position. Again, this is necessary since the trajectory to plunge the printheads down needs to be built in advance by inputting the distance into the MATLAB program. In this case, Control Desk is used to override the position commands and manually position the printheads within range of home position when the program is paused and waiting for operator acknowledgement (Figure 4.16). The X and Y axes were also included in the Control Desk interface to more easily position the printheads over a specific area of the substrate and avoid having to constantly switch back and forth between the internal router controller and dSPACE. However, in this thesis, a homing routine has not been developed for the X and Y axes.

Loading the controllers to dSPACE takes a significant amount of time. Since the controller has already been designed and should be stable at this point, the same controller implemented for printing was used for jogging the axes instead of having to continuously switch between two different controllers. In the Control Desk interface, the user specifies the distance and direction of travel as a constant value. The constant position command is smoothed for jogging into continuous motion using two low-pass filters, whose time constants determine how long it takes for the axes to travel the specified distance. Once the desired position is reached, the axes are manually disabled and the encoders are reset to zero. If the axes are not disabled first, then the delay between the encoder reset and the control signal will cause the axis to jump to its previous zero location, which should not be done when jogging large distances. The one exception is that since the Z2 motor will back-drive due to its weight without the presence of a control signal, the Z2 axis must be constantly activated before running the printing routine. Thus, it is recommended to first position the Z2 axis within 10 mm of home position, disable the Z2 axis and then reset it. If the Z2 axis is still out of position, then the Z2 axis can be kept activated, re-positioned, and then the encoders reset, which will cause it to attempt to move back to its previous zero before settling at its new zero position.

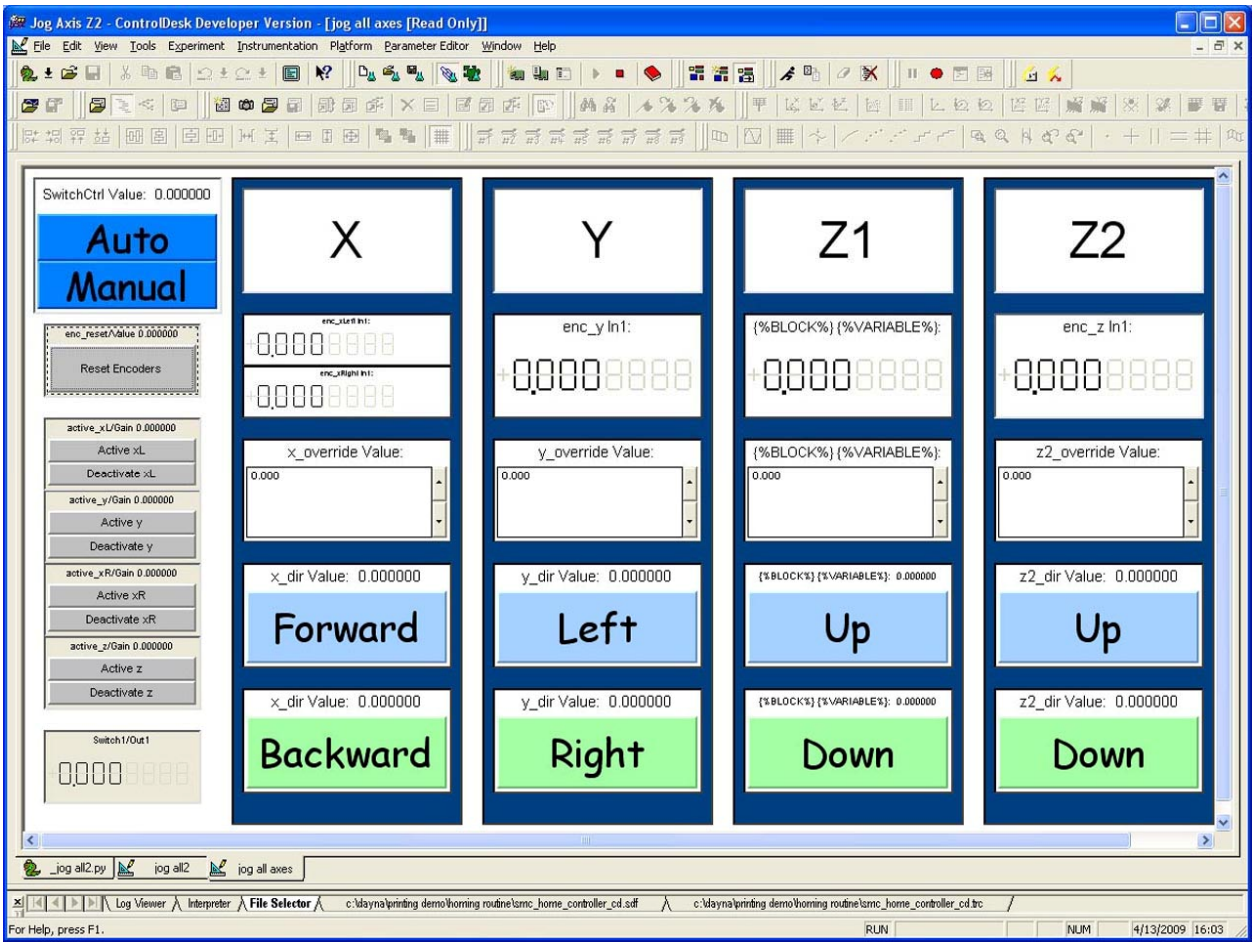

Figure 4.16: Axis Jogging Interface

An image is typically composed of multiple swaths, printed one swath at a time. A smooth trajectory decreases the risk of misplaced droplets, as the printheads are very susceptible to noise and vibration. This was done by implementing a jerk-limited trajectory as developed by Michele Heng and shown in Figure 4.17 for one pass along the y-axis [9]. In addition, the start of each swath is offset such that the printheads fire only when the motion is under constant velocity, which is set at the maximum speed of the router, 250 mm/sec. The maximum magnitude of acceleration and deceleration was chosen as 500 mm/sec^2 with a maximum jerk of 25 000 mm/sec^3 based on previous testing to limit the effect of shock and vibration. The printheads maintain a height of 1 mm over the substrate throughout the print. For unidirectional printing, the printheads only print along the forward swath and then move forward along the x-axis while retracting in the y-axis before printing the next swath (Figure 4.18). Bidirectional printing prints in both the forward and reverse directions, which requires the x-axis to move forward before moving back along the y-axis for the reverse swath (Figure 4.19). At the end of a print, the printheads return to their home position. This trajectory uses a significant amount of memory, which the

dSPACE cannot handle for images over a certain size. Since each pass is basically the same repeated motion except with an increase in the x-direction, the trajectory should be separated into segments and sent to a buffer, as is typically done in commercial printers. Alternatively, real-time trajectory interpolation can also be used to solve this problem. Based on the trajectories, bidirectional printing would finish 14.1 seconds faster (15.3% reduction) than unidirectional printing. Acceleration, deceleration, and jerk values could be adjusted to optimise the times, though this was not done in this thesis work. The time reduction is not closer to 50% since the bidirectional method has to move along the x-axis in between swaths, whereas the unidirectional method retracts along the x- and y-axes at the same time.

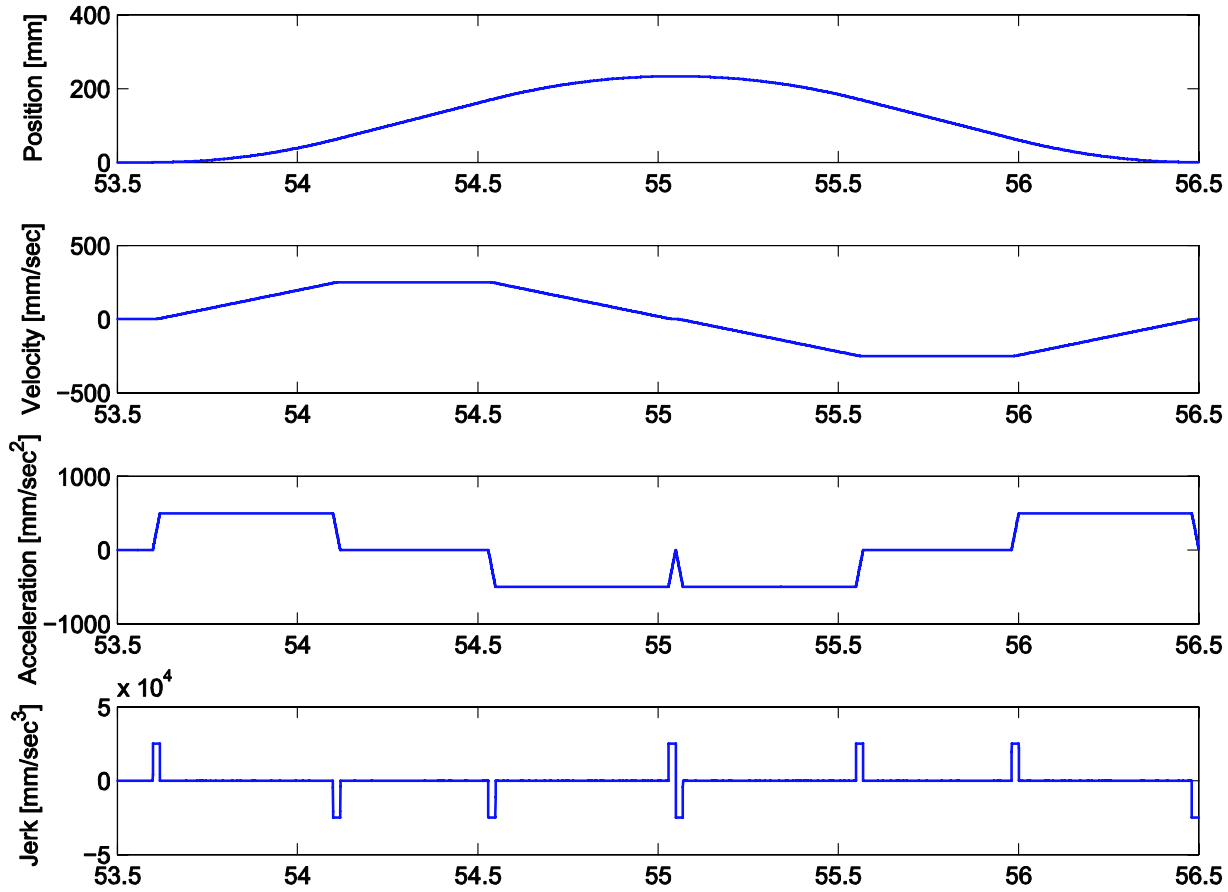

Figure 4.17: Jerk Limited Profile for the y-axis

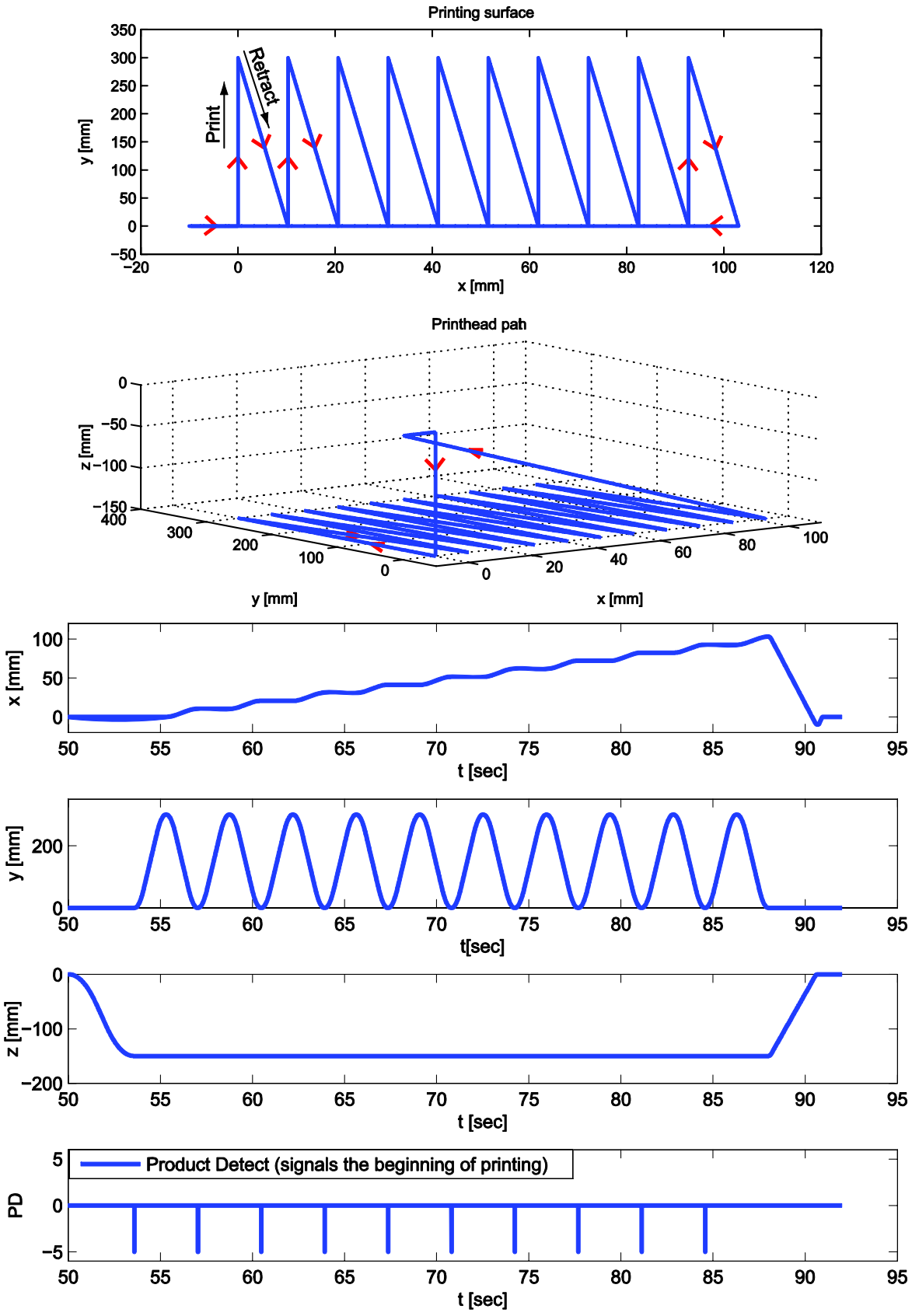

Figure 4.18: Unidirectional Printing Trajectory

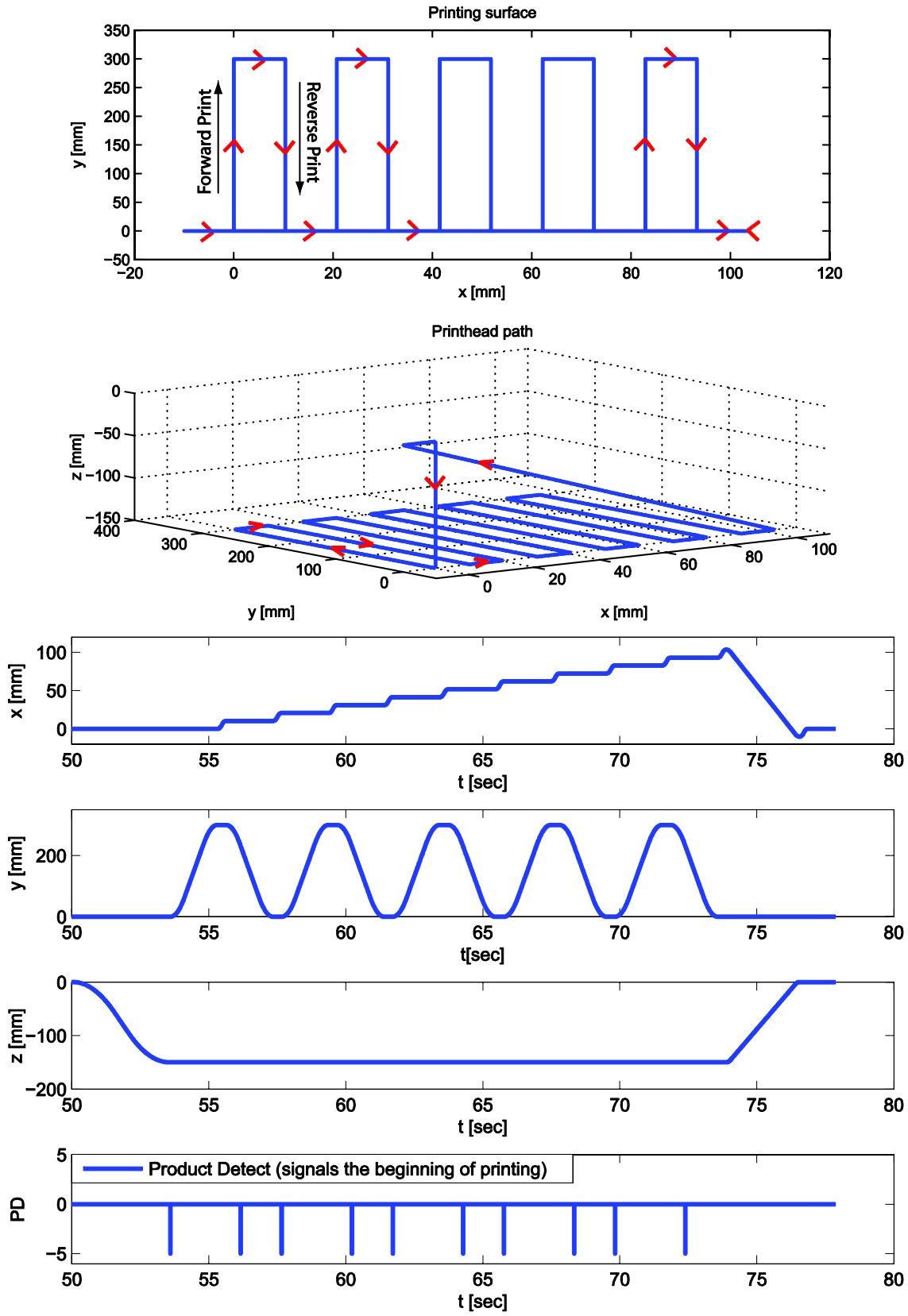

Figure 4.19: Bidirectional Printing Trajectory

Since the XUSB relies directly on the linear encoder measurements, smooth motion to reduce noise in the signal becomes important rather than the positioning accuracy of the controller during unidirectional printing. Tracking error is fairly repeatable, so each swath would be shifted by the same amount. In 1PD bidirectional printing, the reverse PD is generated by the XUSB based on the linear encoder measurements, which can be affected by noise, tilting and vibration of the printheads, and other machine error. The 2PD bidirectional method would be better since it is adjusted by viewing the final image, which includes these errors that are not detected by the linear encoder. However, when generating 2 PD signals, there will be positioning error along the forward swath and an opposite positioning error along the reverse swath; essentially doubling the error found in unidirectional printing. Tuning the timing of the second PD signal based on the printed image will help, though the timing of the signal is limited to the sampling rate of the controller. With a 5 kHz sampling period and 250 mm/sec motion, the printheads will travel 50 µm for each time step. If the true position of the PD signal is in between each 50 µm step due to tracking error, then the only way to further improve the swath to swath positioning accuracy is through controller design to reduce tracking error.

Section 4.5: Conclusions

In this chapter, the controller design for improved tracking control and droplet placement accuracy was explained, which is essential for printing quality images using the 2PD bidirectional method and when milling shapes around the printed image features. A loop-shaping controller was designed with better performance than an SMC by identifying the actual plant FRF. This was achieved by injecting sinusoidal excitation signals into the control signal and using least squares fitting to estimate the input and output amplitude and phase values at each frequency. A proportional gain integrator was used to increase the gain at low frequencies for better tracking and rejection of disturbances, such as friction and cutting forces. Two notch filters were added to remove the resonances found in the sensitivity function, and a double-lead filter compensated for the phase loss due to the dynamics of the drive and added filters. Lastly, a second order low-pass filter was incorporated to lower the gain at high frequencies. The loop-shaping controller improved the maximum tracking error over the SMC during 250 mm/sec motion from roughly 80.75 to 20.2 µm.

It was necessary to develop a homing routine since the print trajectory is planned in advance of motion and there is no visual detection system. A Control Desk interface was developed to manually move the printhead mount within the range of a predefined home position along all three axes. Then, the homing routine was implemented for the secondary Z-axis based on the 5.08 mm lead and the Z-pulse from the encoder. To prevent back-driving of the printhead mount due to its weight, the Z2 axis should be kept activated throughout homing and printing. A jerk-limited trajectory was used to ensure smooth motion in order to avoid vibrating during the firing pulses. It was found that bidirectional printing would be approximately 15% faster than unidirectional printing.

Chapter 5: Inkjet Printing Calibration

The human eye possesses excellent visual acuity, given that a person with normal 20/20 vision is capable of resolving discrepancies as small as 1 minute of arc (1/60 of a degree) [35]. This means that, for example, if an image is 300 mm away from the eye, then the smallest distance a dot can be distinguished from another dot is 0.087 mm. A print resolution of 309 dots per inch (DPI) results in a centre-to-centre dot separation of 0.082 mm, such that any mono-colour print resolution higher than 309 DPI is sharp and adequate for most purposes, and a resolution of less than 309 DPI may result in noticeably pixelated or blurry images or jagged edges. Calibration is thus an extremely crucial process for an inkjet printing system since accurate placement of ink droplets, in addition to droplet absorbability with the substrate, defines the resolution, and in turn, the quality of the image. However, one must keep in mind that 20/20 vision is just an average that has been deemed acceptable for human eyesight, though there are people who have better than 20/20 vision. As well, for future material deposition applications in areas such as MEMS or nanotechnology, a much higher resolution would be necessary. A detailed explanation of the calibration process followed in this thesis is given in Section 5.1.

Colour printing, on the other hand, is a much more complicated process than monochrome printing. With a CMYK printer, most colours besides cyan, magenta, yellow, and black are made up of some combination of the other colours and white, which is typically the assumed colour for the substrate. White spaces help lighten colours and black dots darken them. For example, green would be mostly composed of cyan and yellow, with some magenta, black, and blank dots depending on the shade of green. If all these dots were the same size, as it is for binary printing, and were to be deposited in a single position, then the result would be a black dot of diameter larger than 0.087 mm. Thus, for the binary printing system developed in this work, error diffusion dithering is used to simulate the desired colours by spreading out the droplets of each individual colour, which means that the resolution for a colour image is significantly less than 309 DPI. It is easy to acknowledge that even slight colour changes are readily distinguished with the human eye, and therefore a higher resolution would be needed for colour printing. Greyscale printing would also be another option to improve colour resolution, since dot size is more controllable and several colours could potentially make up one pixel. Colour is an exhaustive field that will not be investigated here beyond qualitative judgement.

Recalling the layout of the printhead mounting plate in Section 3.2.1, in order to achieve a specific resolution, the printheads need to be aligned at a specific angle, as well as have close alignment with the other printheads both vertically and horizontally. Mechanical alignment (i.e. making slight

changes in angle and vertical alignment where necessary) is done through the adjustment screws holding the printheads in position with respect to spring-loaded thrust pins. Software settings for the printhead controller allow for changes in horizontal offsets that can be applied to each printhead individually in terms of number of pixels. Large images are printed with multiple swaths, where each swath is printed in the direction of the printhead sweeping motion. This means that each swath must be placed directly below the previous swath, or else the image will have a jagged appearance. Vertical displacement between swaths is determined by the trajectory and the motion control system.

It was found that printing on non-glossy paper such as Xerox Premium Inkjet paper weighing 90 g/m^2 would allow the ink to absorb into the fibres of the paper, making quantitative microscopic analysis much more difficult, even though the image is aesthetically fine. Therefore, testing was done with HP Premium Plus Photo Paper, which is 280 g/m^2 high gloss paper designed for inkjet printing. The oil-based ink did not absorb into the glossy paper since HP uses water-based ink with thermal inkjet technology, where the ink solidifies after cooling, rather than piezoelectric, which relies on absorption or evaporation. However, that is exactly why the high gloss paper was ideal for testing calibration. Since the droplets do not absorb into the paper, they remain in the exact position and shape in which they were deposited with minimal distortion. The disadvantage is that factors such as physical contact, air convection, imperfections in the paper surface, dust contamination, tilting the sample, and settling time could affect the droplets while preparing and transporting the sample to a microscope. [18]

Section 5.2 will present the verification results from calibrating the printheads and the problems involved. This section is further divided into subsections by implementing one element at a time, starting from a unidirectional monochrome print to a full-colour bidirectional image for reduced production time. All tests were done using the loop-shaping controller developed in Section 4.3 for the y-axis motion. Section 5.3 details the additional issues encountered while printing and how they were resolved, including printhead maintenance. Section 5.4 gives the conclusions for this chapter.

Section 5.1: Printhead Calibration Methodology and Operation

Calibration can be separated into mechanical and software components. First, the printheads were manually aligned by tightening or loosening the adjustment screws that hold the printheads in place. The tapered heads of the adjustment screws determine how far the printhead is pushed against the thrust pin, which can be considered a deformable spring. This means the fixed reference point changes depending on which screw is being adjusted, making adjustment more complicated. As shown in Figure 5.1, by tightening screw A, the force will push the thrust pin (highlighted in green) down and to the left and the printhead will rotate counter-clockwise around screw B. Conversely, tightening screw B will move the thrust pin up and to the left and rotates the printhead clockwise about screw A. The more a screw is tightened, the greater the force it exerts against the printhead and thrust pin. However, one screw can limit the extent to which the other screw affects the printhead. For example, if both screws are significantly tightened and screw A is tightened further, screw B will prevent the printhead from shifting down further until screw B is loosened. Quantification to ascertain exact printhead displacement in relation to screw rotation was concluded to be outside the scope of this thesis. It should be noted that the adjustment screws are only for minor adjustments since the printhead angle is mainly determined by the mounting plate. Excessive tightening may bend the thrust pin and cause it to break.

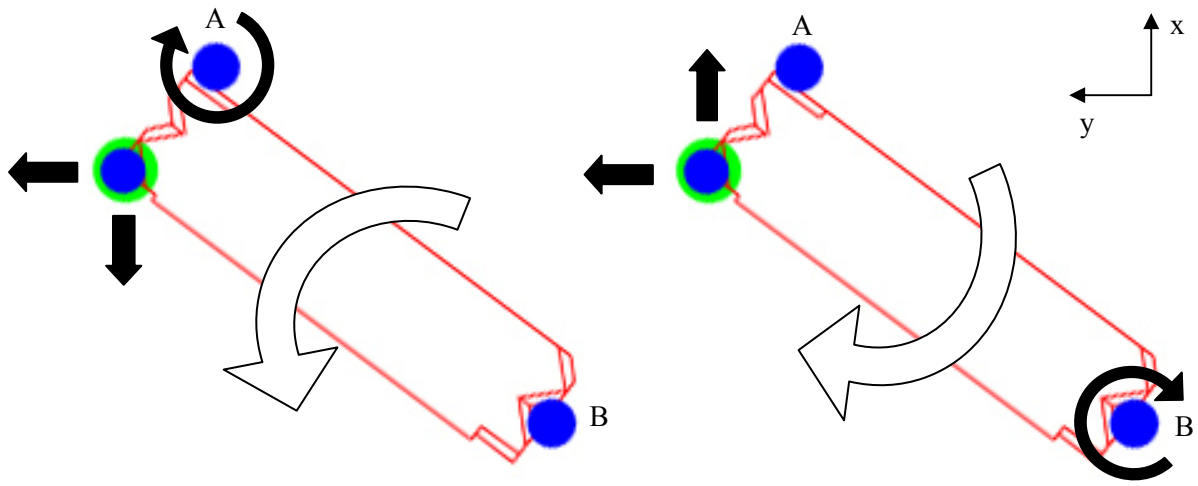

Figure 5.1: Direction of Printhead Adjustment - Turning adjustment screws A or B results in the corresponding motion of the printhead (outlined in red) and the thrust pin (highlighted in green).

Software calibration is controlled through the XUSB software provided by the printhead manufacturer, Xaar, and MATLAB trajectory generation. In the XUSB software, each printhead has an offset in units of pixels that determines the distance that the printhead should delay after receiving the

product detect signal to start printing in each swath. Since there is a gap between each printhead, the offsets will need to be adjusted accordingly, increasing with their respective distances from the first printhead. The trajectory determines how far the printheads travel in the x-direction to the next swath. In other words, the XUSB software has some control over the horizontal displacement, while the trajectory controls the spacing between swaths, though not the spacing between droplets within a swath.

The results from printing on HP glossy paper were viewed under an Olympus microscope at 50x magnification, which was the lowest magnification available, and captured and measured using Image-Pro 6.3 software. Samples were held down with tape while the platform on which the sample rests can be jogged with a joystick to move around within the limited field of view. Microscope images are inverted both horizontally and vertically. Thus, when printing two colours directly on top of each other, if the dots of one colour appear to be offset to the right of the other, then it is actually shifted too far left and requires a respective change in offset value or a mechanical shift to the right to align with the other colour. Conversely, the angular adjustment direction is the same as viewed under the microscope, since the horizontal and vertical flips are equivalent to a rotation of 180 degrees. However, it is much easier to adjust the printheads in terms of horizontal and vertical movement. It should be noted that the colour depicted in the microscope images of printed results may not reflect the actual colour of the sample due to various visual settings in the Image-Pro software.

Droplets are ejected from the printhead nozzles using piezoelectric shear mode firing (Figure 5.2). The nozzles eject ink when the two walls of a nozzle are activated by an electric field, supplied by metal electrodes on the upper half of both sides of the channel wall. Voltage signals applied to the electrodes produce shear mode deformation of the upper halves of the walls and the lower halves follow their motion. As the walls move outwards, the pressure within the channel is reduced. Acoustic waves restore atmospheric pressure to bring fluid into the channel. The waves cross in the middle, producing a high pressure region in the centre. When one acoustic period passes, which is the time for a wave to travel the length of the channel, the pressure along the channel is elevated. Next, a step in the waveform applied to the channel and an opposing step in the waveform of the neighbouring channels cause the walls to move inwards, creating more pressure. Finally, acoustic rarefaction waves reduce the pressure back to atmospheric level, which allows fluid to flow into the nozzle to produce a droplet. Since the two walls of a channel are shared by its neighbouring channels, this means that the nozzles must be separated into at least groups of three to prevent undesired firing. The nozzles within each group are known as A, B, and C channels. For example, if the nozzles were split into only two groups, A and B, and all the A channels were activated, then the B channels would also fire since they share two walls with two A channels. [13, 36, 37]

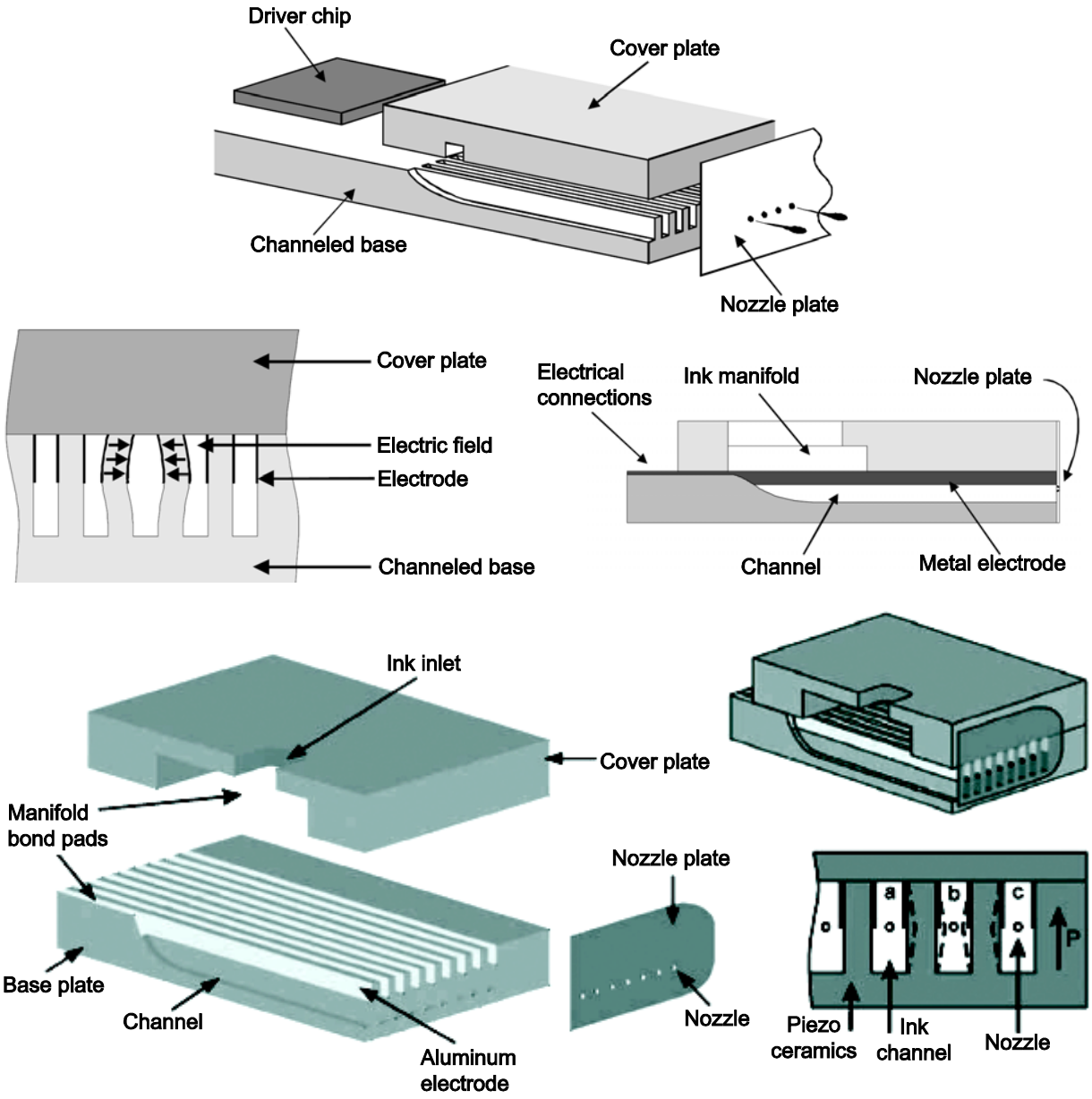

Figure 5.2: Piezoelectric Shear Mode Printhead - Reprinted with permission of IS&T: The Society for Imaging Science and Technology, sole copyright owners of *Recent Progress in Ink Jet Technologies II,* and reprinted from Piezoelectric shear mode drop-on-demand inkjet actuator, Brunahl, J. and Grishin, A., *Sensors and Actuators*, pp. 371-382, 2002, with permission from Elsevier [13, 36]

Based on the orientation of the printhead, the C channels will fire first during print, followed by the B channels, and then the A channels. This order reverses in bidirectional printing. There is a set period of settling time, which cannot be changed, between each firing of a channel before the next channel can release an ink droplet. Due to this delay, the droplets from the A, B, and C channels will not fall in the same exact horizontal locations. This results in a horizontal resolution that is less than the vertical resolution. Figure 5.3 shows an image under the microscope illustrating the limitations of the A-B-C firing of the nozzles. The A, B, and C labels show where the droplets should have been

deposited and A′ and B′ are where they were actually deposited. The crosshair image file is composed of two perpendicular lines, yet due to the A-B-C firing, the vertical line appears jagged. Instead of a straight vertical line for the crosshair, a repeated pattern of three diagonal dots is seen. The angle of the printhead could influence the alignment of the A-B-C firing, though it would require a greater change in angle than is achievable by the adjustment screws alone and would also mean misalignment from swath to swath. It may be necessary to decrease the vertical resolution in order to achieve better horizontal resolution. However, this is not recommended since higher resolution is more desirable as explained at the beginning of this chapter. As the issue of the A-B-C firing presents problems in aligning the printheads within a certain resolution, measurement comparisons were only made within each group of A, B, and C nozzles. It was later found that a better A-B-C firing compensation could be made depending on the settings in the XUSB software. Nonetheless, the horizontal resolution is simply much less exaggerated with the correct settings and the alignment process is the same as described in this chapter. Due to the latency of this discovery, the results from using the correct XUSB image settings can be found in Appendix D.

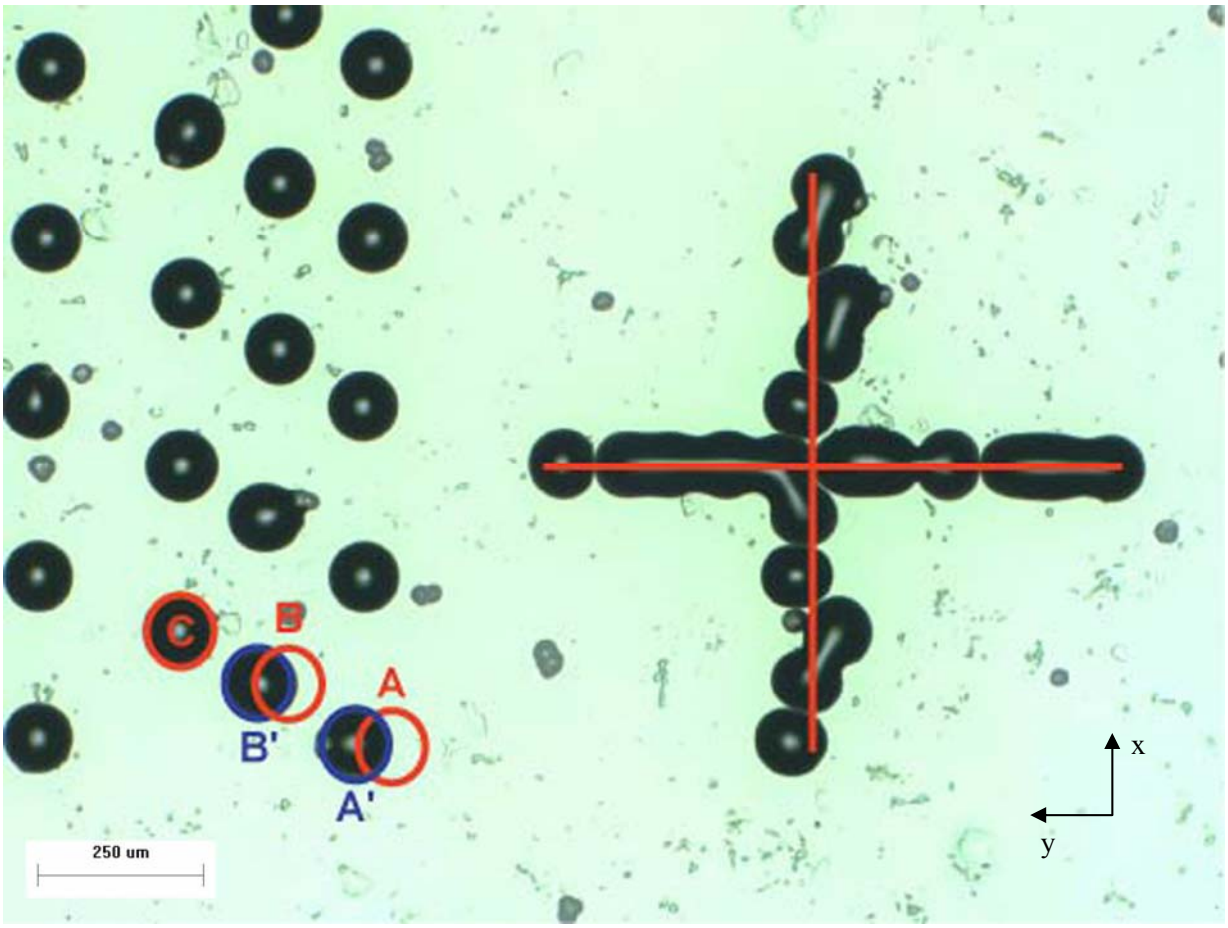

Figure 5.3: Droplet Placement Error due to A-B-C Firing - It is believed that the droplets A′ and B′ should have been deposited at locations A and B based on the original image shown in Figure 5.4.

Section 5.2: Calibration Experiments

A calibration image was designed to test the alignment and droplet placement accuracy of the printheads, as shown in Figure 5.4. Using the resolution of 309 DPI, the image height was made equal to the combined height of two swaths, in order to test swath-to-swath alignment. In this thesis, the first swath always represents the top of the image. Each dot represents one droplet from a nozzle, which means there are 126 dots corresponding to the 126 nozzles. Since all the A, B, and C nozzles fire in succession, three columns of dots were made to show repeatability, making it easier to check vertical alignment in each group of nozzles, and reduce potential bleeding between dots. Originally, the image also had vertical lines to show alignment of the three groups of nozzles together and horizontal lines to demonstrate the repeatability of the droplet firing accuracy. However, the solid lines meant higher density of dots, which tended to blend together and prevent extrapolation of any meaningful results. A crosshair was added to determine the straightness of the image, though later the first nozzle was used as a straight line in order to measure the angle for each group of nozzles. All images were printed at the maximum motion speed available from the router, 250 mm/sec. The x-y axes in the top-left corner show the direction of printhead motion and are not part of the test image.

Figure 5.4: Calibration Image Shown rotated 90°clockwise- 126 dots will be printed to test each of the 126 nozzles.

Since the printheads are at an angle, each nozzle will travel ahead of the next nozzle and sending a normal image will result in each swath being angled at the same angle as the printhead. The XUSB software attempts to compensate for the angle of the printhead and the A-B-C firing based on the predefined image resolution. It does this by displacing each row in the bitmap by a certain number of pixels. Figure 5.5 shows the calibration image that should actually be sent to the printheads for a trailing edge (bottom of image prints before the top of the image). Notice that not all pixels are shifted equally and as mentioned, Figure 5.3 shows the misalignment caused by the A-B-C firing despite the angle compensation.

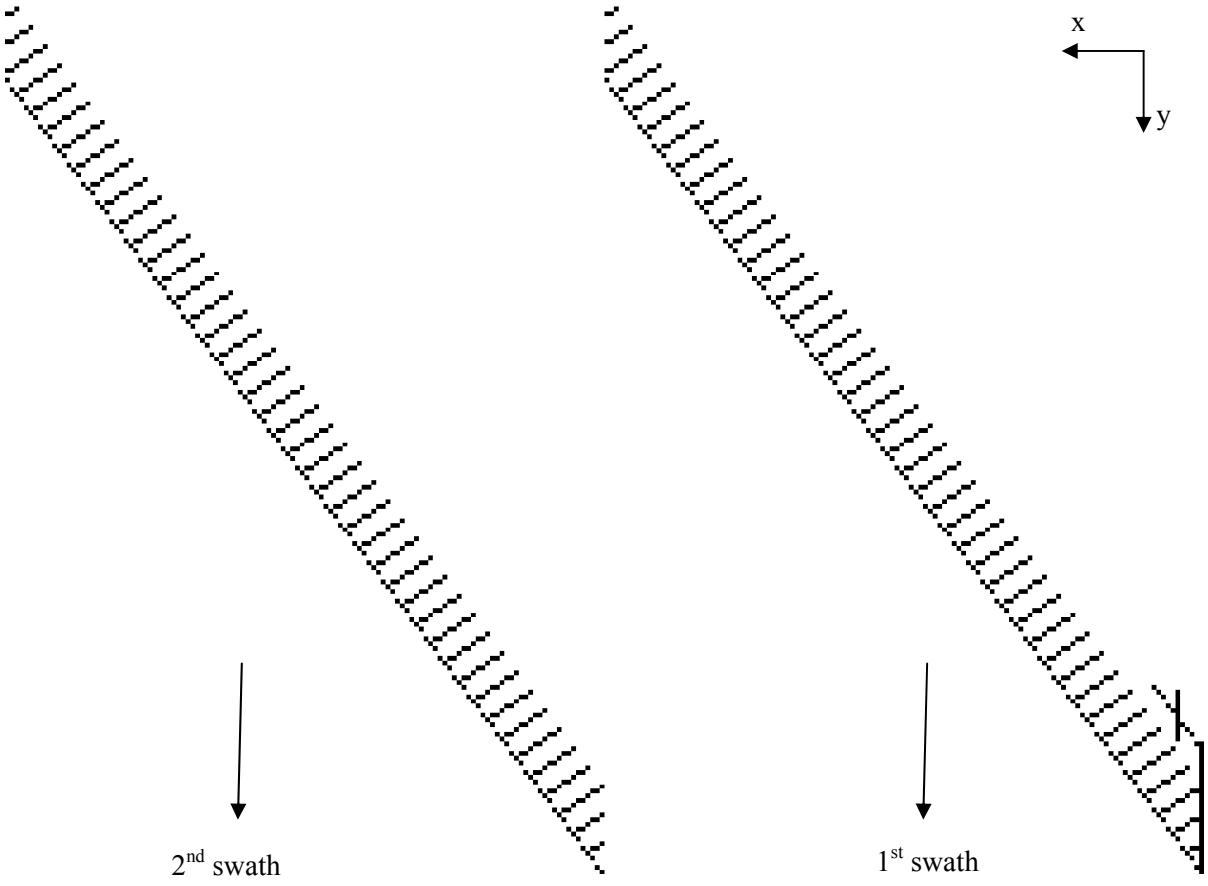

Figure 5.5: Test Image After XUSB Angle Compensation - The angled image is to compensate for the orientation of the printhead. In this case, it is a trailing edge image, in which the top of the printhead trails behind the bottom of the printhead. Since the printhead sees the left of this image first (when rotated 90° counter-clockwise), the bottom of the printhead will print before the top.

Section 5.2.1: Unidirectional Monochrome Printing

The only concern in single colour printing is that the printhead is angled correctly to produce a straight image with dimensions corresponding to the print resolution. This is controlled through the mechanical calibration of the adjustment screws. If the image appeared to be rotated counter-clockwise, then the printhead was rotated in the clockwise direction, and vice versa. Each printhead angle was initially adjusted for straightness by eye and then fine-tuned by viewing the results under the microscope. As can be seen in Figure 5.6, which is made up of several field of view pictures combined in Photoshop, there is a very slight angle perceived in the results when compared with the straight edge of the figure border. Also note that the three column groups of the A, B, and C nozzles are distinctly separated from each other, unlike the original image, due to a combination of the A-B-C firing and the angle compensation from the XUSB software. It is believed that since the C channels fire first, the B and A channels are delayed, causing them to appear further to the left than desired. Given that the C channel fires at the correct time there is a larger gap between where the A channel left off and the C channel next fires. The Yellow ink droplets appear significantly larger than the other colours, despite having the same material properties according to the MSDS sheets. It is not known whether the difference in sizes is due to incorrect efficiency values or a property of each ink, since it is reasonable to assume that less black ink would be required to darken a pixel. Average measurements for dot radii can be found in Table 1.

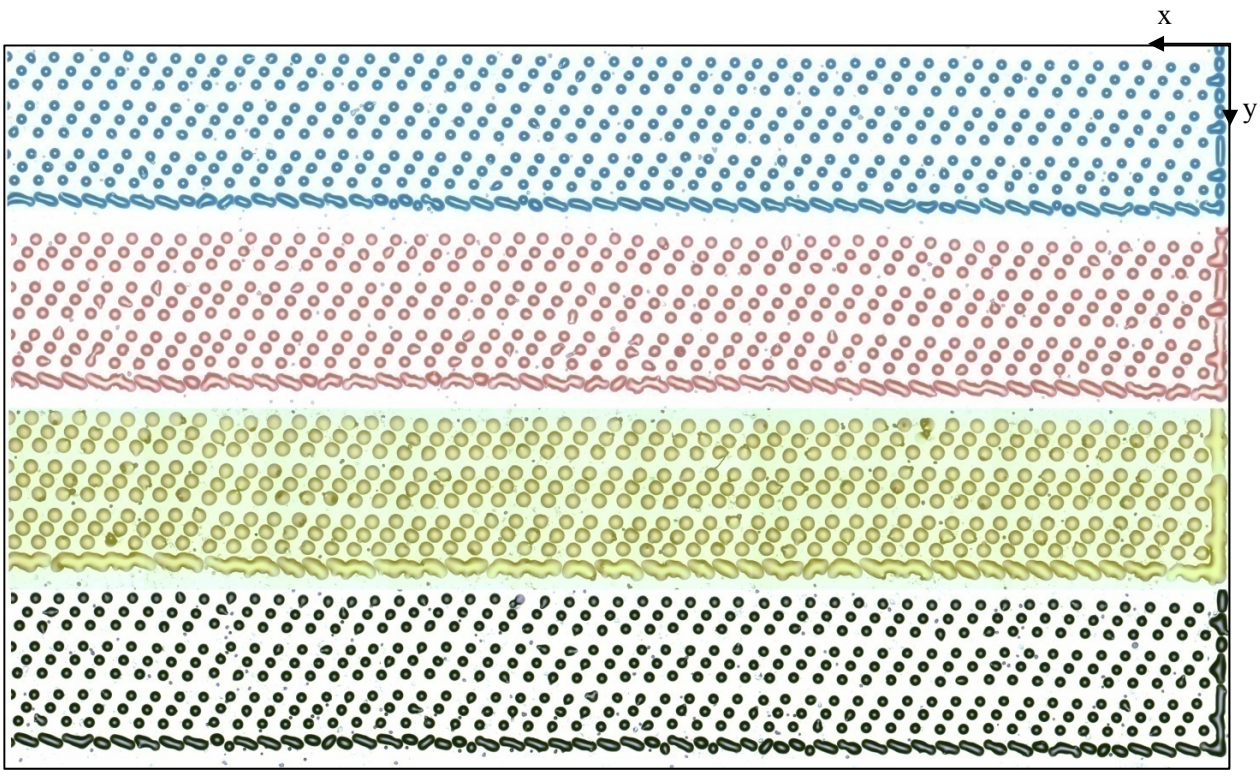

Figure 5.6: Unidirectional Printed Microscope Results

Table 1: Dot Radii Measured from Microscope Images

	Cyan Dot Radius [µm]	Magenta Dot Radius [µm]	Yellow Dot Radius [µm]	Black Dot Radius [µm]
Average	58.8392	63.0349	77.7197	56.6914
Maximum	62.9350	65.6322	80.0173	58.4396
Minimum	57.5406	61.1368	75.5220	55.7424

ImagePro has geometric tools to measure various features from microscope images. In Figure 5.7, a line (L1) was drawn through the centre of the droplet sequence from the first nozzle and the corresponding lines (L2 – L10) for each set of A, B, and C nozzle droplets were roughly drawn through the mean of the droplet centres. Then the angle between L1 and each droplet group line was measured (AF1 – AF9). The data for the angular measurements is found in Table 2, yet these values do not clearly suggest that the printheads are misaligned. There also appears to be a switch in angle after approximately half of the measurements are taken, from either above 90° to below 90° or vice versa. Inconsistent angles may be a sign that the angle is slightly off, though it does not explicitly indicate in which direction the angle should be changed. Using Figure 5.6 as a visual guide, the printheads were adjusted accordingly and the results were re-measured, as shown in the last column of Table 2 for Cyan. The consistency of the measured angles improved over the previous results as indicated by the decrease in standard deviation from 1.55 to 0.64, while the average is also slightly closer to 90°. Figure 5.8 gives the visual outcome. Failure to accurately measure the angles using the ImagePro software could be due to the limited field of view, errors in the positioning accuracy of the table on which the print sample was placed, lack of a suction system to ensure the sample is flat, or human error in measuring, which is estimated to be within ±3 µm (found by making slight adjustments in the position of the lines). Measured dot radii could also be affected by inaccurately tuning the depth of focus of the microscope.

Table 2: Droplet Placement Accuracy [degrees]

Column	Cyan Angle	Magenta Angle	Yellow Angle	Black Angle	Cyan Angle After Calibration
AF1	91.68	89.39	90.12	89.51	90.34
AF2	91.78	89.58	90.12	89.67	90.77
AF3	91.87	89.57	90.3	89.09	91.07
AF4	92.29	90.01	90.33	89.72	91.05
AF5	88.23	90.56	90.70	89.09	89.42
AF6	88.67	89.71	88.63	90.37	89.46
AF7	89.17	88.94	88.83	91.33	89.79
AF8	89.76	88.87	88.34	91.11	90.00
AF9	89.9	88.82	88.10	91.63	90.53
Average	90.37	89.49	89.50	90.17	90.27
Standard Deviation	1.55	0.57	1.00	0.98	0.64

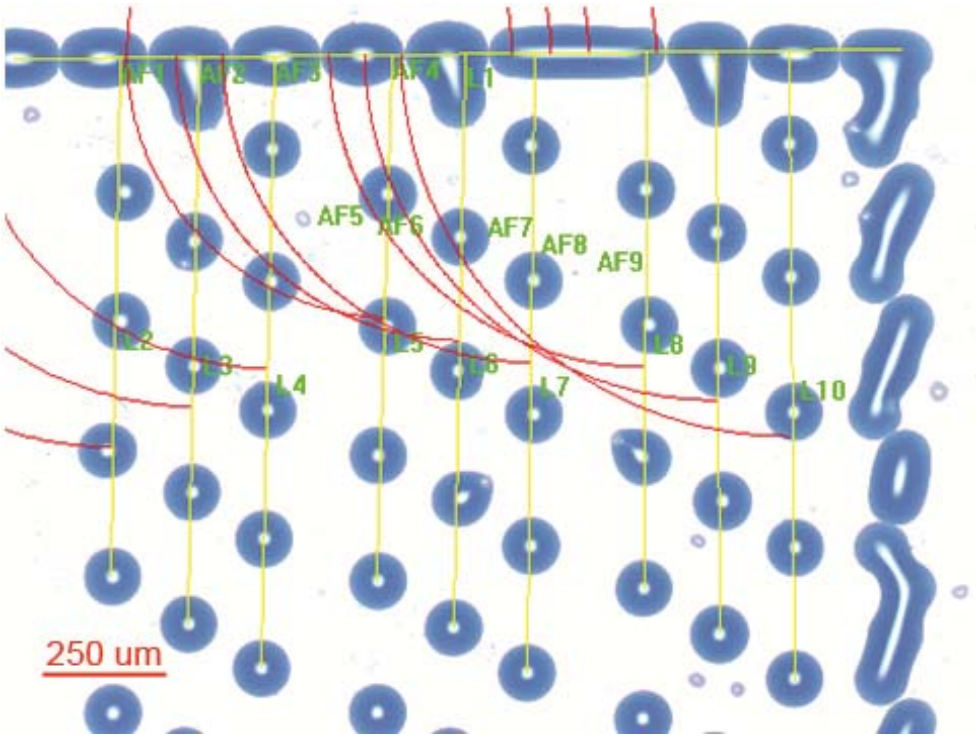

Figure 5.7: Angle Measurements

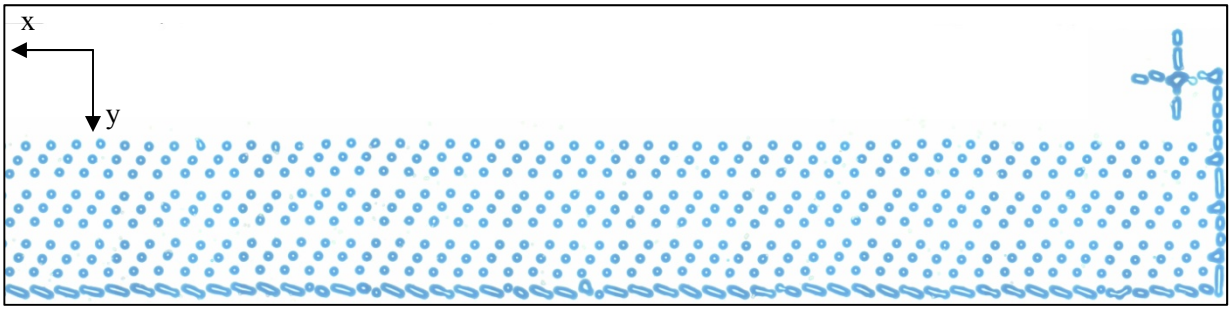

Figure 5.8: Microscope Image of Cyan Printed After Calibration

Section 5.2.2: Unidirectional Multi-colour Printing

In multi-colour printing, each printhead must be aligned with the other printheads such that each droplet from the nozzles of one printhead will directly overlap the droplets from the nozzles of the next printhead when the same image is sent to both printheads. This requires vertical alignment by mechanical adjustment from the screws and horizontal alignment achieved through the software offsets. First, it was assumed that one printhead was in the correct position, and then each printhead was aligned relative to the first printhead. It may be necessary to recheck the alignment of each printhead, in case the angle was accidentally changed during the vertical calibration. Test images were viewed as soon as possible after printing, since the inks merged together after extended periods of time and any difference in alignment between the two colours would be indistinguishable.

For example, when aligning magenta with cyan, if magenta printed too late, then the offset value in the XUSB software was decreased. Similarly, if magenta printed too early, then the offset value was increased. If the magenta image was printed slightly lower than the cyan image, then it would need to be shifted up using the adjustment screws. Both screws would need to be adjusted equally so as not to shift the angle. In the first image of Figure 5.9, with Magenta overlapping Cyan, the dots are slightly distorted, indicating that the two colours are not perfectly aligned. The Magenta printhead needs to be shifted to the right and slightly upward, which could be accomplished by loosening screw A, loosening screw B, or some combination of both. It may even be necessary to decrease the delay for the magenta printhead in the XUSB software. An attempt was made to measure the distortion between Cyan and Magenta, as shown in Appendix D. Since the dots were not very circular, the smallest and largest diameters were taken. The average of the large diameters was actually roughly equal to the radius of dots when Cyan and Magenta are correctly aligned, so it is difficult to use this information when aligning the printheads.

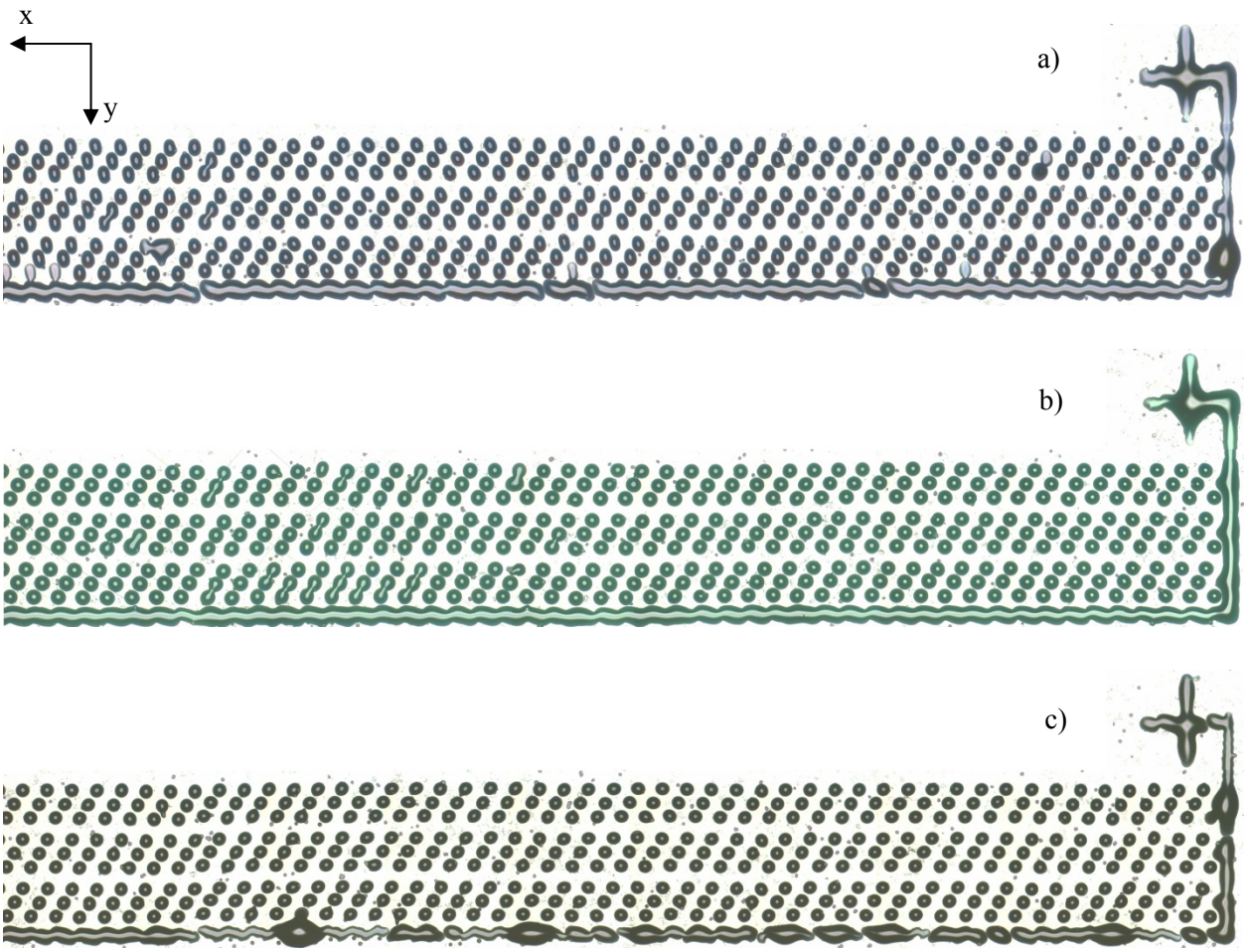

Figure 5.9: Multicolour Unidirectional Printed Microscope Results- a) Magenta on Cyan, b) Yellow on Cyan, c) Black on Cyan.

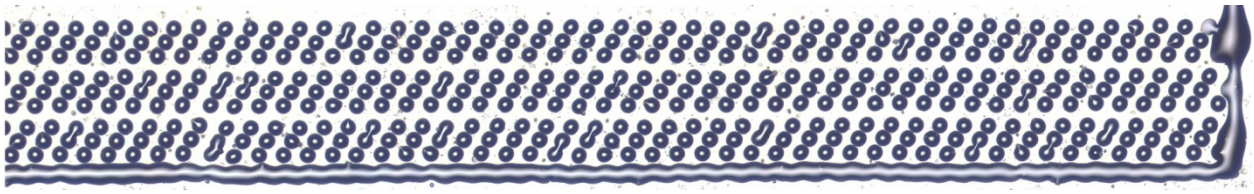

Figure 5.10: Microscope Image Printed After Realignment of Magenta

Section 5.2.3: Unidirectional Multi-swath Monochrome (Large Image) Printing

A large image is basically an image made of multiple swaths, though the size of the image is limited to that of bitmap format as the XUSB software only accepts bitmaps for binary printing and Photoshop does not support images larger than 300 000 x 300 000 pixels. Blank lines that appear between swaths indicate that the printheads are moving in the x-direction a distance greater than the height of a swath (due to vertical offset). Similarly, dark lines or an image that is too short suggest that the change in motion in the x-direction needs to be increased. Each swath must also be positioned directly below the previous swath, or else jagged edges appear in the image (due to horizontal offset). Figure 5.11 shows the two possible offset errors between successive swaths, using blocks to represent sections of an image. Since it was necessary to separate the droplets from the A, B, and C channels, all measurements were made between droplets from the same channel set. The overall image angle due to sample misalignment was straightened in Photoshop and the angle was incorporated into the measurements. However, this angle was typically less than ±0.5°, which had an effect of less than 0.0001 µm on the measurements and thus compensation was unnecessary.

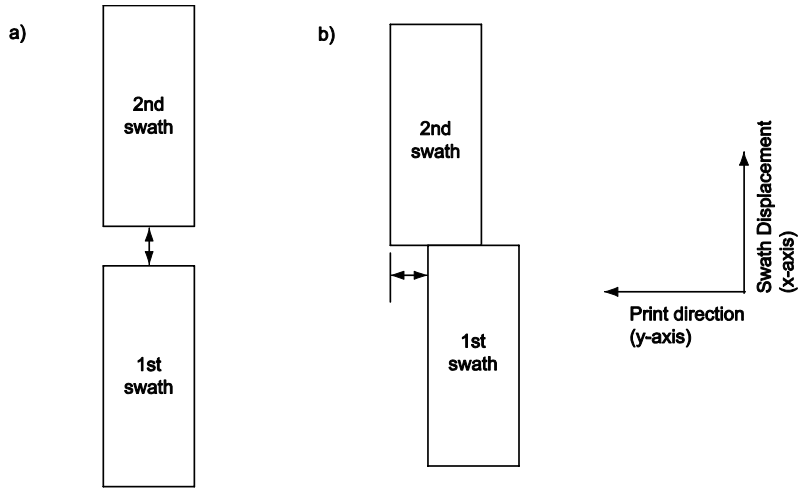

Figure 5.11: Alignment Errors - a) Vertical Offset, b) Horizontal offset

It was estimated that the distance between any two dots should be 82.6 µm for a resolution of 309 DPI, based on the printhead specifications and calculations in Section 3.2.1 and Appendix B. Therefore, the distance between two successive dots from the same channel group is three times this amount, which is approximately equal to 247.9 µm. As there are three groups of A-B-C droplets, there are a total of nine samples to get an average from. Figure 5.12 shows an example of how the offsets were measured. Circles (C) were drawn as close to the actual droplet diameters and positions as possible and the vertical (horizontal) offsets were calculated as the difference in vertical (horizontal) positions (i.e. C2y – C1y). The average distance between dots from an arbitrary section within the first

swath of Figure 5.13a was found to be 245.1 µm, which is reasonably close to the estimated value. The vertical offset between swaths should also be about 245.1 µm to provide a continuous image from swath to swath. Recalling that this vertical offset is mostly affected by the x-axis trajectory, the offset can be adjusted accordingly. Since the image is composed of two swaths and the image was set to repeat, there are a total of four swaths. However, between swaths 2 and 3, there is a line representing the first nozzle, making it difficult to measure the offsets. Thus, only the vertical offsets between the first two swaths and the last two swaths of the image were measured.

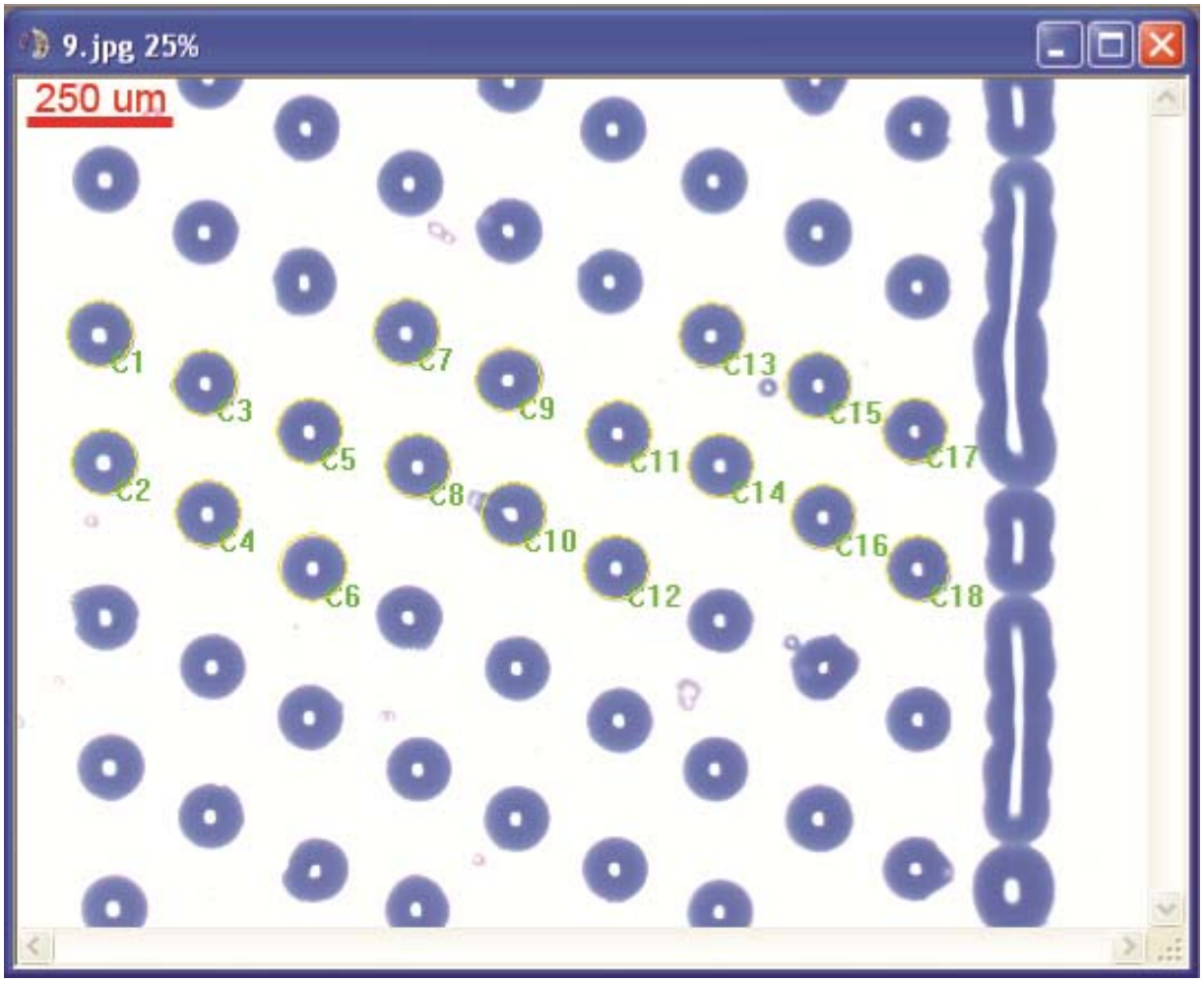

Figure 5.12: Measuring Droplet Radius and Position

Table 3 gives the vertical offsets measured from the microscope images for a unidirectional monochrome print. Between the first two swaths, the average vertical offset was measured to be 221.5 µm, while the distance between the last two swaths was 264.4 µm. At first, only the distance between the first two swaths was taken into account and the trajectory change in the x-direction was increased by 0.01 mm. Subsequent tests revealed that the discrepancy between the first two swaths and the last

two swaths remained. It was then concluded that the low values from the first to second swaths could be caused by motor backlash. As the printheads always return to home position at the end of a print, the gears must reverse direction from the first swath to the second swath at the start of the next print job. As a temporary solution, the x-axes were manually jogged forward in Control Desk before starting to print. The trajectory was later changed to retract past the home position at the end of a print before moving forward to zero.

At this point, it was realised that the printheads were still angled out of alignment and were consequently realigned. This may have been a result of printing slightly more than 1.0 mm above the substrate due to a miscalculation in homing position. However, the same alignment process was followed and afterward, the swath width was changed from 10.41 mm to 10.42 mm to compensate for the vertical offset between swaths. Looking at the new results after fine-tuning the alignment, the difference of 3.494 µm between the average vertical offset for swaths 1 to 2 and the average vertical offset for swaths 3 to 4 is reasonable considering the amount of measurement error.

Table 3: Vertical Offset Measurements

	Between Two Dots Within a Swath [µm]	Before Fine-tuning Alignment		After Fine-tuning Alignment	
		Between Swath 1 and Swath 2 [µm]	Between Swath 3 and Swath 4 [µm]	Between Swath 1 and Swath 2 [µm]	Between Swath 3 and Swath 4 [µm]
Average	245.1250	221.4844	264.4398	240.3494	236.8553
Maximum	257.2617	242.3910	274.5937	251.2971	257.1343
Minimum	231.2729	216.6836	249.0882	223.2748	217.5752

Figure 5.13a shows the image for the unidirectional multi-swath results. The measured horizontal offsets can be found in Table 4. The horizontal offset is slightly worse between swaths 3 and 4. Considering the accuracy of the loop-shaping controller is within +/- 28 µm, as shown in Section 4.3, it was determined that the accuracy of droplet placement was reasonable. An error of ±20.2 µm in addition to the estimated ±3 µm of measurement error corresponds to around 40.6% of the average droplet diameter of 57.19 µm or 28.3% of the 82 µm dot separation for 309 DPI.

Table 4: Horizontal Offsets for Unidirectional Printing

	Swaths 1-2 [µm]	Swaths 3-4 [µm]
Average	9.541611	37.2616
Maximum	23.503	53.0452
Minimum	1.8079	16.184

Given the difficulty in adjusting the vertical offset discussed earlier, testing was also done at 1.5 mm above the substrate and 0.5 mm above the substrate as shown in Figure 5.13b and Figure 5.13c

to determine how printing at heights other than 1 mm would affect the results. The 1.5 mm gap showed significantly worse positioning accuracy such that the entire image appears slanted, while the 0.5 mm spacing increased the chances of smearing the print as the bottom plate or dust particles touched the surface. Both the 0.5 mm and 1.5 mm clearances produced droplets of slightly smaller radius than at the standard clearance [Table 5]. This could indicate that 1.0 mm is the optimal clearance, though the varying droplet size could also be due to other factors, such as settling time or measurement error. Nevertheless, these results show that a smaller substrate clearance is preferable to a larger one.

Table 5: Droplet Radius [µm] Comparison for Different Substrate Clearances

	1.0 mm Above	0.5 mm Above	1.5 mm Above
Average	56.74776	55.9422	54.64355
Maximum	59.66048	58.4396	56.64148
Minimum	52.4289	53.9443	52.14613

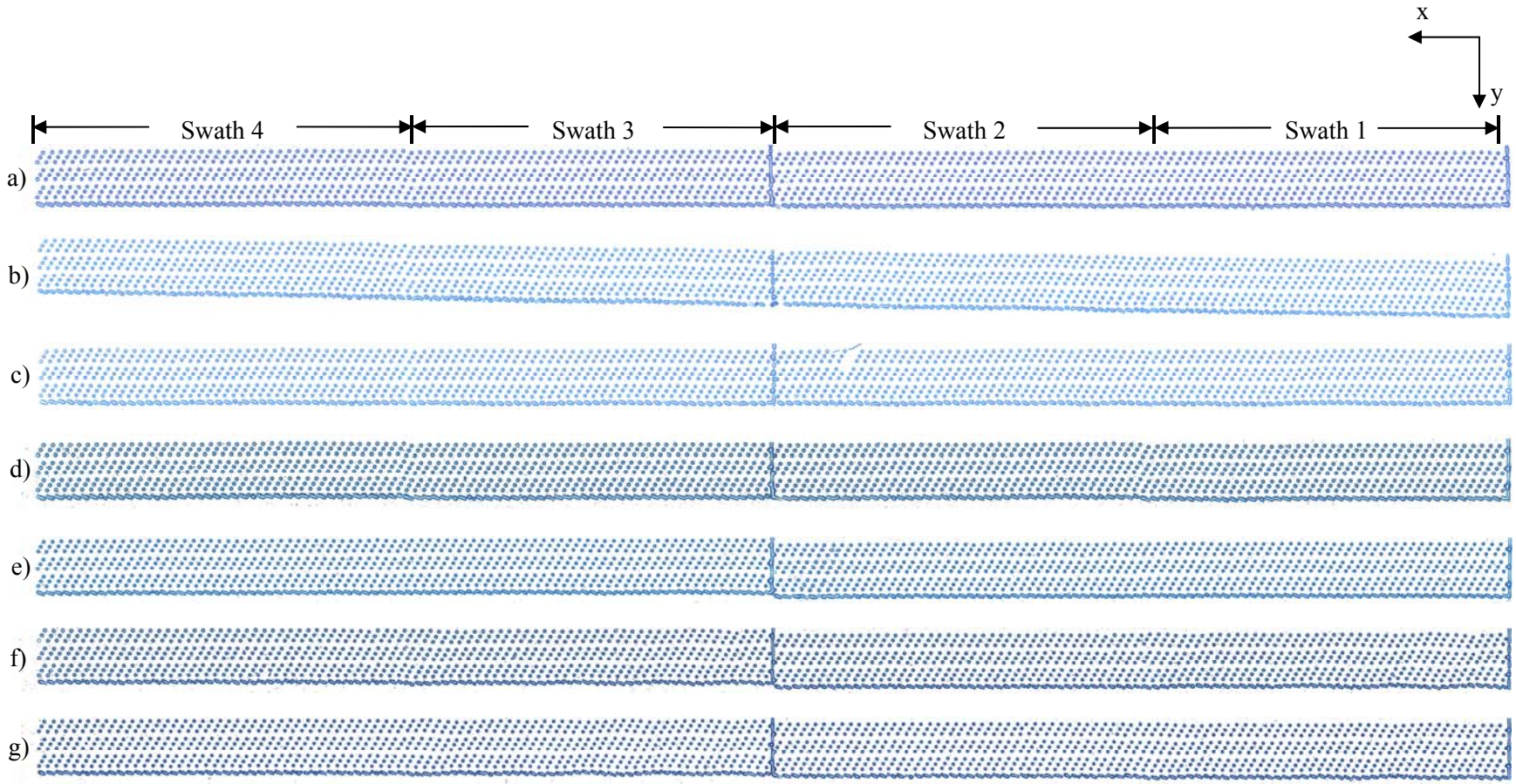

Figure 5.13: Calibration Results – a) Unidirectional Monochrome, b) 1.5 mm Above Substrate, c) 0.5 mm Above Substrate, d) Bidirectional with 1PD at 250 mm/sec, e) Bidirectional with 2PD at 250 mm/sec, f) Bidirectional with 1PD at 50mm/sec, g) Bidirectional with 2PD at 50 mm/sec

Section 5.2.4: Unidirectional Multi-swath Multi-colour Printing

A verification of all the steps taken until this point would be to print a large, multicolour image to show that all the colours are aligned individually and with each other. The original photograph in Figure 5.14 was taken with a digital camera, courtesy of Ivan Chin. This test image was arbitrarily chosen based on its range of colour composition and complex feature detail. Though it is more difficult to differentiate each colour in a photograph, it will provide proof of concept. Figure 5.15 shows the full-scale scanned image of the actual print on Xerox paper. The high droplet density causes the colours to be much darker than the original image.

Figure 5.14: Unidirectional Multi-swath Multi-colour Test Image - Courtesy of Ivan Chin (1:1 scale)

Figure 5.15: Scan of Unidirectional Multi-swath Multi-colour Image Printed on Xerox Paper - Darker and less clear than original photograph (1:1 scale)

Section 5.2.5: Bidirectional Monochrome Printing

The benefit of bidirectional printing is that the print is completed in significantly less time, approximately 15% reduction from unidirectional printing in this thesis work, as mentioned in Section 4.4. One issue is ensuring that the reverse swath prints exactly where the forward swath left off, which can be achieved with several methods available from the XUSB software, two of which will be discussed. The first method allows the XUSB to determine where it should start the reverse print based solely on the PD signal from the forward swath and the encoder counts it receives from the linear encoder. It is believed that some error could be introduced in this method due to signal noise in decoding the sinusoidal encoder signals into multiple pulses and tilting or vibration of the printhead assembly, which would lead to different displacement than that registered from the linear encoder. This would result in an offset between the forward and reverse swaths. A second method involves calculating where a second PD signal should be placed along the reverse swath, based on the printing trajectory. This method is more difficult than it sounds since the trajectory will overshoot the position where the forward swath printing finishes, which compensates for deceleration of the printheads and the offset between the four printheads. It is also necessary for all printheads to receive an image in bidirectional 2PD printing; otherwise the offset will not be correct (cyan prints first in the forward direction and black prints first in the reverse direction).

Droplet placement error is a combination of nozzle placement error with respect to the absolute position of the printheads and the jet trajectory error as a result of the angle deviation of the droplet trajectory from the absolute vertical [38]. Xaar specifications state that at 1 mm clearance above the substrate the printheads can print at a linear speed up to 635 mm/sec with a maximum droplet deviation of 1°. According to Equation (5) in Section 2.2, if the droplets travel at a vertical velocity of 6000 mm/sec and the print speed is 250 mm/sec, then during the time it takes for the droplet to travel the 1 mm distance to the substrate, it will have undergone a horizontal displacement of 0.0417 mm. This droplet placement error corresponds to approximately 2.39° deviation, higher than the specified deviation angle. Travelling at the maximum speed of 635 mm/sec would result in a 6.04° deviation, whereas the 1° deviation is only achievable at print speeds of approximately 105 mm/sec or less. The displacement at 250 mm/sec is quite significant, considering the dot separation should only be 0.082 mm. For unidirectional printing the droplet momentum had little effect, since all the dots would be equally shifted by 0.0417 mm. However, this error could be problematic when attempting to print bidirectional, since it will, in effect, be doubled as the forward swaths are shifted forward and the reverse swaths are shifted backward. There may be some error since the equations are specifically for a horizontally ejected droplet and it was assumed that air convection was not significant based on the size

of the droplets. The results correspond almost exactly with calculations based on simple geometry. Detailed calculations can be found in Appendix D for the droplet diameter and ink density specified by Xaar.

The 1PD and 2PD bidirectional prints can be found in Figure 5.13d and Figure 5.13e, respectively. The results are summarised in Table 6, where it is evident that the method of bidirectional printing with 2PD signals produced a much more accurate horizontal offset compared to the 1PD and even the loop-shaping controller unidirectional prints. When using the 1PD method, the option to adjust the reverse swath offsets is not available since it relies on the XUSB controller and software. Thus, the maximum measured displacements are fairly close to the 0.0834 mm calculated based on the print and droplet velocities. The 2PD method is more versatile due to the option of manually adjusting the reverse offsets for each printhead separately in the XUSB software and by adjusting the start of the second PD signal established by the trajectory and encoder readings; thereby compensating for some of the displacement caused by droplet momentum and possibly some of the steady-state error inherent in the machine. It should be noted that the bidirectional 2PD test revealed a large offset between swaths 2 and 3, though it was difficult to measure due to the line of ink printed from the first nozzle (used as a straightness edge). Printing at a lower speed of 50 mm/sec resulted in over 50% reduction in horizontal offset for the 1PD case (Figure 5.13f). For the 2PD bidirectional method, the offset was accounted for by adjusting the second PD signal so that the lower speed did not have a significant effect on the accuracy, which indicates that the offset is dependent on velocity (Figure 5.13g). This concludes that the 2PD bidirectional method should be used for high-speed precision printing. All methods showed less offset than was calculated using the droplet placement error calculations.

Table 6: Bidirectional Horizontal Offsets [µm]

	1PD Swaths 1-2 at 250 mm/sec	1PD Swaths 3-4 at 250 mm/sec	1PD Swaths 1-2 at 50 mm/sec	1PD Swaths 3-4 at 50 mm/sec	2PD Swaths 1-2 at 250 mm/sec	2PD Swaths 3-4 at 250 mm/sec	2PD Swaths 1-2 at 50 mm/sec	2PD Swaths 3-4 at 50 mm/sec
Average	57.8403	49.0494	20.8784	15.6839	18.8805	14.18538	17.9815	14.1853
Maximum	71.0266	63.834	42.2563	44.055	26.9721	28.7703	41.357	23.3758
Minimum	42.257	36.862	0.899	1.7981	8.0916	2.697	1.7981	0.899

Section 5.2.6: Bidirectional Multi-colour Printing

Theoretically, multi-colour bidirectional printing should operate similarly to monochrome bidirectional printing. However, another problem discovered with bidirectional printing is that the printheads will print in a specific order pre-determined by their positions on the mounting plate. Based on this single row setup, Cyan will print first and then Magenta will print on top of Cyan, followed by Yellow, and then Black. However, in the reverse direction the printheads will print in the opposite order, starting with Black, then Magenta, then Yellow, and then Cyan on top. The result is a slightly different overall colour for the reverse swath than would be found in the forward direction, and occurs both for images where the same image is sent to each colour and for images where the colours have been properly separated in Photoshop. Upon close inspection of Figure 5.16, there is a noticeable striping pattern of light (KYMC) and dark (CMYK) swaths. In this figure the first swath is actually a KYMC pass. Since there are an odd number of swaths, a blank swath was inserted at the top of the image. The striping is less apparent in the whiter areas of the image since the droplet density is significantly lower and there are fewer overlapping colours. Due to this colour disparity, it is believed that commercial printers typically print single-colour images in bidirectional, while multi-colour prints are printed in unidirectional, based on the smaller length of time needed to complete a monochrome image versus a multicolour image. The problem of colour disparity can be solved by having another set of CMYK printheads in the opposite order alongside the original printheads, either on the same swath or on a separate swath, so that one set will only print in the forward direction, and the other set will only print in the reverse direction. However, this method would be costly to implement and may not be possible using the XUSB software.

Figure 5.16: Scan of Colour Disparity in Bidirectional Printing - Dark swaths represent ink deposited in the order of CMYK and light swaths represent ink deposited in the order of KYMC (1:1 scale).

Another solution is to offset the printheads in the x-axis so that, regardless of the printing direction, the printheads will always print in the same sequence. To implement this solution, a new printhead mounting plate was designed and re-implemented to accommodate for bidirectional multicolour printing, shown in Figure 5.17. If the printheads are vertically offset from each of the previous printheads by one swath width (measured to be 10.41 mm in Section 5.2.3), then the furthest colour, Cyan, will always print first since it prints one swath in advance of Magenta. When the order of printheads is KYMC the colour actually appears brighter than the CMYK order. However, the order was maintained as CMYK for simplicity and compatibility with the earlier work. Since there is no setting in the XUSB software to offset an image by swaths, the images need to be manually adjusted in Photoshop before printing and the trajectory must include an extra three swaths. For example, since Cyan prints first, there will be three swaths at the end of the print where the Cyan printhead does not print anything while it is waiting for the other three colours to finish printing. In Photoshop, this corresponds to adding three blank swaths, 378 pixels, to the canvas size at the bottom of the Cyan image if the image information is sent from top to bottom. For Magenta, there is a delay of one swath while it waits for Cyan to print first. Thus, one blank swath was added to the top of the Magenta image and two blank swaths were added to the bottom. Similarly, two blank swaths were added to the top of the Yellow image, followed by one blank swath at the bottom, and Black had three blank swaths added to the top of its image. Figure 5.18 illustrates the bitmap files (rotated clockwise) for each colour. Printhead angle correction has also been applied to these images, prior to adding the blanks swaths. It should be noted that the time improvement from unidirectional printing to bidirectional printing would be slightly less than 15% now that the bidirectional method requires three additional swaths.

To align the printheads, the same calibration methods as outlined in the previous sections were employed. The home position was reset and the offsets for bidirectional printing were readjusted. It was found that when printing with the new mounting plate, the swath-to-swath displacement had changed significantly from 10.41 mm to 10.31 mm. This could be due to a number of reasons, including changing the angle of the printheads from 36.87° to 36.9°. Since the vertical offsets between each printhead were designed based on the 10.41 mm offset, there is a significant offset between the black and cyan printed images of approximately 0.7 mm, which cannot be compensated for using the adjustment screws. Another plate was designed using the 10.31 mm distance between printheads and all four colours were able to be aligned with each other. An image was successfully printed without the bidirectional striping or vertical offset errors.

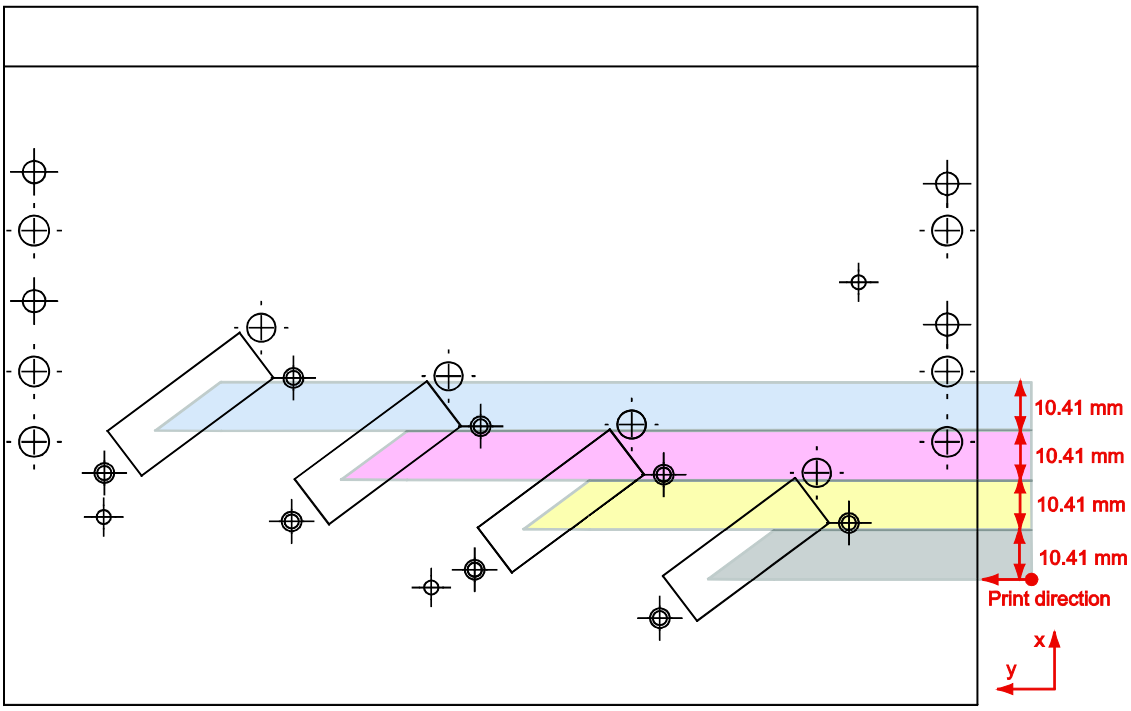

Figure 5.17: Mounting Plate for Bidirectional Multicolour Printing (Top View) [mm] - Cyan will always print first.

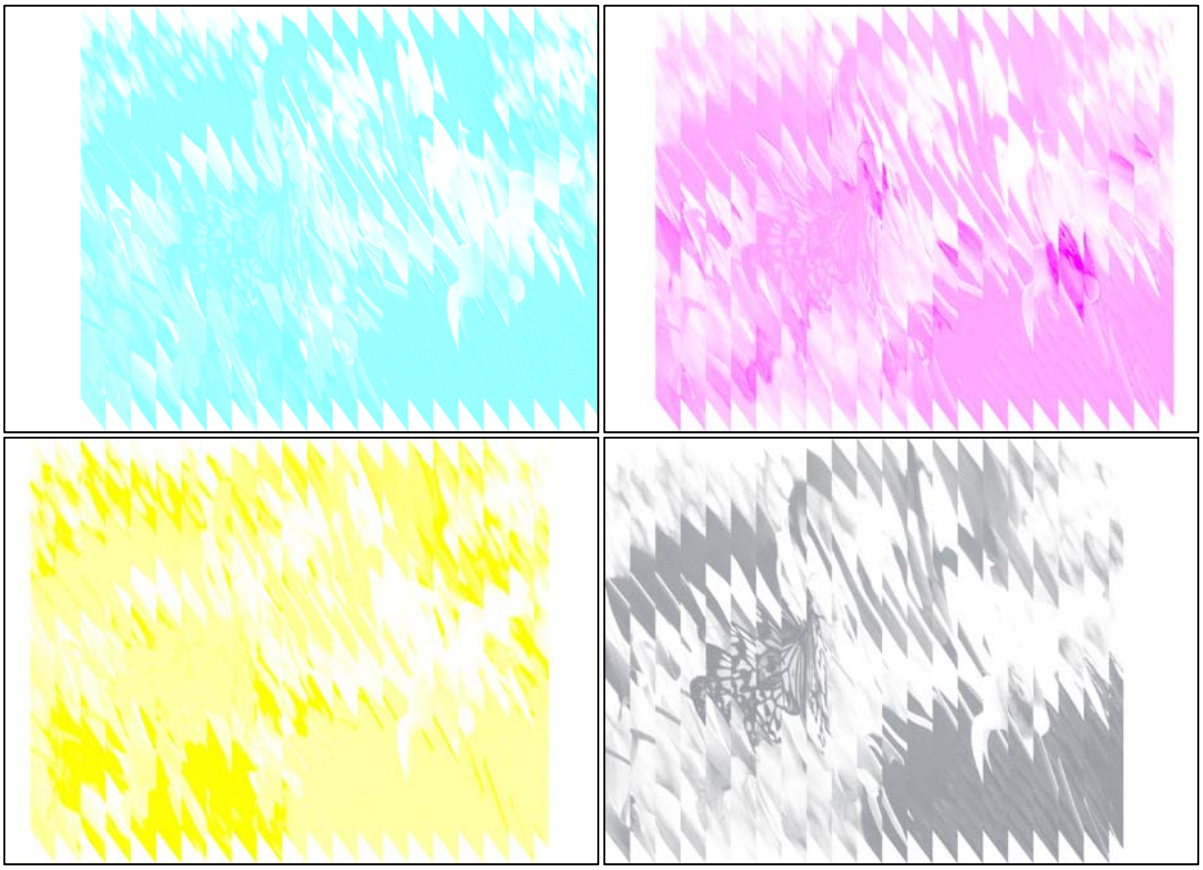

Figure 5.18: Image Processing for a Bidirectional Image - Top-left is Cyan, top-right is Magenta, bottom-left is Yellow, and bottom-right is Black (images have been colourised for visual effect)

Section 5.3: Additional Issues

During testing, it was found that a nozzle on the Magenta printhead would not print. Upon closer inspection, it was determined that the ink droplets from the nozzle were being ejected in a different location. This problem would not disappear even after purging and wiping the nozzle plate at different pressures and time periods or wiping with the printhead cleaning solution. The printhead was then flushed with the cleaning solution and then viewed under the microscope. From the printed calibration image in Figure 5.19, it was noted that the droplet came from the 43rd nozzle (47th including the four dummy nozzles at the ends). The second missing droplet appears to have merged with another droplet. At first glance there was no apparent damage to the nozzle shown in Figure 5.20. However, careful inspection shows a very faint line leading to the nozzle. Though it does not appear to affect the nozzle, this line is likely a scratch causing the nozzle to deform, while similar scratches seem to have no influence on the other nozzles. A test print after flushing verified that the printhead was not clogged and the printhead was replaced.

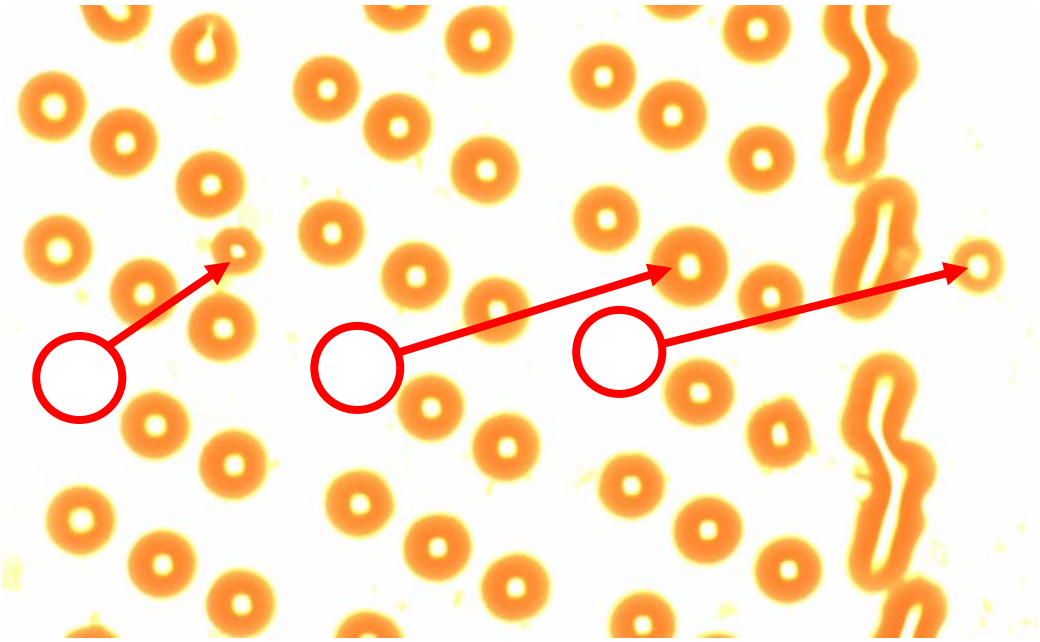

Figure 5.19: Print from Damaged Magenta Nozzle - Droplets from one nozzle are being misdirected.

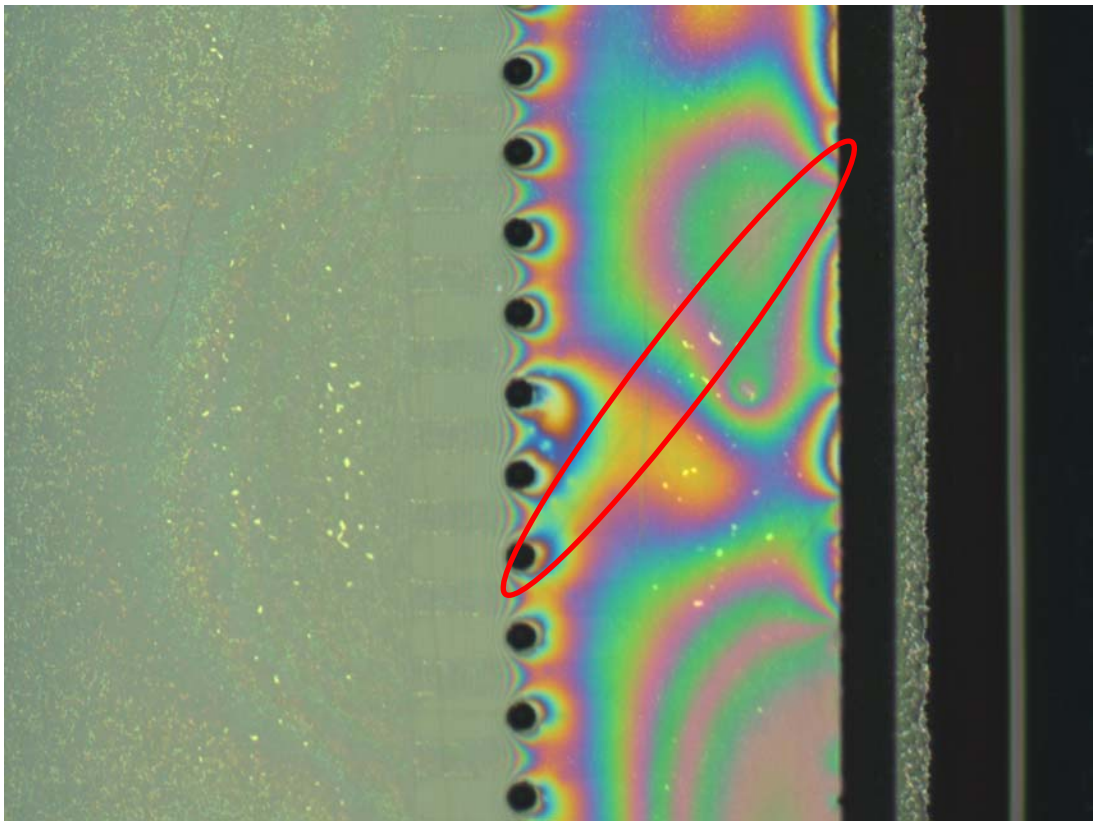

Figure 5.20: Damaged Nozzle on Magenta Printhead - Malfunctioning nozzle is likely due to a faint scratch.

Another issue found was that the printheads were prone to leak when the system was turned off for long periods of time. Though each component was examined carefully, the leakage was possibly caused by air gaps or cracks in fittings, dysfunctional printheads, malfunctioning header tank pressure sensors, or insufficient negative pressure to maintain ink meniscus. On one occasion, a header tank was believed to have failed. After printing for a variable period of time the printhead would continue to leak almost as much as when the vacuum is not being applied and the manual valve is open. When the manual valve was closed, the ink would slowly move toward the ink trap bottle and vacuum as when there is too much pressure applied. Once the pressure stabilised after the system had been turned off overnight, the printhead would print several images normally and then suddenly start to leak again. Since then the issue has not occurred and may have been due to overdriving the printhead while testing various settings. A replacement header tank should be ordered in case the problem has not been resolved.

Section 5.4: Conclusions

This chapter described the process and issues involved in calibrating Xaar 126 printheads, as well as characterising the droplet placement accuracy. The precision of droplet placement is very important in generating a quality image, and even more so for future MEMS and nanotechnology applications. There are many factors which influence the accuracy of the printheads including droplet firing speed, print speed, printhead orientation, and precise motion tracking. Printhead orientation was adjusted mechanically using fine thread screws or through software offsets. PD signals, trajectory generation, and motion control influenced the overall swath offsets. Calibration images were printed on high gloss HP photo paper to reduce droplet distortion and measurement error, while pictures were printed on Xerox inkjet paper for optimal absorption and minimal bleeding. The calibration images were used to align the printheads and were viewed under a microscope at 50x magnification and analysed using ImagePro software for droplet size and relative position. The horizontal resolution of the printheads is inherently worse than the vertical resolution due to the frequency of nozzle firing in the piezoelectric shear mode design. Thus measurements were only made within nozzles of the same group.

The system was tested and calibrated systematically by adding one element of complexity at a time to determine the accuracy and capability of the printheads. These main modes were single colour unidirectional, multicolour unidirectional, single colour bidirectional, and multicolour bidirectional printing. Bidirectional tests were further divided into different speeds and whether one or two PD signals were generated. Monochrome unidirectional printing provided the basis for the swath angle, which was found to be roughly 90°±1°. Multicolour unidirectional printing evaluated how well each colour aligned with each other both vertically and horizontally. From the unidirectional results, the vertical swath-to-swath displacement was corrected to 10.42 mm. It was also shown that printing clearances higher than 1 mm significantly reduced the quality of the print. Smaller clearances may be possible at an increased risk of smearing either the print before it absorbs into the substrate or any ink found on the bottom of the plate or the printhead nozzles, depending on the surface finish of the substrate. Bidirectional printing reduced print time with little increase in horizontal offset between swaths. For high-speed printing accuracy, generating 2PD signals produced much better results than the 1PD option. A new printhead mounting plate was designed where the printheads were offset vertically from each other by one swath width to eliminate the colour striping problem resulting from switching the order in which the colours were deposited during bidirectional printing. This solution required additional image processing of adding blank swaths to the beginning and ending of each image corresponding to the printhead position on the plate. Bidirectional colour printing was achieved at the maximum speed of the router (250 mm/sec) with comparable accuracy to unidirectional printing.

Chapter 6: Printing on Different Media

To prove the integration of printing and cutting for sign and furniture industries, it was necessary to show the capability of printing on substrates such as wood. Cutting, or engraving, which would follow the printing process, has already been researched on the router and so will not be investigated further in this thesis. As discussed in the previous chapters, the main factor in printing high quality images is precise droplet placement. In order to print on materials such as wood and improve the colour appearance, ink jet printers generally require a special pre-coating to help the ink cure and prevent bleeding. Most satisfactory results on wood in industry have been achieved using water-based inks. However, the ink used in this thesis is oil-based, which relies mainly on direct absorption into the substrate and is intended for paper rather than wood. As the ink tends to absorb into the grain of the substrate, different types of wood and coatings were tested to find the optimal conditions for a high quality image.

Hymmen uses three major steps for direct printing on wood: preparation of the substrate, preparation of printing base, and sealing of the surface. The surface of the substrate should be clean and is prepared by sanding, filling, and smoothing, depending on the substrate material. For particle boards there is usually a section for a water-based filler and a section for a UV-filler, followed by drying. MDF requires a water-based primer to prepare for adhesion of the filler and just one section for filling and drying. Next, two to three base coats are applied, each followed by a dryer, and then two or more printing machines. Sealing consists of two layers of UV-lacquer with subsequent curing; corundum particles are added to lacquer layers for abrasion protection. This process developed by Hymmen was not found until later in this research. However, a few steps could be applied to the initial case studies found in this section, such as preparing the MDF with an oil-based primer, sanding, applying an oil-based filler, and an oil-based base coat before printing the image. [1]

This chapter will present the results from printing on different types of wood and coatings. A walnut wood pattern was chosen to simulate the effect of manufacturing furniture or flooring with inexpensive materials. The original image can be found in Figure 6.1, with the actual size of the image being 211.67 mm x 159.3 mm. A darker image such as this one was preferred in order to test the limits of the system, since the lower density of ink in lighter images makes them more easily adaptable to different substrates. Conclusions are provided in Section 5.4.

Figure 6.1: Wood Pattern Test Image- 211.67 mm x 159.3 mm. Courtesy of www.designyourwall.com [39]

Testing was first done with various types of paper. The Technical Association of the Pulp and Paper Industry (TAPPI) recently introduced the brightness standard, TAPPI T 452, in order to compare different paper products against each other [40]. Here, brightness is defined as the measurement of blue reflectance of paper, based on a light source shining onto the paper at 45° while optic receivers view the same spot at 0° to simulate the natural viewing position when looking at the paper. Higher numbers indicate more light is reflected off the paper; whiter sheets of paper are generally more appealing due to better image contrast. It was found that the paper was susceptible to ripples and would often become smeared with ink left on the bottom of the mounting plate or from the printheads themselves. Since there is only roughly 0.75 mm distance between the paper surface and the mounting plate, there is not much room for variation in the surface flatness. Thus, for paper tests, the sides of the paper were taped down while trying to ensure tension in the paper. Wood substrates were assumed to have better surface finish and therefore no risk of contact between the substrate and the printhead mount.

The results of Hammermill paper, weighing 75 g/m^2 and brightness of 92, shown in Figure 6.2 were found to be acceptable, though there was some slight bleeding along the edges of the image and

the image colour was much darker than the original image. Xerox inkjet paper, 90 g/m^2 and brightness of 92 was found to have less bleeding along the edges and brighter colour, as seen in Figure 6.3. The heavier Xerox paper was likely able to handle a heavier application of ink than the Hammermill paper, which is more suitable for high-volume printing. Both were still unacceptable in terms of calibration as the droplets would absorb into the fibres of the paper, making it difficult to determine the exact size and location of droplet deposition. HP high-gloss paper, weighing 280 g/m^2, was also tested with a calibration image, though the oil-based ink provided by Xaar would not absorb into the HP paper even after a long period of time. However, this also allowed the ink droplets to be highly visible, since the droplets were not distorted by the fibres in the paper, as in the Xerox inkjet paper. Calibration tests were thus printed on glossy paper and viewed under a microscope, as demonstrated in Chapter 5.

MDF is made out of wood waste fibres glued together with resin by heat and pressure, and has been shown to be readily milled into parts depending on feed parameters, cutting tool, and workpiece quality. The low cost of MDF makes it an ideal choice for the sign and furniture industries and was thus one of the main test materials. Each layer in an MDF panel has an effect on the final surface roughness, which is a factor in how well ink droplets are placed [41]. As shown in Figure 6.4, printing directly on MDF showed more bleeding than on paper, causing the image to appear much darker and losing sharp details, despite the image being significantly lightened in Photoshop. The non-paper images may be distorted as a result of the digital camera viewing angle. Various coatings were also tested that did not absorb the ink very well, taking several days for the ink to dry. Coatings that were manually applied were painted with a fine latex brush and allowed to dry according to their respective instructions. Figure 6.5 shows MDF coated with semi-gloss varnish, which allowed the colours to bleed together to form an incoherent image. A double coat of rust paint on MDF produced a dark image with heavy bleeding in Figure 6.6.

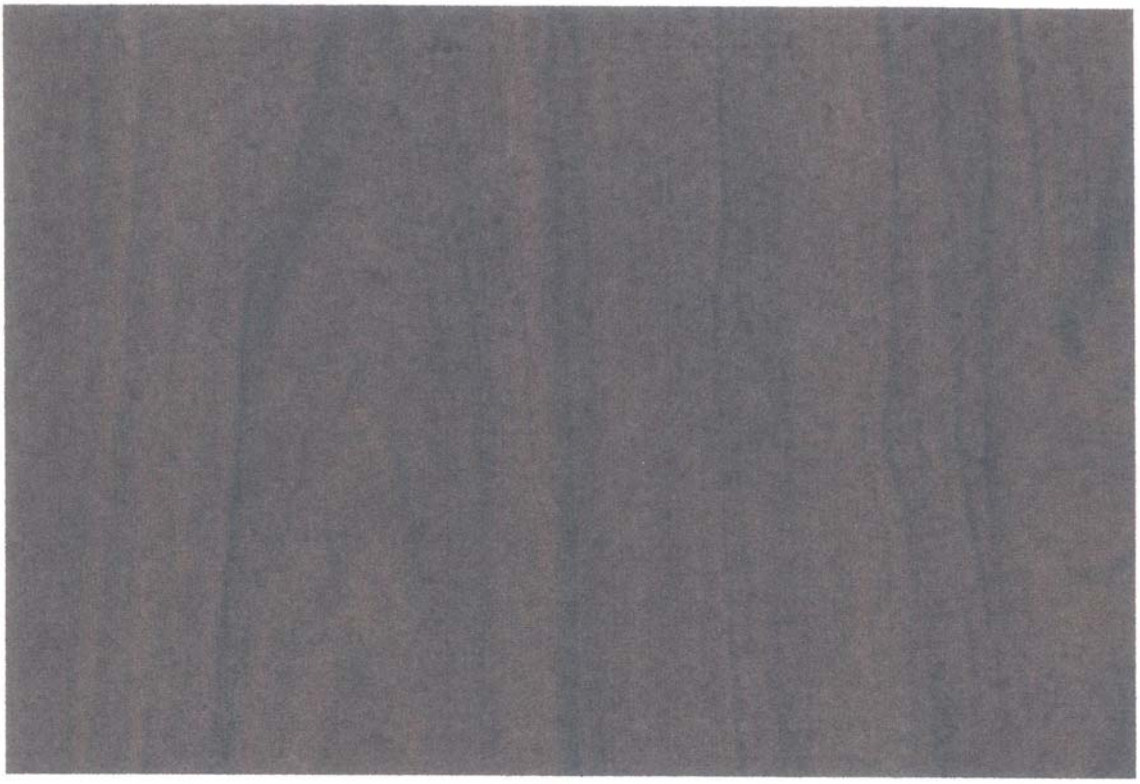

Figure 6.2: Wood Pattern Printed on Hammermill Paper

Figure 6.3: Wood Pattern Printed on Xerox Inkjet Paper

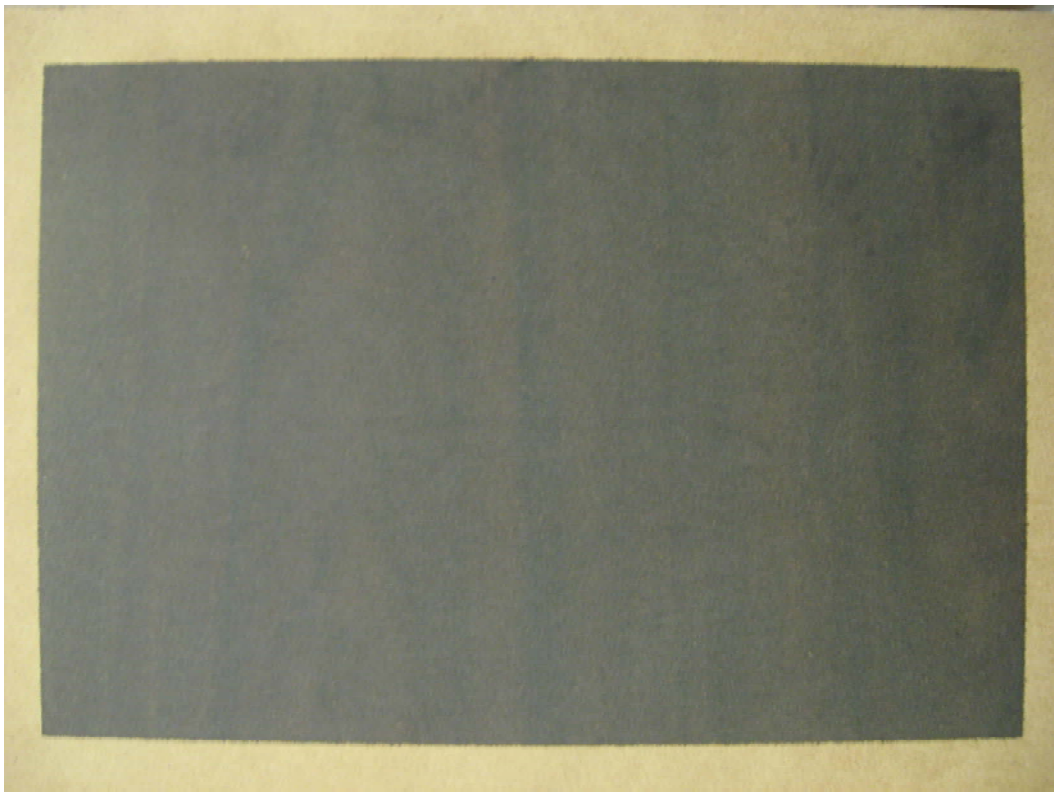

Figure 6.4: Wood Pattern Printed on MDF

Figure 6.5: Wood Pattern Printed on Varnished MDF

Figure 6.6: Wood Pattern Printed on MDF Painted with Rust Paint

Other inexpensive building materials such as drywall were also tested. Subsequently, as seen in Figure 6.7, printing directly on drywall produced results close to paper, though slightly darker due to the greyish hue of the drywall. However, drywall is typically coated with a primer to seal it from water and thus, printing directly on drywall would not be reasonable. Drywall painted with a double-coat of primer resulted in a dark image worse than plain MDF, losing much of the sharper details due to colour bleeding (Figure 6.8). Plywood was then tested and resulted in the ink absorbing into the grain of the wood such that the image details were very poor, taking on the appearance of the plywood rather than the walnut image (Figure 6.9). Next, MDF pre-coated with a white paint, likely oven-baked, was purchased from a public consumer store. The result was an image close to the original image, though the colour was slightly washed out and the cracks in the coating could be seen through the image when viewed within roughly 1 m (Figure 6.10). The abnormal coloured swath on the right is thought to be a consequence of electrical noise interfering with the yellow printhead. It is believed that the cracks are a result of the oven-baking process and possibly a spray-painted version could be found that would create

a higher quality image. It was determined that the paint was produced by a company called Chemcraft, however, further investigation was not completed. Finally, Gesso, a primer for oil-based paints when painting on canvas or wood, was painted onto MDF and allowed to dry. This actually gave one of the worst results with the ink bleeding heavily into the gesso; a close-up of which is found in Figure 6.11. It is believed that the lower viscosity of oil-based paints compared to the oil-based inks was significant enough that the inks did not behave the same as the paints would on Gesso.

Figure 6.7: Wood Pattern Printed on Drywall

Figure 6.8: Wood Pattern Printed on Primed Drywall

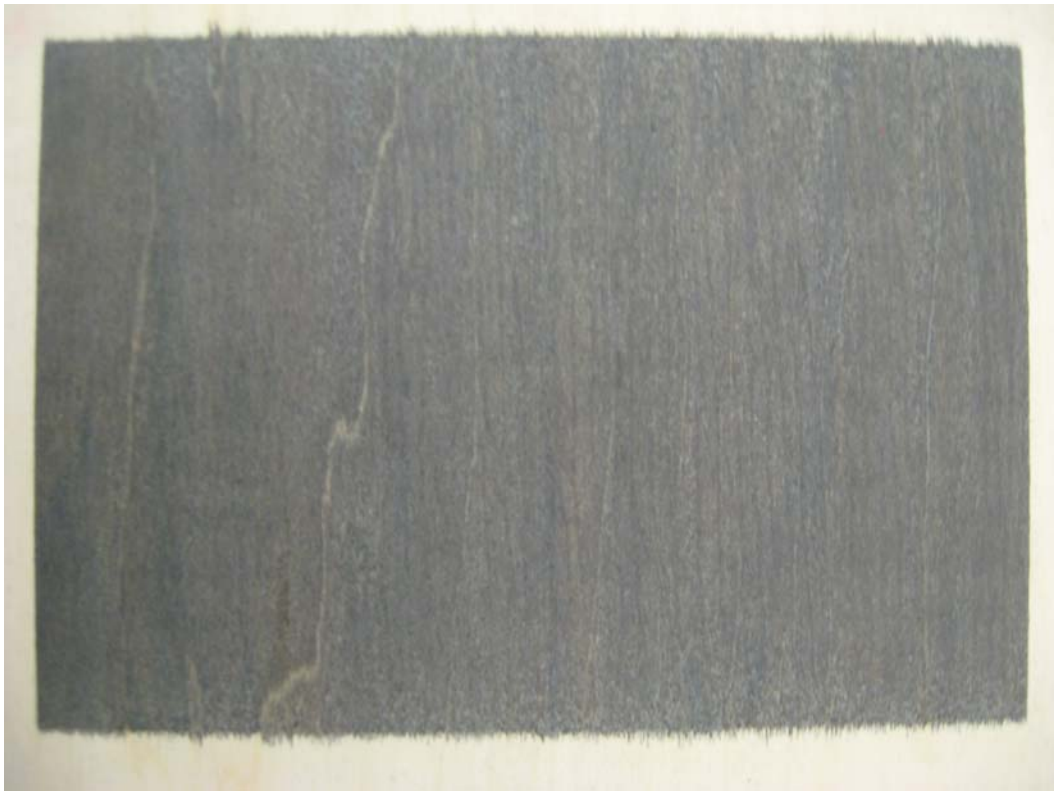

Figure 6.9: Wood Pattern Printed on Plywood

Figure 6.10: Wood Pattern Printed on Pre-coated MDF

Figure 6.11: Wood Pattern Printed on Gesso (not full image)

It was determined that the MDF image could not be significantly improved upon without a more extensive research of special coatings based on the fluid properties of the oil-based ink. The actual constituents of the ink were kept confidential by Xaar and there was no suggestion from Xaar for a specific coating or substrate that would improve image quality. Instead, they suggested switching to solvent inks or a UV printing system, which is a much more reliable and flexible process with known application, and should be investigated despite the added system complexity and cost in order to obtain satisfactory results for the sign and furniture industries. Another option would be to change the droplet volume in relation to the substrate, though this would require specific knowledge of the interaction between the ink and the substrate. It was thought that harder, non-lacquer paints would produce a sharper image. Thus, melamine, sanded melamine, industrial primer, and industrial paint over the industrial primer were later tested. However, the results still showed significant bleeding as the ink did not absorb into the material. Due to limited time and resources, further substrate material testing has not been completed.

Section 6.1: Conclusions

Oil-based ink produced the best images on Xerox inkjet paper, with almost no bleeding and high resolution. Since the oil-based ink did not absorb into the HP high-gloss photo paper, the droplets could be clearly seen as close as possible to the original image size and position, as shown in the previous chapter. The best results on wood were achieved by printing directly onto MDF or MDF pre-coated by an oven-baked white paint. However, the image on unfinished MDF was significantly darker than on paper and had to be drastically lightened in Photoshop before printing. There was also some noticeable bleeding into the MDF grain. The image on the pre-coated MDF allowed the cracks in the paint to show through the ink when viewed at close range and also required a much longer drying time than for plain paper or MDF. If the correct coating could be found that absorbs oil-based ink with minimal bleeding, then any substrate that is compatible with the coating could be first coated then printed with the desired image. Image quality on wood could be significantly improved with the use of UV-inks, which have been shown in industry to provide better quality, minimal colour bleeding, and reasonable durability even in outdoor conditions. An alternate approach would be to vary the dot size based on the substrate, though a more in depth knowledge of the printhead waveforms and interaction between ink and substrate would be necessary.

Chapter 7: Conclusions and Recommendations

This thesis has presented the integration of an inkjet printing system onto a low-grade, industrial flatbed router. The benefits of such a combined printing and cutting system include reduced waste, faster operation, and it provides the potential for applications outside of paper products, such as the manufacture of signs, furniture, and laminate flooring.

The Xaar 126 printing system was chosen as the introductory tool for learning about the printing process due to its ease of assembly, low cost compared to other systems, simple operation, and potential for future applications with alternative inks. All necessary electrical, mechanical, and software connections were made to allow communication between the computer and printing components, while adhering to the structure of the existing router. A secondary z-axis was designed and assembled alongside the existing spindle axis in order to actuate the printheads over substrates of variable thickness. For any future work, the mechanical assembly between the printhead mount and the spindle should be minimised for increased work area.

A loop-shaping controller was designed based on the frequency response of the machine to account for the resonant and high frequency dynamics of the servo system in the y-axis, which is the main motion contributing to droplet placement accuracy and is particularly important for bidirectional printing, as well as subsequent milling operations. The loop-shaping controller showed a 75% improvement in tracking error over the Sliding Mode Controller and 79% improvement over the industrial benchmark. A homing routine was developed for the secondary z-axis and an interface was made in Control Desk in order to position the printheads where desired before starting to print. Consistently starting in the same position is necessary since the thickness of the substrate may change and a 1 mm clearance between the printheads and the substrate must be maintained for quality image results. Homing routines should also be developed for the x- and y-axes, similar to that of the secondary z-axis. Smooth, jerk-limited trajectories were used to diminish the influence of vibrations on the printheads. It is likely that the dSPACE memory will overrun due to the long trajectories necessary for larger images. Further investigation should be made to create a buffer as is applied in typical printers so that only small sections of the image are sent to the printheads at a time and the back and forth trajectory can simply be repeated with an increase in x-position values. Alternate printing hardware may be necessary since the XUSB only handles bitmaps or similar file types, which have a limit on image size.

Alignment of the printheads is accomplished through mechanical and software means by the adjustment screws holding the printhead in place relative to a thrust pin, offsets defined in the XUSB

software, and the swath-to-swath displacement. Calibration images were printed onto high-gloss HP paper and viewed under a microscope at 50x magnification to evaluate the accuracy of droplet placement. One element of complexity was added at a time, first starting from a monochrome, unidirectional image for the alignment of a single printhead, then aligning the rest of the printheads with respect to the aligned printhead. Next, large images were tested to determine the swath-to-swath accuracy in terms of vertical and horizontal offsets, which are mostly controlled by the trajectory and Product Detect signal, respectively, as well as positioning accuracy. Finally, bidirectional printing was implemented using both 1PD and 2PD signals, where the 2PD method provided more reliable droplet placement. A new mounting plate was designed to eliminate the bidirectional colour striping as a result of alternating the order in which colours are deposited. This was accomplished by offsetting the printheads from each other by one swath each so that they always print in a specific order. It is necessary to add extra blank swaths to the images to compensate for these offsets. Bidirectional printing was shown to be at least 15% faster than unidirectional printing, with comparable droplet placement accuracy.

Various substrates were tested, with pre-coated MDF showing the best results in terms of colour and resolution. It was difficult to achieve satisfactory results, since the ink absorbs into the material, allowing the substrate grain to show through the image. Darker substrates also reduced the colour quality of the image significantly, despite image processing in Photoshop. More testing should be done with different substrate coatings or preparation to obtain better quality results. Much of the image resolution is lost when converting from various file types to bitmap. Greyscale printheads would improve the colour of the printed images since they can control the amount of ink that is being deposited in order to produce more vibrant colours, corresponding more closely to the original digital image. A white pre-coating should also be incorporated into the system to allow images to be printed on any substrate without significant colour loss or colour compensation in Photoshop. In order to improve the quality of print on MDF wood and other materials, a UV system should be installed onto the router. This would require obtaining UV inks, UV-proof tubing, and a UV lamp. Changes to the system and/or environment would need to be made to ensure that no external UV light reaches any ink, otherwise undesirable curing will take place. In a UV system, colours can be cured one at a time or all at once, depending on the strength of the UV light. Curing one colour at a time could cause over-curing and cracking of the lower ink layers. Different curing intensities and durations would need to be adjusted to prevent over-curing.

The final combined printing system was able to print on various paper and wood substrates with calibration results showing droplet positioning errors of less than 4 μm in the vertical direction and

less than 30 µm in the horizontal direction, using a 2PD bidirectional trajectory at the maximum drive speed of 250 mm/sec. These results are significantly better than the 100 µm feed accuracy specified by the printing systems currently manufactured by Zünd. The ideas developed in this thesis could also be used to implement material deposition for applications such as manufacturing microchips, LEDs, and 3D printing and cutting. However, these technologies would require machines of higher positioning accuracy than was presented in this thesis.

References

[1] Lentner, A., 2006. Direct Multi-Colour Printing on Wood and Wood Composite Panels, *Decorative and Industrial Laminates Symposium,* August 21-23 2006, Technical Association of the Pulp and Paper Industry pp1-15.

[2] Graedel, T.E. and Howard-Grenville, J.A., 2005. Forest Products and Printing. *Greening the Industrial Facility.* Springer US, pp. 369-387.

[3] Madou, M.J., 2002. Fundamentals of Microfabrication. 2 edn. CRC Press.

[4] Lee, E.R., 2003. Microdrop generation. Boca Raton, Fla.; London: CRC Press.

[5] Hon, K.K.B., Li, L. and Hutchings, I.M., 2008. Direct Writing Technology - Advances and Developments. *Annals of the CIRP,* **57**.

[6] Wallace, D.B., 1989. Automated Electronic Circuit Manufacturing Using Ink-Jet Technology. *Journal of Electronic Packaging,* **111**(2), 108-112.

[7] Bharathan, J. and Yang, Y., 1998. Polymer electroluminescent devices processed by inkjet printing: I. Polymer light-emitting logo. *Applied Physics Letters,* **72**(21), 2660-2662.

[8] Dong, H., 2007. *Improving Gantry Style Router Tracking Accuracy through Optical Linear Encoder Retrofit and Error Compensation Using Laser Interferometry.* Work report. Waterloo, Ontario, University of Waterloo, Faculty of Engineering.

[9] Heng, M., 2008. *Smooth and Time-Optimal Trajectory Generation for High Speed Machine Tools*. Master's thesis. Waterloo, Ontario, University of Waterloo, Faculty of Engineering.

[10] Kamalzadeh, A., 2009. *Precision Control of High Speed Ball Screw Drives*, PhD thesis. Waterloo, Ontario, University of Waterloo, Faculty of Engineering.

[11] Le, H.P., 1999. Progress and Trends in Ink-jet Printing Technology. *Recent Progress in Ink Jet Technologies II.* Society for Imaging Science and Technology, pp. 1-14.

[12] Martin, G.D., Hoath, S.D. and Hutchings, I.M., 2008. Inkjet printing - the physics of manipulating liquid jets and drops, *Engineering and Physics - Synergy for Success,* 03/01 2008, IOP Publishing Ltd. pp1-14.

[13] Beurer, G. and Kretschmer, J., 1999. Function and Performance of a Shear Mode Piezo Printhead. *Recent Progress in Ink Jet Technologies II.* Society for Imaging Science and Technology, pp. 151-155.

[14] Heinzl, J., 2008. Ink Jets. *Comprehensive Microsystems.* Oxford: Elsevier, pp. 335-368.

[15] McConnell, J.J., 2006. Computer Graphics: Theory into Practice. Jones and Bartlett Publishers, Inc.

[16] Hancock, A. and Lin, L., 2004. Challenges of UV curable ink-jet printing inks - a formulator's perspective. *Pigment and Resin Technology,* , 280-286.

[17] Whitcher, J., 2006. Getting Wider. *Graphic Arts Online,* (6), pp. 14-19.

[18] Beeson, R., 1999. Thermal Inkjet: Meeting the Applications Challenge. *Recent Progress in Ink Jet Technologies II.* Society for Imaging Science and Technology, pp. 43-46.

[19] Schofield, J.D., 1999. Ink Systems for the Xaar Ink Jet Printhead. *Recent Progress in Ink Jet Technologies II.* Society for Imaging Science and Technology, pp. 430-434.

[20] Rioboo, R., Marengo, M. and Tropea, C., 2002. Time evolution of liquid drop impact onto solid, dry surfaces. *Experiments in Fluids,* **33**(1), 112-24.

[21] Yarin, A.L., 2006. Drop Impact Dynamics: Splashing, Spreading, Receding, Bouncing... *Annual Review of Fluid Mechanics,* **38**, 159-192.

[22] Marx, D., 2005. Flatbed inkjet expands printing possibilities. *Canadian Printer,* **113**(5), 30-34.

[23] Zünd, 2010-last update, zünd - swiss cutting systems. Available: http://zund.com/ [March 2, 2010].

[24] Hymmen and Xaar, 2009. Jupiter Digital Printing Line News Release, *LIGNA 2009,* 18-22 May 2009.

[25] *DPR laminate flooring from Egger.* 2008. Lamniat-Magazin.

[26] Hymmen, 2009. Hymmen Develops own Digital Printing Technology.

[27] Mills, R.N. and Demyanovich, W.F., 2005. Materials and Process Development for Digital Fabrication Using Ink Jet Technology. *Digital Fabrication,* **1**, 8-12.

[28] Xaar System Manual. 2008. Cambridge, UK: Xaar.

[29] Moon, A., 2008. *Design and Installation of Inkjet Printing System on a Flatbed Router.* Waterloo, Ontario: University of Waterloo, Faculty of Engineering.

[30] Heidenhain, 2007. Interface Electronics.

[31] Baqai, F.A., Lee, J.-., Agar, A.U. and Allebach, J.P., 2005. Digital color halftoning. *IEEE Signal Processing Magazine,* **22**(1), 87-96.

[32] Anastassiou, D. and Pennington, K.S., 1982. Digital Halftoning of Images. **26**, 687-697.

[33] Altintas, Y., Erkorkmaz, K. and Zhu, W.-., 2000. Sliding Mode Controller Design for High Speed Feed Drives. *CIRP Annals - Manufacturing Technology,* **49**(1), 265-270.

[34] Franklin, G.F., Powell, J.D. and Emami-Naeini, A., 2009. Feedback Control of Dynamic Systems. 6 edn. Prentice Hall.

[35] Hofstetter, H.W., Griffin, J.R., Berman, M.S. and Everson, R.W., 2000. Dictionary of Visual Science and Related Clinical Terms. 5 edn. Butterworth-Heinemann.

[36] Brunahl, J. and Grishin, A.M., 2002. Piezoelectric shear mode drop-on-demand inkjet actuator. *Sensors and Actuators A (Physical),* **A101**(3), 371-82.

[37] Kretschmer, J. and Beurer, G., 1999. Design Parameters of a Shear Mode Piezo Printhead for a Given Resolution. *Recent Progress in Ink Jet Technologies II.* Society for Imaging Science and Technology, pp. 156-162.

[38] Wang, X., 2009. Piezoelectric Inkjet Technology - From Graphic Printing to Material Deposition, *Nanotech Conference & Expo 2009,* May 3 - 7 2009, Dimatix Fujifilm.

[39] Design Your Wall, 2010-last update, walnut self-stick wood grain wall contact paper [Homepage of Design Your Wall], [Online]. Available: www.designyourwall.com [April 5, 2010].

[40] Brightness of pulp, paper, and paperboard (directional reflectance at 457nm), Test Method T 452 om-08. 2009. Technical Association of Pulp and Paper Industry.

[41] Davim, J.P., Clemente, V.C. and Silva, S., 2009. Surface roughness aspects in milling MDF (medium density fibreboard). *The International Journal of Advanced Manufacturing Technology,* **40**, 49-55.

Appendix A: Xaar Printhead Specifications

Active Nozzles	126
Nozzle Pitch [mm]	137.1
Nozzle Diameter [µm]	40
Typical Drop Volume [pl]	50
Typical Drop Velocity [m/s]	6.0
Max Drop Deviation [degrees]	1.0
Ambient Temperature Range [°C]	15 – 35
Ambient Humidity (non-condensing) [%]	10 – 90 RH
Max Frequency [kHz]	7.5
Max Linear Speed (single pass) [mm/s]	635
Pixel Resolution, swathe x traverse [dpi]	300 x 300
Print Height at Given Resolution [mm]	10.6
Weight (dry) [g]	35
Dimensions (WxHxL) [mm]	43x11.8x45
Recommended Printing Distance [mm]	1
Internal Fluid Volume [ml]	2
Maximum Printhead Acceleration [m/s^2]	9.81

Appendix B: Printhead Angle Calculations

DPI stated in XUSB software	309
Number of printhead nozzles, *n*	126

Swath Width, *w* [mm]:

$$w = \frac{DPI}{n} = \frac{309}{126} \times \frac{25.4mm}{inch} = 10.3573$$

Distance Between Nozzles, *d* [mm]:

$$d = \frac{w}{n-1} = \frac{10.3573}{126-1} = 0.0829$$

Distance from one swath to the next, δ_x, [mm]:

$$\delta_x = d + w = 0.0829 + 10.3573 = 10.4401$$

It can be seen that the swath width of 10.3 mm mentioned in the manual is not accurate.

The datasheet from the website gives the distance from the first nozzle to the last nozzle as 17.2 mm, while the manual claims it is 17.1 mm.

Angle for distance of 17.2 mm [degrees]:

$$\theta = \sin^{-1}\left(\frac{w}{17.2}\right) = \sin^{-1}\left(\frac{10.4401}{17.2}\right) = 37.0253$$

Angle for distance of 17.1 mm [degrees]:

$$\theta = \sin^{-1}\left(\frac{w}{17.1}\right) = \sin^{-1}\left(\frac{10.4401}{17.1}\right) = 37.2784$$

The manual states that the printheads should be angled at 36.9° though it correlates this with 300 DPI and 10.3 mm swath width, neither of which is accurate:

Angle, θ [degrees]	36.9
Distance from first to last nozzle [mm]	17.2

Swath Width, *w* [mm]:

$$w = 17.2\sin(36.9) = 10.3272$$

DPI:

$$DPI = \frac{126}{10.3272} \times 25.4 = 309.8992$$

Distance between nozzles, *d* [mm]:

$$d = \frac{w}{n-1} = \frac{10.3272}{125} = 0.0826$$

Distance from one swath to the next, δ_x, [mm]:

$$\delta_x = d + w = 0.0826 + 10.3272 = 10.4098$$

Angle, θ [degrees]	36.9
Distance from first to last nozzle [mm]	17.1

Swath Width, *w* [mm]:

$$w = 17.1\sin(36.9) = 10.2672$$

DPI:

$$DPI = \frac{126}{10.2672} \times 25.4 = 311.7115$$

Distance between nozzles, *d* [mm]:

$$d = \frac{w}{n-1} = \frac{10.2672}{125} = 0.0821$$

Distance from one swath to the next, δ_x, [mm]:

$$\delta_x = d + w = 0.0821 + 10.2672 = 10.3493$$

It was thought that the 36.9° was an approximation for the angle of a right triangle with side length ratios 3-4-5.

Angle, θ [degrees]	36.8699
Distance from first to last nozzle [mm]	17.2

Swath Width, *w* [mm]:

$$w = 17.2\sin\left(36.8699\right) = 10.3200$$

DPI:

$$DPI = \frac{126}{10.3200} \times 25.4 = 310.1163$$

Distance between nozzles, *d* [mm]:

$$d = \frac{w}{n-1} = \frac{10.3200}{125} = 0.0826$$

Distance from one swath to the next, δ_x, [mm]:

$$\delta_x = d + w = 0.0826 + 10.3200 = 10.4026$$

Angle, θ [degrees]	36.8699
Distance from first to last nozzle [mm]	17.1

Swath Width, *w* [mm]:

$$w = 17.1\sin\left(36.8699\right) = 10.2600$$

DPI:

$$DPI = \frac{126}{10.2600} \times 25.4 = 311.9298$$

Distance between nozzles, *d* [mm]:

$$d = \frac{w}{n-1} = \frac{10.2600}{125} = 0.0821$$

Distance from one swath to the next, δ_x, [mm]:

$$\delta_x = d + w = 0.0821 + 10.2600 = 10.3421$$

The swath width in the manual is 10.3 mm.

For Nozzle Plate Width of 17.2 mm:

DPI:

$$DPI = \frac{126}{10.3} \times 25.4 = 310.7184$$

Distance between nozzles, *d* [mm]:

$$d = \frac{w}{n-1} = \frac{10.3}{125} = 0.0824$$

Distance from one swath to the next, δ_x, [mm]:

$$\delta_x = d + w = 0.0824 + 10.3 = 10.3824$$

Angle, θ [degrees]:

$$\theta = \sin^{-1}\left(\frac{w}{17.2}\right) = \sin^{-1}\left(\frac{10.3}{17.2}\right) = 36.7867$$

For Nozzle Plate Width of 17.1 mm:

DPI:

$$DPI = \frac{126}{10.3} \times 25.4 = 310.7184$$

Distance between nozzles, *d* [mm]:

$$d = \frac{w}{n-1} = \frac{10.3}{125} = 0.0824$$

Distance from one swath to the next, δ_x, [mm]:

$$\delta_x = d + w = 0.0824 + 10.3 = 10.3824$$

Angle, θ [degrees]:

$$\theta = \sin^{-1}\left(\frac{w}{17.1}\right) = \sin^{-1}\left(\frac{10.3}{17.1}\right) = 37.0376$$

Appendix C: Operation of Printing System

Operation of the router is given in a recommended order, though the sequence of some steps can be interchanged.

Image Processing

1. Open Adobe Photoshop.
2. Open the image to be processed.

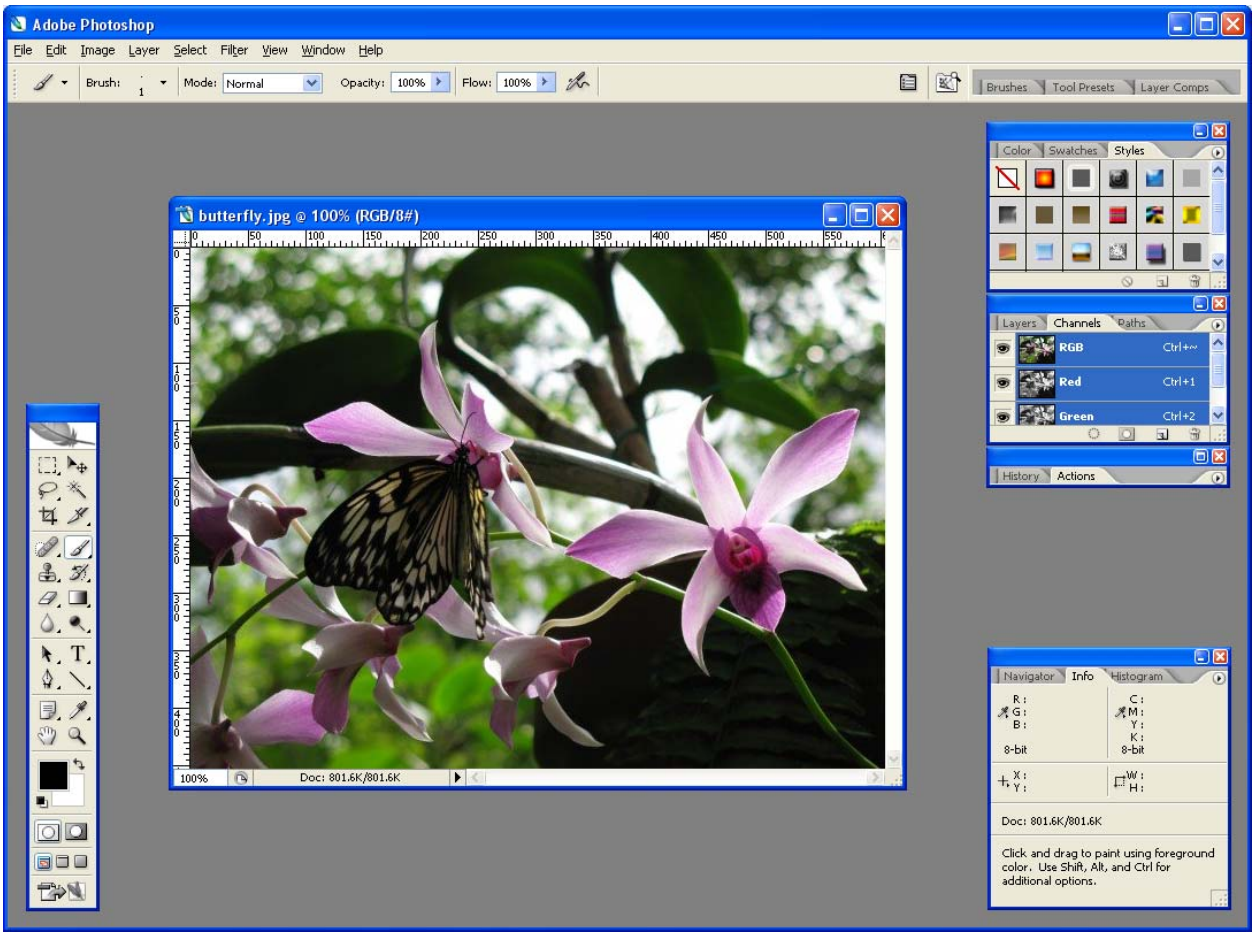

3. Change the image mode to CMYK (Image -> Mode -> CMYK color).
4. Preserve highlights and shadows for printing (Image -> Adjustments -> Levels…). Generally, shift the middle arrow of the Input Levels histogram to the left until the image is significantly lightened.

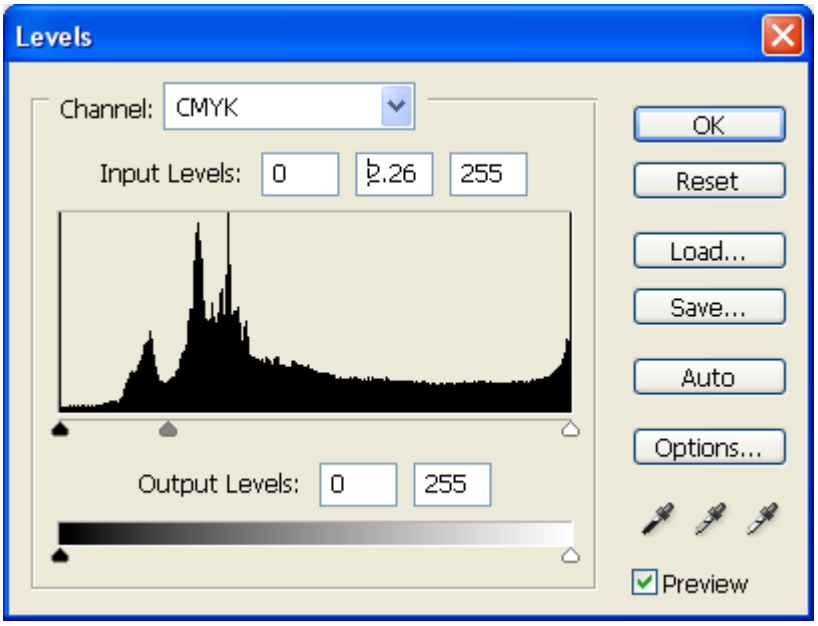

Alternatively, adjust the tonality and colour of the image (Image -> Adjustments -> Curves…). Shift the curve with the mouse or manually input the values. Suggested values are Input: 25 and Output: 50.

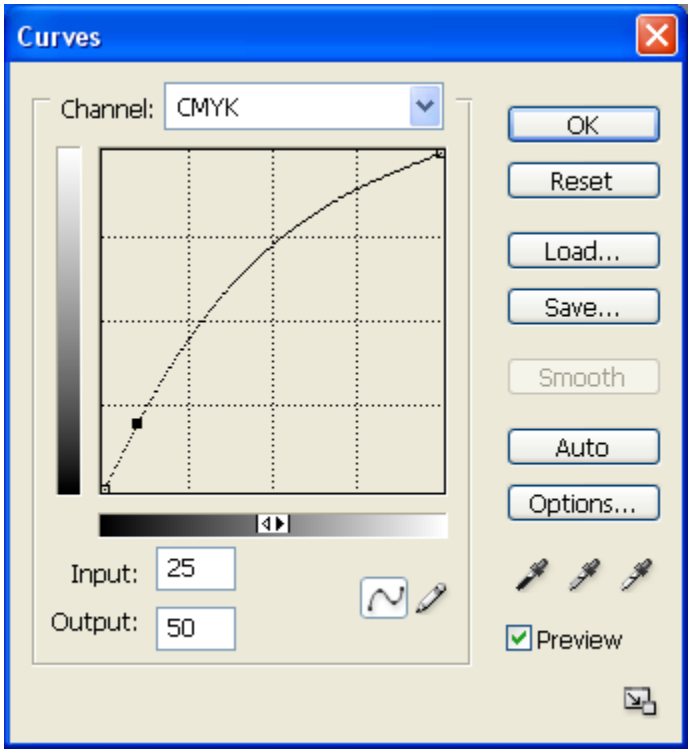

Press OK to close the dialog box.

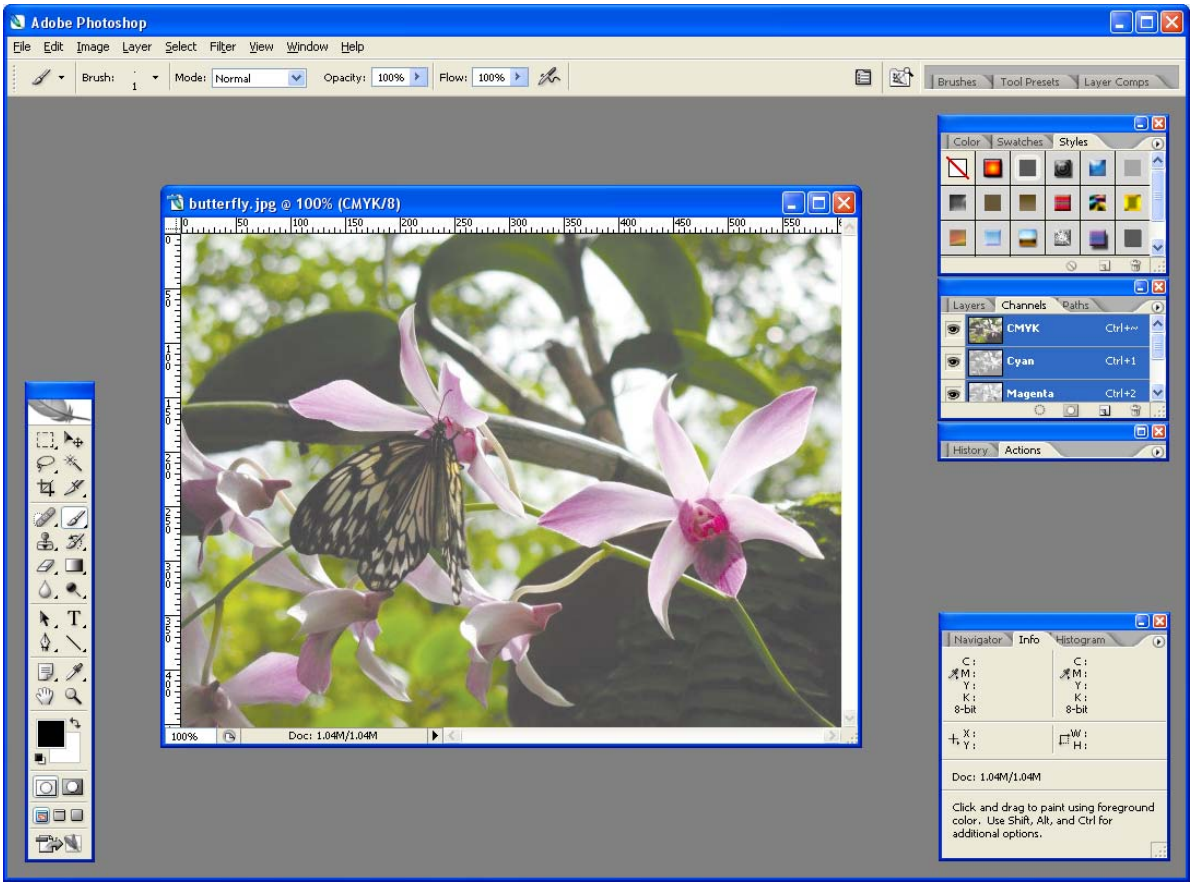

5. Change the resolution to 309DPI (Image -> Image Size…). In the Resolution input box, enter 309.

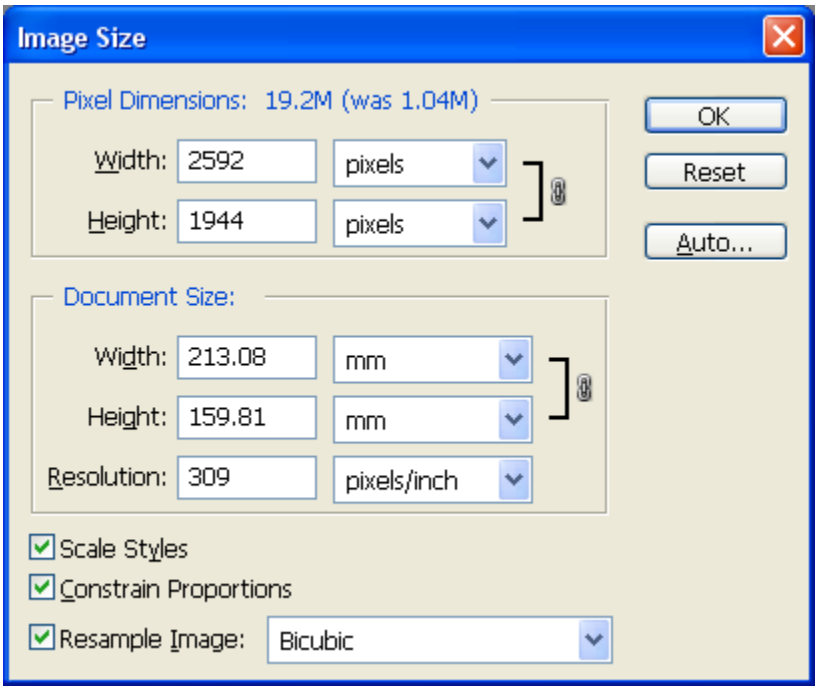

Press OK to close the dialog box.

6. If desired, change the view so that the image fits on the screen.
7. Rotate the image 90 degrees clockwise if necessary (Image -> Rotate Canvas -> 90°CW.

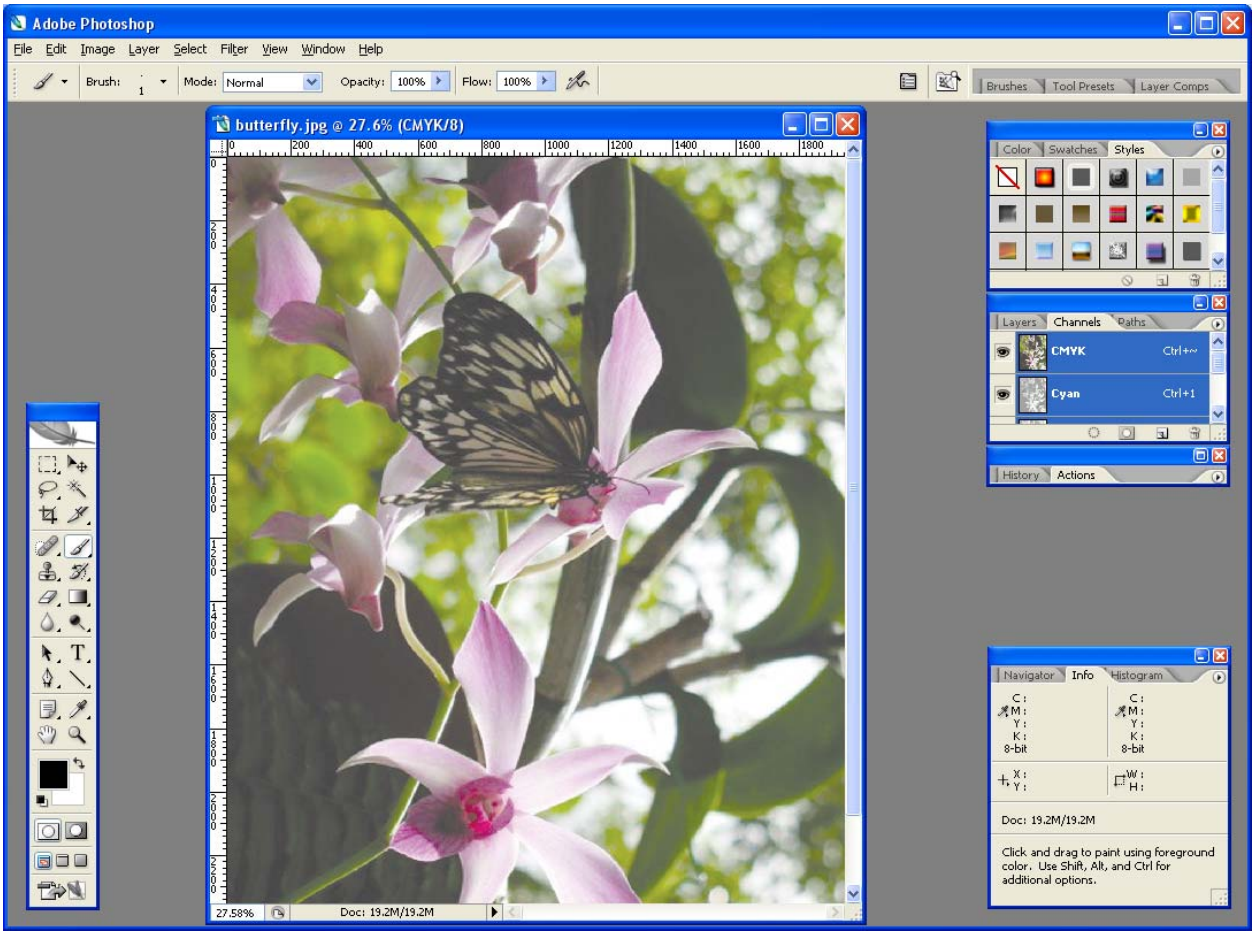

8. Split the image into its separate CMYK images. Click on the arrow button in the top-right corner of the Channels tab and select Split Channels. If the option is not available, then selecting Image -> Mode -> Multichannel might work.

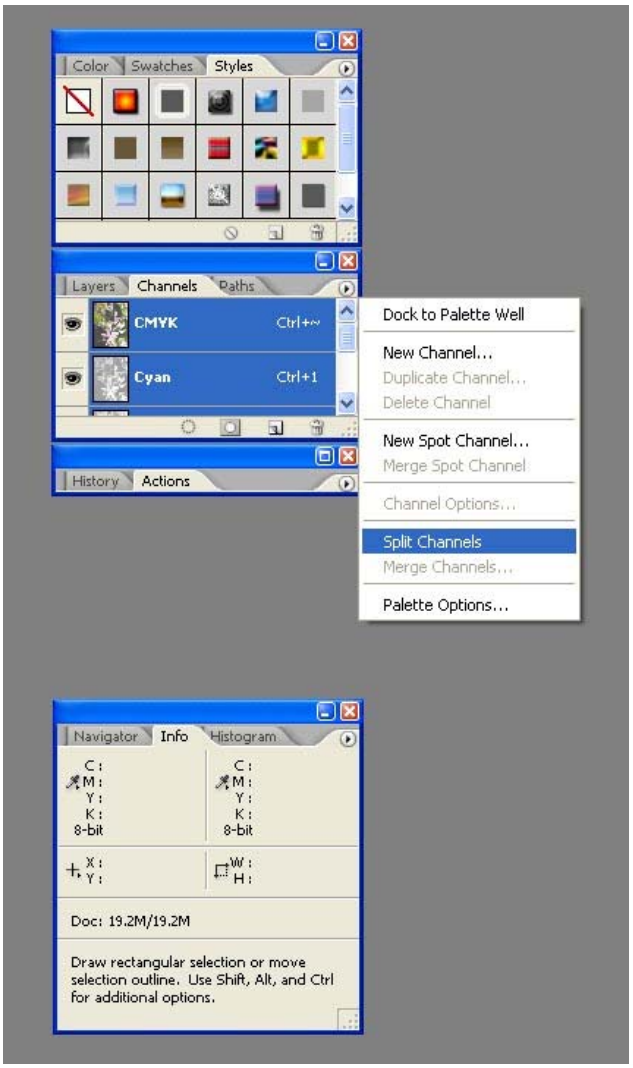

9. Change each image to a bitmap (Image -> Mode -> Bitmap…). This opens a dialog box. Make sure the Output is 309 pixels/inch and use Diffusion Dither. Press OK to close the dialog box.

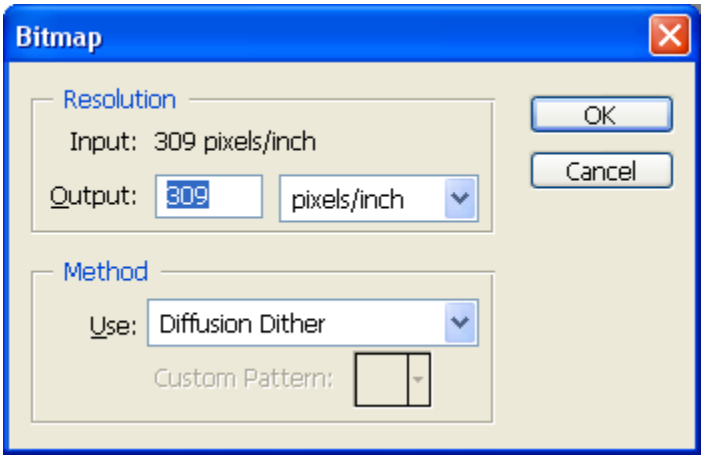

10. Save each image according to the following naming convention, where *Name* is whatever the file will be called:

Cyan	*Name*11A.bmp
Magenta	*Name*11B.bmp
Yellow	*Name*12A.bmp
Black	*Name*12B.bmp

Make sure that the file format is set to BMP.

Setting up

1. Plug the power cable for the router into the 400V outlet, pushing as far as possible and twisting counter-clockwise to ensure complete contact.
2. On the fuse box, flip up the switch labelled "router control" to the ON position.
3. Flip up the corresponding "router control" fuse switch at the back of the router.
4. Press the green button on the lower left side at the front of the router to supply power to turn on the router.
5. In the same area, check that the ink supply controller is properly connected to power, the ink pumps, header tanks, and the RS232 cable to the computer. Also check that the two RS232 extension cables are secure.
6. Turn on the ink supply controller by pressing the switch. Green lights will indicate the status of the device.
7. Remove the hitch pins and cover from the bottom of the printheads and place away from router.
8. Turn the manual valves leading to the printheads so that the ink is free to flow. The valves are open when they are pointing in the same direction as the tubing. DO NOT open the valves before turning on the ink supply controller. Without the vacuum to maintain negative pressure at the nozzle plates, ink will leak from the printheads.
9. Check that the router has been configured for external control.
10. Place the dSPACE close to the encoder cables from the router.
11. Plug the power cable for the dSPACE into a nearby outlet.
12. Plug the network cable into the dSPACE and the computer.
13. Verify that the software license key for the dSPACE is in one of the available USB ports.
14. Open MATLAB 7.0.4 on the computer connected to the router. Only version 7.0.4 is compatible with the dSPACE controller.
15. Open the printing demo file.

16. Open the model.
17. Check that the dSPACE configuration for digital (rotary) and analog (linear) ports corresponds to the ports needed in the model. If not, then either the leadscrew model must be changed to match the dSPACE configuration or the chips must be manually changed on the board inside dSPACE. Be sure to remember the orientation of the metal cover to the dSPACE when taking it apart, as one side is specially coated. When changing the leadscrew model, check that the encoder counts have been changed to correspond with the linear (4096) and rotary (4) encoders.
18. Connect the BNC connectors according to the layout defined in the model. Failure to make the proper connections will result in highly undesirable control. Opposite ends of the BNC connectors should also be connected to the corresponding ports on the Pulse Width Modulator (PWM).
19. Ensure all necessary cables are connected to the XUSB: two firewire cables to the head personality card unit, power supply connector, and USB cable connected to a USB 2.0 port on the computer with no other devices sharing the same board, otherwise the XUSB software will not load properly. The USB cable also has two USB repeaters which should be secured. DO NOT change connections while the XUSB is powered. Hot-plugging will cause damage to the electronics.
20. Turn on the power supply for the XUSB, located on the lower right side at the front of the router. Green lights will indicate the status.
21. Clear the router area and surface.
22. Turn on the dSPACE and PWM.
23. On the computer, open the InkSystem software.

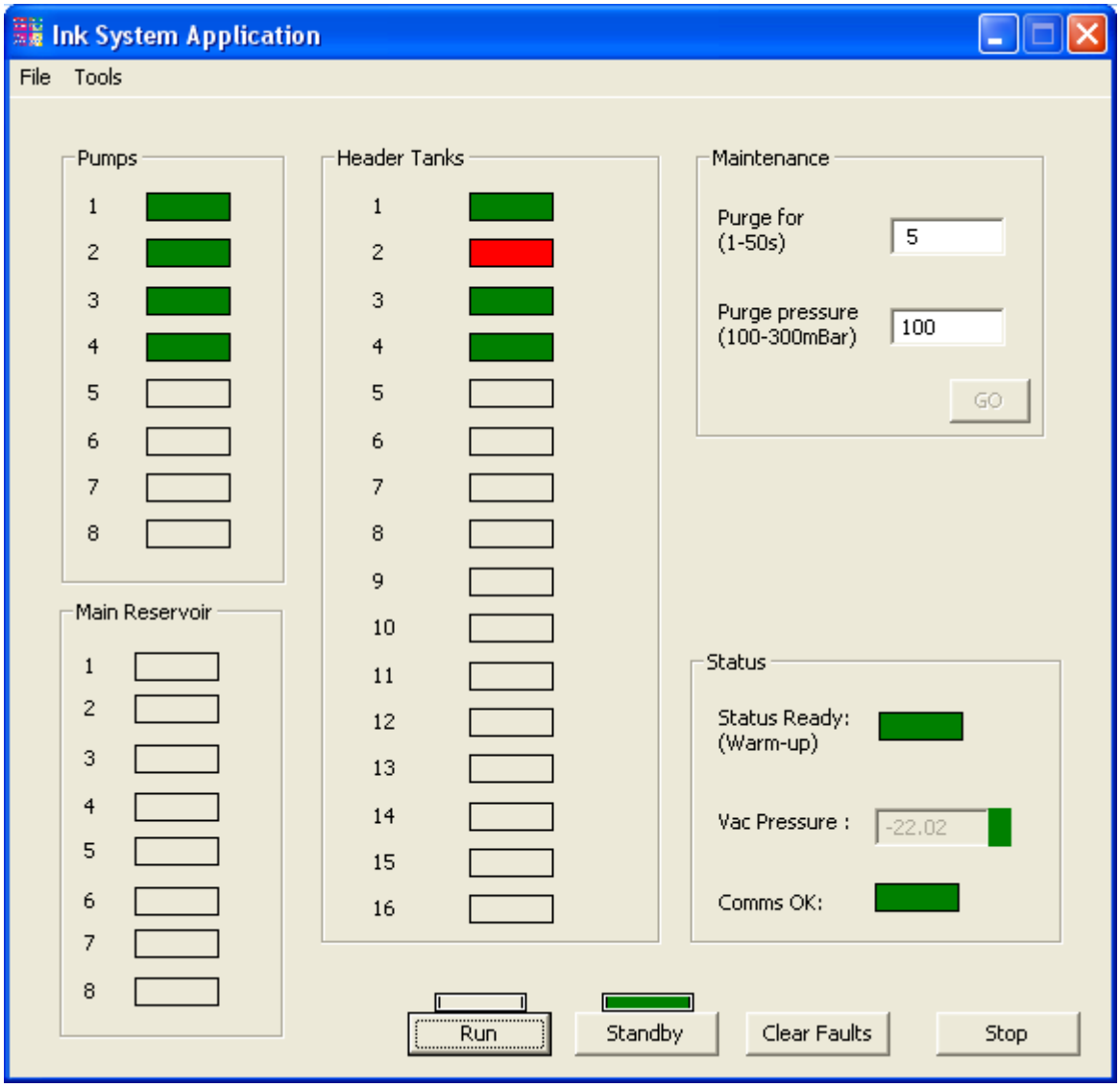

24. Place a drip tray underneath the printheads.
25. Press the RUN button. This will fill any header tanks low on ink, indicated by a red box in the Header Tanks section and a red LED on the header tank itself.
26. If there is ink in all of the purge tubes then skip to Step 30. Otherwise, close the valves leading to printheads that have ink in the purge tubes. It is recommended that only one printhead be filled at a time.
27. Change the purge pressure to the lowest setting, 100mBar. Recommended time for purge is 5 seconds.
28. Open the plug to the purge tube to be filled.
29. It is HIGHLY RECOMMENDED that a second person helps with this step. Press the GO button to start the purge. Quickly close the plug to the purge tube as ink fills the tube.

30. Purge the printheads. Set a purge pressure and length of time for the purge. Press GO to start the purge. Remove the drip tray.
31. Wipe the nozzle plate with lint-free swabs in one direction only (along the length of the plate), being extremely careful not to scratch the plate. If there is an excessive amount of ink, then remove some of the ink with lint-free wipes, being careful not to touch the nozzle plate. DO NOT reuse wipes or swabs. DO NOT mix colours.
32. Open the XUSB software. If a window pops up saying it is unable to load the device driver, then make sure the power supply is powered, the USB cable is connected properly, and then try restarting the computer. If that does not work, then the driver for the XUSB software will need to be reloaded (Scorpion.exe version 4.1 or higher), possibly followed by restarting the computer.
33. Check the settings (XaarPrint -> Parameters).
34. Activate the printheads to be used in the XUSB/PrintHead Select tab. PrintHead1 is really the first board of the Head Personality Card unit and PrintHead2 is the second card. Each card goes to two printheads. So the first checkbox beside PrintHead1 represents Cyan and the checkbox to the right of that is Magenta. Likewise, the checkbox beside PrintHead2 represents Yellow and the one to the right of that is Black. Ensure that the Power is checked for both cards.

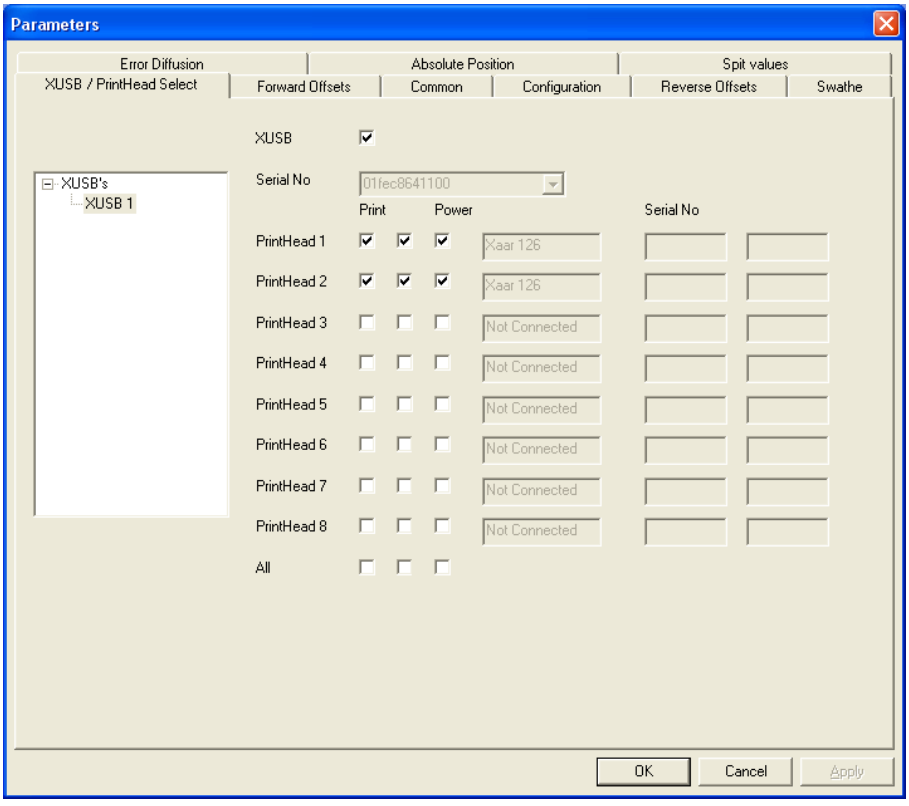

35. Nothing should be changed in the Forward Offsets tab:

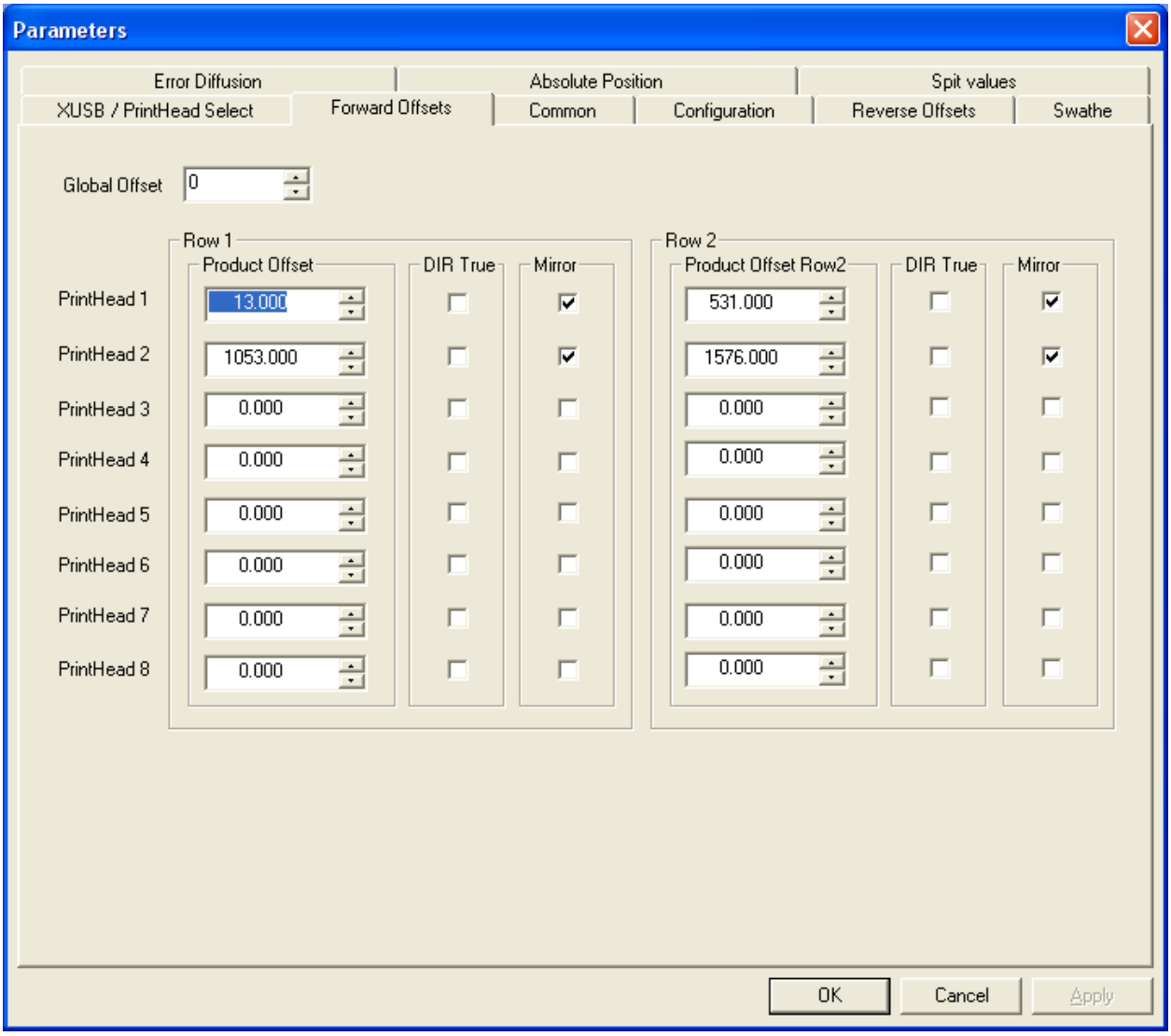

36. Common tab:

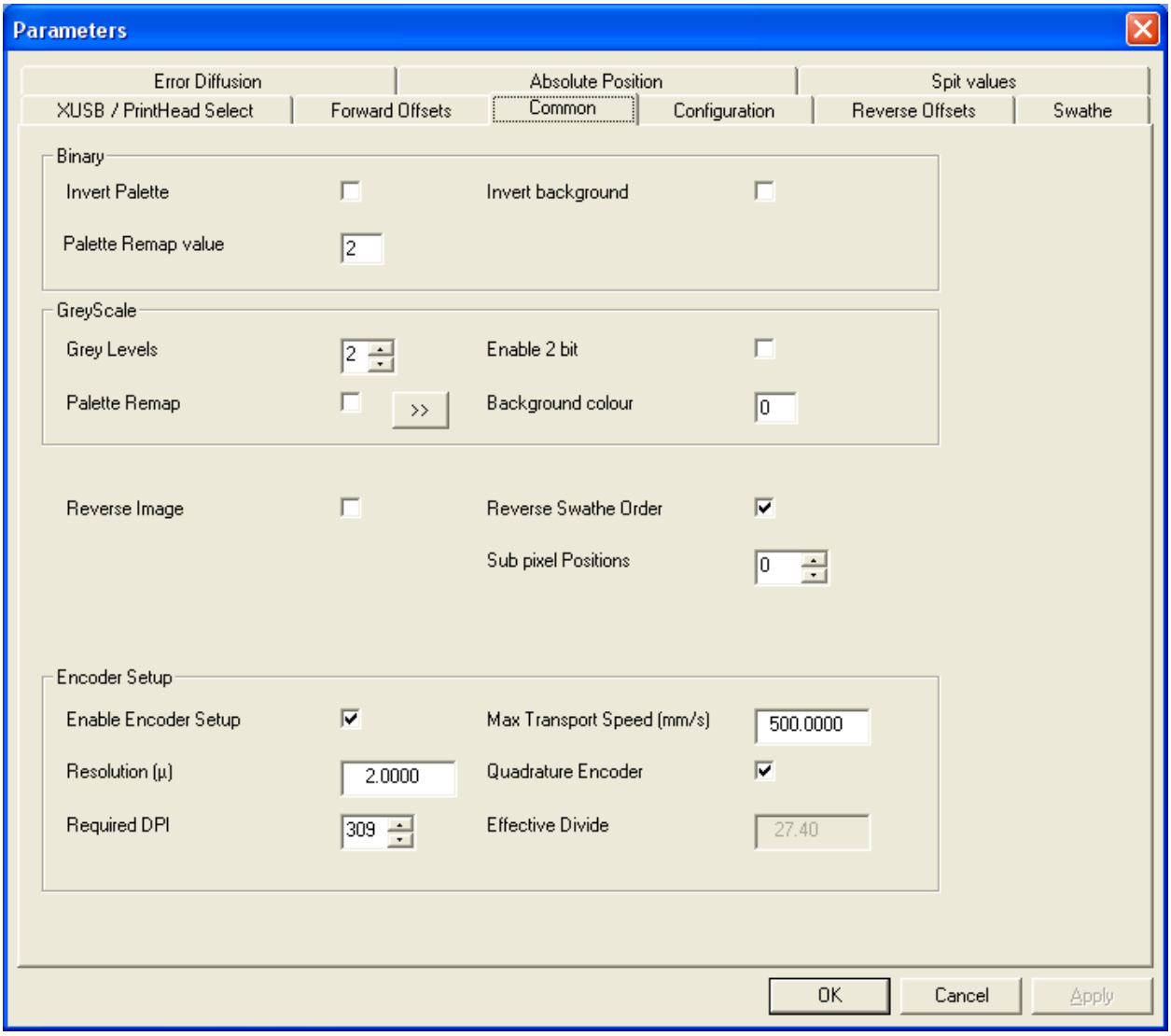

37. Go to the Configuration tab. Change the Print Transport Type according to the desired mode of print (Scanning, Uni-Direction; Scanning, Bi-Direction; Scanning, Bi-Direction – 2 PD). It is generally better to have the Print Once option checked to ensure reliable operation from one print to the next.

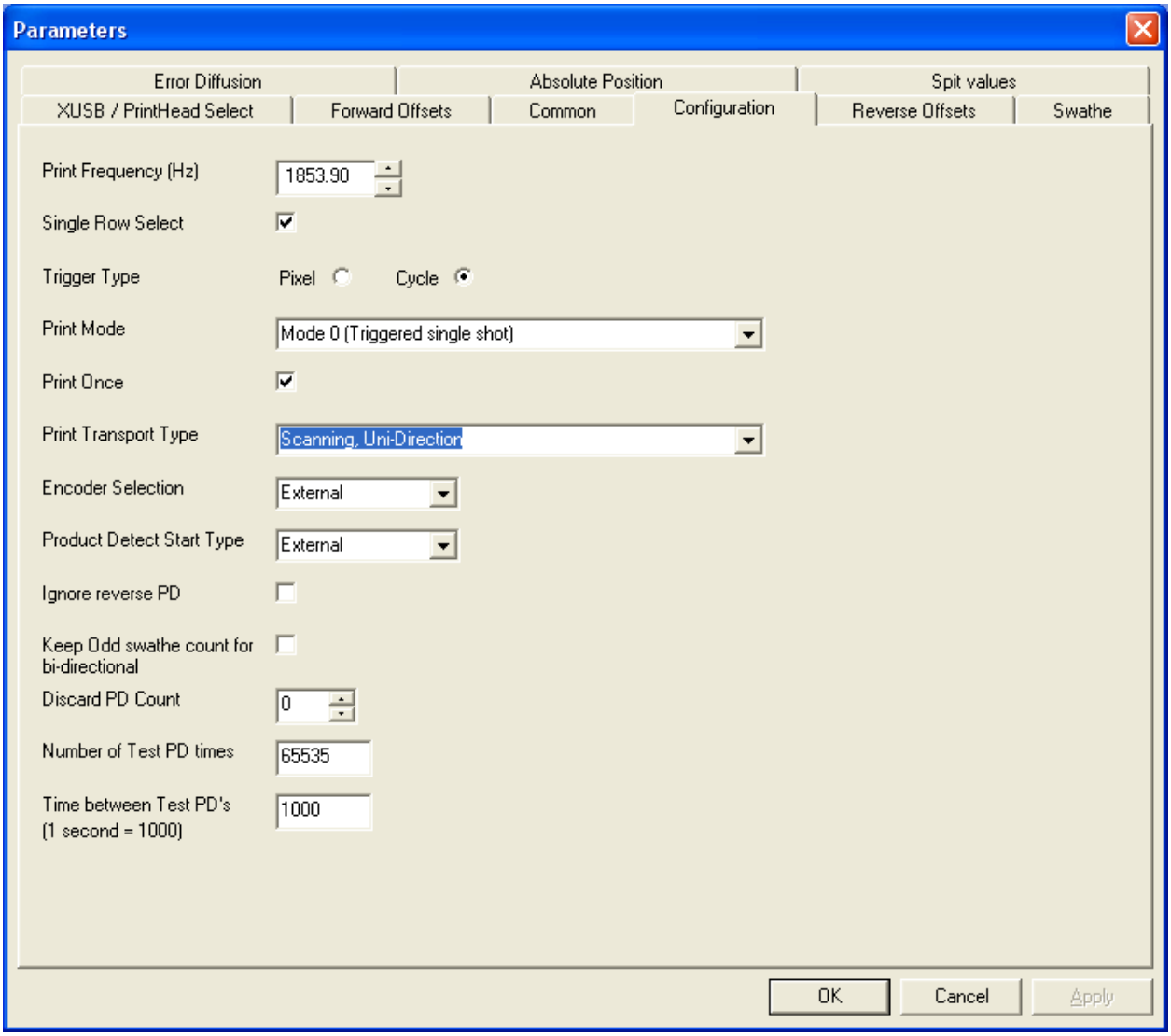

38. The remaining tabs do not need to be changed. Press OK to acknowledge the changes and close the Parameters window.
39. Open the image(s). When opening more than one file (multi-colour printing), go to File -> Open Multiple files.. and select the first file in the sequence (i.e. *Name*11A.bmp). This will open all the files according to which printheads are activated.
40. If the images have already been angled, then set the active window to the first file in the sequence and skip Steps 41-42. Otherwise, angle each image (File -> Angle 126 Image). Select the following options (leading edge for the unidirectional plate, trailing edge for bidirectional plate with no mirror if already set in offset tab):

Press OK to accept.

41. Save each image over its original file and close each file.
42. Reopen the image(s) and set the active window to the first image in the sequence (i.e. *Name*11A.bmp).

Running the Printing Program

1. Check the image dimensions in Photoshop.
2. Change the image height as the width and the image width as the height in millimetres into the MATLAB code.
3. Select the method of print: 1 for unidirectional, 2 for bidirectional – 1PD, and 3 for bidirectional – 2PD. This must match the setting chosen in the XUSB software parameters.
4. Place the substrate into the desired position.
5. Measure the thickness of the substrate.
6. Enter this value into the MATLAB code plus the 1mm clearance between the substrate and printheads.
7. Run the MATLAB program.
8. When the model finishes loading to dSPACE, open Control Desk.
9. Load the .sdf created from compiling the model to the DS1002 platform by dragging the file onto the platform symbol.
10. When it finishes loading, open the jogging experiment.
11. Select RUN.
12. Turn on the router (green button at front-right of router) and wait by the emergency stop (red push-button next to the green button) to verify that all axes are stable. Turning on the router

before this step could result in undesirable motion. Non-terminated signals from other MATLAB code have been known to continue sending signals while the router is turned off.

13. In Control Desk, press the RESET button to reset all the encoders. None of the axes should be activated.
14. Activate all axes.
15. Press the MANUAL button.
16. Enter a travel distance in millimetres into the input box for Z2 (press ENTER to submit the value while in the input box cursor or use the arrow buttons to increase or decrease the value).
17. Press the Up or Down buttons accordingly to move the printhead mount within range of home position. Be careful not to exceed the limitations of movement.
18. Similarly move the X and Y axes into the desired position. Both XL and XR must be activated at the same time.
19. If Z2 has travelled a large distance (> 5mm), then deactivate the Z2 axis before resetting the encoders. Otherwise, leave it activated.
20. IMPORTANT: Deactivate XL, XR, and Y axes.
21. Reset the encoders.
22. If Z2 has dropped out of range, then activate Z2 and repeat steps 16 through 22 as necessary.
23. IMPORTANT: switch the program back to Automatic control to allow MATLAB to control the router motion.
24. Return to the MATLAB window and press a key to start the homing routine.
25. Once it is finished, verify that the displayed graph shows the axis has been homed. If it does not, then the Control Desk program may have been left in Manual mode and all axes except Z2 MUST be deactivated and the program restarted. If the axis still does not home, then close Control Desk, restart MATLAB (CTRL+C to end the program), and go back to step 7. The last solution would be to close all programs, turn off the router, restart the computer and necessary programs, and go back to step 7.
26. Go to the XUSB software and start the print.

27. Return to the MATLAB prompt and press a key to continue and again to start the printing routine.
28. Place a hand over the emergency stop while the printing routine is running. Possible reasons for stopping include erratic motion, printhead mount contacting substrate, and safety.

29. When printing has completed and the axes have returned to home position, check the printed image for any flaws.
30. Go to the XUSB software, acknowledge the print completion, and stop the print.

To continue printing, the steps are fairly similar and can begin with the software steps. If the trajectory does not need to change, then the model does not need to be built to the dSPACE environment. The memory allocated to the trajectory should be fairly large; otherwise the .sdf may need to be reloaded to the DS1002 platform in Control Desk (stop the program and then remove the platform by pressing the red button). Remember to activate the Z2 control since the printhead mount may have dropped due to the weight when the control was deactivated after printing. If printing the same image over again, the "print once" option can be deactivated under the printhead configuration and the start print will only need to be pressed once. However, when making changes to the settings in Scorpion version 4.1, such as powering on and off certain printheads or changing offsets, then the changes must be made while print mode is stopped.

Shutting Down

1. Press the Emergency stop button on the router.
2. Stop the animation in Control Desk. Remove the platform by pressing the red button. Close Control Desk.
3. Stop the Ink System program. Close Ink System.
4. Stop print mode in the XUSB software if this has not been done already. Close the XUSB software.
5. Turn off the XUSB.
6. IMPORTANT: Close the manual valves above the printheads. Handles should be pointed in the direction opposing the motion of ink flow.
7. Place the cover back over the bottom of the printheads using the hitch pins.
8. Turn off the Ink Supply Controller.
9. Turn off the router panel.
10. Turn off the two fuse switches.
11. Unplug the router.
12. Turn off the pulse-width modulator.
13. Turn off the dSPACE.

Appendix D: Additional Calibration Measurements and Calculations

Cyan and Magenta Alignment

	Minimum Distortion Radius [µm]	Maximum Distortion Radius [µm]	Combined Aligned Radius [µm]
Average	63.5843	84.9622	82.5647
Maximum	66.5313	89.0081	85.4118
Minimum	60.2378	81.8155	80.9164

Results from Correct XUSB Image Settings

Note: It was not until the new mounting plate for bidirectional printing was installed that the image settings were corrected. It is believed that the discrepancies between swaths 1-2 and swaths 3-4 are a result of the mounting plate being tilted.

Unidirectional Printing:

Vertical Offset Measurements

	Between Swath 1 and Swath 2 [µm]	Between Swath 3 and Swath 4 [µm]
Average	212.1808	243.6483
Maximum	219.3734	253.5381
Minimum	202.291	235.5567

Horizontal Offset Measurements

	Swaths 1-2 [µm]	Swaths 3-4 [µm]
Average	9.541611	37.2616
Maximum	23.503	53.0452
Minimum	1.8079	16.184

Bidirectional Printing:

Bidirectional Horizontal Offsets [µm]

	1PD Swaths 1-2 at 250 mm/sec	1PD Swaths 3-4 at 250 mm/sec	1PD Swaths 1-2 at 50 mm/sec	1PD Swaths 3-4 at 50 mm/sec	2PD Swaths 1-2 at 250 mm/sec	2PD Swaths 3-4 at 250 mm/sec	2PD Swaths 1-2 at 50 mm/sec	2PD Swaths 3-4 at 50 mm/sec
Average	71.626	10.4892	14.5849	53.6449	14.2854	11.5880	8.4913	25.0742
Maximum	92.604	26.073	25.174	80.0173	26.973	32.367	19.7796	44.0544
Minimum	58.4396	0.899	4.4953	21.5777	2.6972	4.4954	1.7981	3.596

Again, the 2PD results show significant improvement and more consistency over the 1PD results.

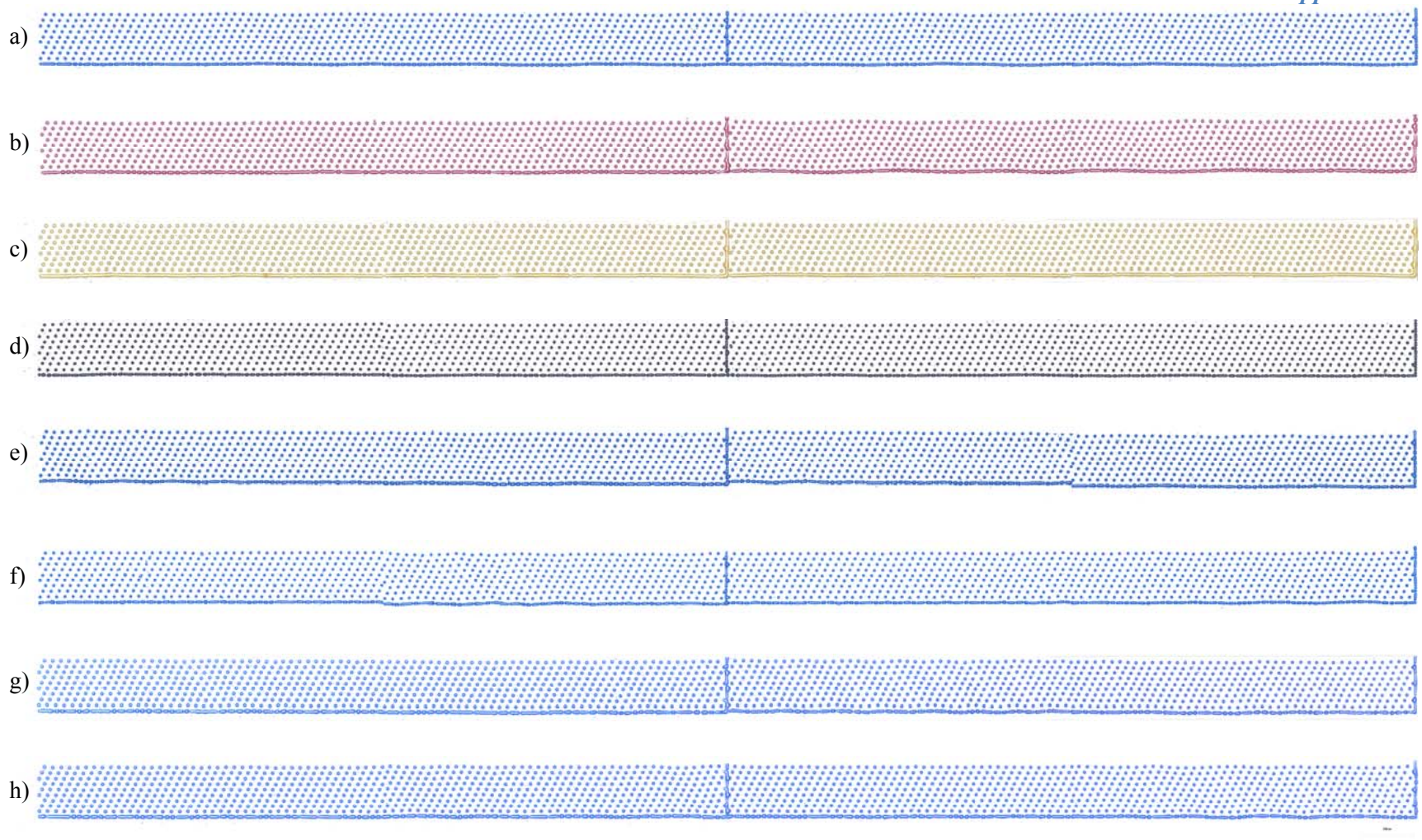

a) Unidirectional Cyan, b) Unidirectional Magenta, c) Unidirectional Yellow, d) Unidirectional Black, e) 1PD at 250 mm/sec, f) 1PD at 50 mm/sec, g) 2PD at 250 mm/sec, h) 2PD at 50 mm/sec.

Droplet Placement Error Calculations

Parameters

Density of Ink [g/cm^3]	0.87
Vertical Velocity [m/sec]	6
Volume of Droplet [pL]	50
Horizontal Velocity [mm/sec]	250
Viscosity of Air [g/cm·s]	0.0001827

Diameter of Droplet [cm], *D*:

$$D = 2\left(\sqrt[3]{\frac{3}{4}\frac{V}{\pi}}\right) = 2\left(\sqrt[3]{\frac{3}{4}\frac{50\times10^{-9}}{\pi}}\right) = 0.004570781$$

This diameter is within the range such that Brownian motion is not significant.

Relaxation Time Constant, τ [sec]:

$$\tau = \left(\frac{1}{18}\right)\left(\frac{D^2}{\eta_{air}}\right)\rho_{droplet} = \left(\frac{1}{18}\right)\left(\frac{0.00457^2}{0.0001827}\right)0.87 = 0.005526996$$

Time Taken for Droplet to Travel 1 mm from Nozzle to Substrate, *t* [sec]:

$$y_v(t) = \tau g t + \tau\left(v_{vi} - \tau g\right)\left(1 - e^{(-t/\tau)}\right)$$
$$0.001 = 0.00553(9.8)t + 0.00553(6 - 0.00553(9.8))\left(1 - e^{(-t/0.00553)}\right)$$
$$t = 0.000169$$

Horizontal Distance Travelled After *t* Seconds [mm]:

$$y_h(t) = v_{hi}\tau\left(1 - e^{(-t/\tau)}\right) = 0.25(0.00553)\left(1 - e^{(-0.000169/0.00553)}\right) = 0.041661$$

Deviation Angle, θ [degrees]:

$$\theta = \arctan\left(\frac{0.041661}{1}\right) = 2.38562127$$

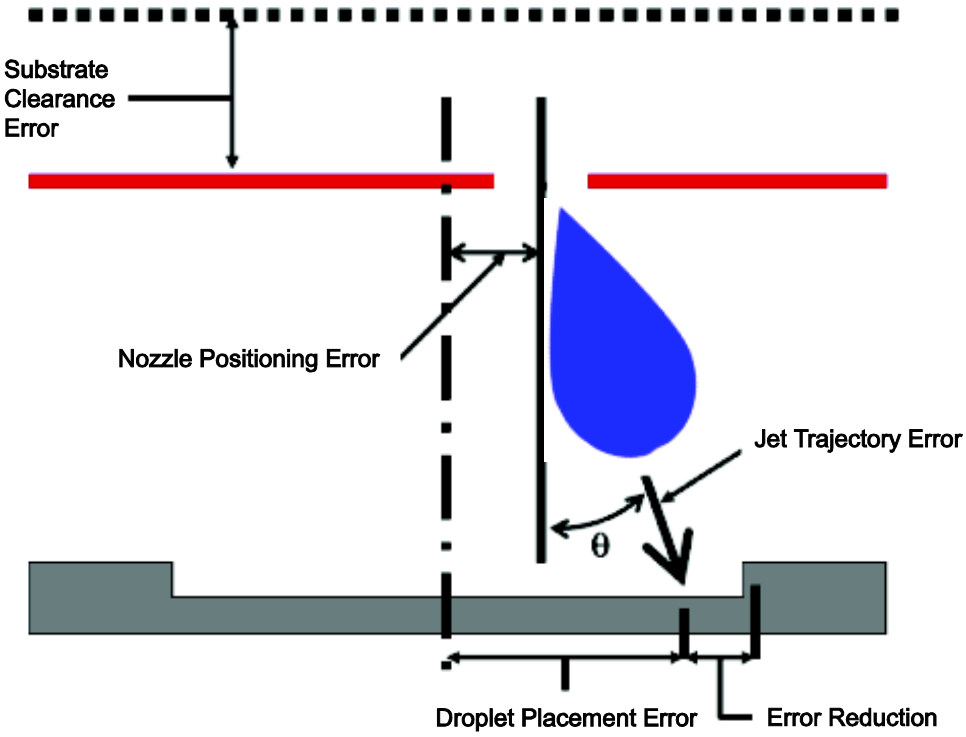

Droplet Placement Error – Adapted from Piezoelectric Inkjet Technology, Wang, X., 2009 [38]

Horizontal Distance Travelled for Different Velocities

Velocity [mm/sec]	Horizontal Offset [µm]	Deviation Angle [°]
635	0.105819	6.0405
105	0.017498	1.0024
50	0.008332	0.4774